AD-A145 215 PEARCE FOCAL SPHERE ANALYSIS OF EXPLOSION AND EARTHQUAKE MECHANISMS(U) TELEDYNE GEOTECH ALEXANDRIA VA ALEXANDRIA LABS K L MCLAUGHLIN ET AL. 10 NOV 83 1/2

UNCLASSIFIED TGAL-TR-83-4 F08606-79-C-0007 F/G 8/11 NL

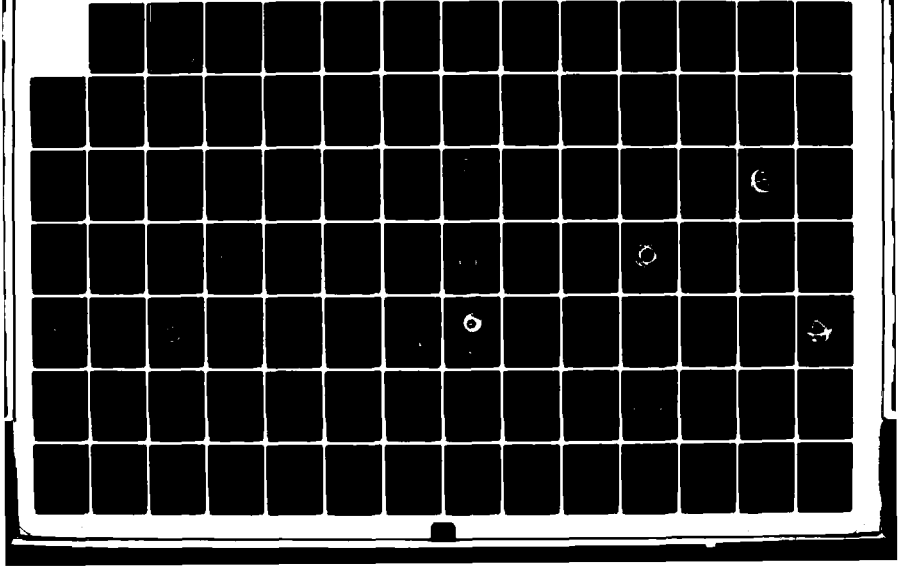

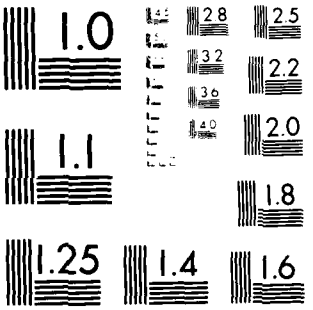

(12)

TGAL-TR-83-4

PEARCE FOCAL SPHERE ANALYSIS OF EXPLOSION AND EARTHQUAKE MECHANISMS

AD-A145 215

K. L. McLaughlin, D. W. Rivers, and M. A. Brennan

TELEDYNE GEOTECH
Alexandria Laboratories
314 Montgomery Street
Alexandria, VA 22314

10 November 1983

Technical Report

APPROVED FOR PUBLIC RELEASE, DISTRIBUTION UNLIMITED.

Prepared for:

DEFENSE ADVANCED RESEARCH PROJECTS AGENCY
1400 Wilson Boulevard
Arlington, VA 22209

Monitored by:

AFTAC/TG
Patrick Air Force Base
Florida 32925

Disclaimer: Neither the Defense Advanced Research Projects Agency nor the Air Force Technical Applications Center will be responsible for information contained herein which has been supplied by other organizations or contractors, and this document is subject to later revision as may be necessary. The views and conclusions presented are those of the authors and should not be interpreted as necessarily representing the official policies, either expressed or implied, of the Defense Advanced Research Projects Agency, the Air Force Technical Applications Center, or the US Government.

REPORT DOCUMENTATION PAGE

1a. REPORT SECURITY CLASSIFICATION: Unclassified	1b. RESTRICTIVE MARKINGS:
2a. SECURITY CLASSIFICATION AUTHORITY:	3. DISTRIBUTION/AVAILABILITY OF REPORT: APPROVED FOR PUBLIC RELEASE; DISTRIBUTION UNLIMITED.
2b. DECLASSIFICATION/DOWNGRADING SCHEDULE:	
4. PERFORMING ORGANIZATION REPORT NUMBER(S): TGAL-TR-83-4	5. MONITORING ORGANIZATION REPORT NUMBER(S):
6a. NAME OF PERFORMING ORGANIZATION: TELEDYNE GEOTECH Alexandria Laboratories; 6b. OFFICE SYMBOL (If applicable):	7a. NAME OF MONITORING ORGANIZATION: AFTAC/TG
6c. ADDRESS (City, State and ZIP Code): 314 Montgomery Street Alexandria, Virginia 22314	7b. ADDRESS (City, State and ZIP Code): Patrick Air Force Base Florida 32925
8a. NAME OF FUNDING/SPONSORING ORGANIZATION: DARPA; 8b. OFFICE SYMBOL (If applicable):	9. PROCUREMENT INSTRUMENT IDENTIFICATION NUMBER: F08606-79-C-0007
8c. ADDRESS (City, State and ZIP Code): 1400 Wilson Boulevard Arlington, Virginia 22209	10. SOURCE OF FUNDING NOS: PROGRAM ELEMENT NO: ; PROJECT NO: VT/0709 ; TASK NO: ; WORK UNIT NO:
11. TITLE (Include Security Classification): (See Block 16)	
12. PERSONAL AUTHOR(S): K.L. McLaughlin, D.W. Rivers, M.A. Brennan	
13a. TYPE OF REPORT: Technical; 13b. TIME COVERED: FROM 7/24/79 TO 1/10/83; 14. DATE OF REPORT (Yr., Mo., Day): 83-11-10; 15. PAGE COUNT: 120	
16. SUPPLEMENTARY NOTATION: PEARCE FOCAL SPHERE ANALYSIS OF EXPLOSION AND EARTHQUAKE MECHNISMS	

17. COSATI CODES		
FIELD	GROUP	SUB. GR.
08	11	

18. SUBJECT TERMS (Continue on reverse if necessary and identify by block number): Pearce processor; Focal planes; Depth phases; Discrimination; Earthquake; Explosion; SRIS; CSS

19. ABSTRACT (Continue on reverse if necessary and identify by block number)

Pearce's (1977) processor for analyzing seismic focal mechanisms has been implemented on two seismic analysis systems, and it has been given limited testing for use as a discrimination aid. This algorithm uses relative amplitudes of the pP and sP depth phases with respect to the P-wave amplitude at each station in a network. If pP and/or sP cannot be identified, then the amplitude of the P-wave coda at the anticipated arrival time of the undetected depth phase may be used as an upper limit on the amplitude of that phase. The solution space of double-couple seismic sources is searched for possible solutions consistent with the relative amplitude bounds which were measured at each station. If no solution can be found, then either the "depth phases" were misidentified or the event was not a double-couple (i.e.,

20. DISTRIBUTION/AVAILABILITY OF ABSTRACT: UNCLASSIFIED/UNLIMITED ☒ SAME AS RPT ☐ DTIC USERS ☐	21. ABSTRACT SECURITY CLASSIFICATION: Unclassified
22a. NAME OF RESPONSIBLE INDIVIDUAL: 1Lt Kenneth M. Ols	22b. TELEPHONE NUMBER (Include Area Code): 305-494-5263; 22c. OFFICE SYMBOL: TGR

19) Continued

it may have been an explosion). The algorithm and support software have been installed at the Seismic Research Center (SRC) on the Seismic Research Information System (SRIS) and at the Center for Seismic Studies (CSS). A description of both systems is given. Examples of the use of the algorithm as a seismic analysis tool are presented.

Theoretical analysis has been performed to evaluate the utility of the constraint on the amplitude of the depth phases which is provided by the amplitude of the seismic coda as a discrimination tool for testing the hypothesis that the event is an earthquake at depth. Analysis using synthetic data suggests that the Pearce algorithm may be a useful discriminant of explosions when the coda remains below the initial P-wave amplitude at five or more teleseismic stations covering all four quadrants. In such a case, it is highly probable that the algorithm will not find any double-couple solutions at depth consistent with small pP amplitudes at all stations. A test on Global Digital Seismic Network (GDSN) data suggests that pP amplitude constraints are sufficient to eliminate the possibility of double-couple sources at depths greater than 3-5 km for explosions of m_b >5, when azimuthal coverage is adequate. Testing of the proposed discriminant on events with smaller magnitudes could not be adequately performed with GDSN data. Analysis of Eurasian earthquake GDSN data demonstrated that pP phases could be detected on short period records for shallow (less than 33 km) events, with acceptable double-couple solutions.

X

A-1

ABSTRACT

Pearce's (1977) processor for analyzing seismic focal mechanisms has been implemented on two seismic analysis systems, and it has been given limited testing for use as a discrimination aid. This algorithm uses relative amplitudes of the *pP* and *sP* depth phases with respect to the *P*-wave amplitude at each station in a network. If *pP* and/or *sP* cannot be identified, then the amplitude of the *P*-wave coda at the anticipated arrival time of the undetected depth phase may be used as an upper limit on the amplitude of that phase. The solution space of double-couple seismic sources is searched for possible solutions consistent with the relative amplitude bounds which were measured at each station. If no solution can be found, then either the "depth phases" were misidentified or the event was not a double-couple (*i.e.*, it may have been an explosion). The algorithm and support software have been installed at the Seismic Research Center (SRC) on the Seismic Research Information System (SRIS) and at the Center for Seismic Studies (CSS). A description of both systems is given. Examples of the use of the algorithm as a seismic analysis tool are presented.

Theoretical analysis has been performed to evaluate the utility of the constraint on the amplitude of the depth phases which is provided by the amplitude of the seismic coda as a discrimination tool for testing the hypothesis that the event is an earthquake at depth. Analysis using synthetic data suggests that the Pearce algorithm may be a useful discriminant of explosions when the coda remains below the initial *P*-wave amplitude at five or more teleseismic stations covering all four quadrants. In such a case, it is highly probable that the algorithm will not find any double-couple solutions at depth consistent with small *pP* amplitudes at all stations. A test on Global Digital Seismic Network (GDSN) data suggests that *pP* amplitude constraints are sufficient to eliminate the possibility

of double-couple sources at depths greater than 3-5 km for explosions of $m_b > 5$, when azimuthal coverage is adequate. Testing of the proposed discriminant on events with smaller magnitudes could not be adequately performed with GDSN data. Analysis of Eurasian earthquake GDSN data demonstrated that pP phases could be detected on short period records for shallow (less than 33 km) events, with acceptable double-couple solutions.

TABLE OF CONTENTS

LIST OF FIGURES

LIST OF FIGURES (Continued)

LIST OF FIGURES (Continued)

LIST OF FIGURES (Continued)

LIST OF TABLES

INTRODUCTION

The traditional method of determining the focal mechanism of an earthquake has been to plot on a stereographic projection the polarities of the first motions of the P waves which were observed for that earthquake at a network of stations. An orthogonal pair of large-circle arcs could then be found graphically which best separated the compressional and dilational first motions into quadrants. These arcs represent the projection of the fault and auxilliary planes of the double-couple mechanism, and their strike and dip could be read directly off the stereonet. The rake of the slip vector could also be calculated by noting that the slip vector is perpendicular to the intersection of the fault and auxiliary planes (*i.e.*, the null axis), so all the parameters necessary for specifying the focal mechanism could be determined from this graphical separation of the first-motion polarities into quadrants. Eventually computer searches over all possible focal mechanisms were used to replace the sometimes subjective process of physically manipulating a stereonet in order to find the best-fitting pair of orthogonal planes (*e.g.*, Wickens and Hodgson, 1967).

Although this traditional technique is sufficient in principle to permit the determination of the earthquake focal mechanism, it uses only a fraction of the information pertaining to the seismic radiation pattern which is available for analysis from the seismogram. The traditional technique has therefore been expanded in the last 20 years or so to incorporate additional information other than simply the P-wave polarities. One such type of additional information is the polarity of the S-waves, which can be measured by taking the ratio of the amplitudes of the SH and SV polarizations. The S-wave radiation pattern is such that, if the directions of the S-wave polarities are plotted as arrows on the same stereographic projection as was constructed for the P-wave polarities, the arrows will be directed from the compression axes to the tension axes, and they

[illegible] the fewest nodal planes. This solution [illegible] thus [illegible] the double-couple solution [illegible] and planes.

[illegible] on the focal sphere is presently [illegible] the *P* [illegible] information about the [illegible] body wave [illegible] amplitudes will be largest at the [illegible] and will be zero at the nodal planes and the *S* wave amplitudes will be largest at the tension, pressure and null axes and will be largest at the positions of the slip [illegible] fault and auxiliary planes. This amplitude information may be [illegible] the focal mechanism solution by inverting the [illegible] amplitudes to obtain the seismic moment tensor. Surface waves rather than body waves [illegible] be used to solve for the seismic moment tensor but surface-wave amplitudes and particularly phases are difficult to trace back to the [illegible] account of differences in the propagation paths from the source to [illegible] stations in the network. (There are similar problems with body [illegible] soon discuss.)

Although adding *S*-wave polarities and body-wave amplitudes to the *P*-wave polarities rectifies the deficiency in the traditional focal mechanism solution of [illegible] pertinent and potentially valuable information which is contained in the [illegible] after the swing of the first motion, there remain a number of [illegible] in this augmented approach. For one thing, near-source focusing [illegible] lateral inhomogeneities along the propagation path may cause the section of the seismic radiation pattern which is actually sampled by a given station to be different from that which would be predicted from the azimuth and take-off [illegible] assumed in plotting that station on the sphere. Signals may be [illegible] either on account of poor signal-to-noise ratio or on account of a [illegible] increasing seismic source time function, and these emergent signals cannot be categorized on the basis of their polarity. Furthermore, the choice of

the particular time window in which one should measure the amplitude of an emergent signal may be rendered ambiguous. Focusing near the receiver and uncertainty in the value which is assumed for the anelastic attenuation parameter t^* for the source-to-receiver propagation path may result in the over- or underestimation of the signal amplitude of either type of body wave. Calculation of the seismic moment tensor will, of course, be particularly sensitive to errors in the amplitude measurement or the path correction for stations close to the nodal planes of the double couple. Finally, S-waves cannot be expected to contribute much information to the solution for small events.

Pearce (1977, 1980) has developed an extension to the traditional method of focal mechanism solution which offers certain advantages over the methods described above. Pearce's technique relies upon the formation of the ratios of the observed amplitudes of the phases P, pP, and sP. Teleseismic radiation from the surface-reflected phase pP samples the upper half of the focal sphere which is not sampled by the downward propagating P waves, so the chances of a given station's being close to a nodal plane, and hence of exerting strong influence on the fault plane solution, are increased when pP amplitudes are added to the data base of P amplitudes. Use of the sP phase allows one to sample the S-wave radiation pattern without having to measure S directly. Perhaps most importantly, forming the ratios P/pP, P/sP, and pP/sP tends to cancel out the effects of attenuation, since the propagation paths for each of these phases are nearly the same for shallow events. By using sP rather than the direct S phase, one can ignore the effects of t^*_S on all of the path except for the upgoing leg, so the amplitude ratio P/sP which is used by Pearce is less sensitive to the effects of attenuation than is the ratio P/S, which was used for focal mechanism solutions by Honda (1957). Another important advantage of Pearce's technique is that, if pP or sP cannot be detected, the amplitude of the seismic coda at the time of the predicted phase arrival can be measured, and

this value can then be used as an upper bound on the [illegible] of the unobserved phase.

In order to implement Pearce's amplitude ratio [illegible] necessary to have an earth model for ray-tracing, which permits us to associate the measurements made at a given station with the proper point on the focal sphere from which the seismic radiation emanated. In this regard it is the same as the traditional technique which associates stations on the stereonet with points on the P-wave radiation pattern by means of the azimuth and take-off angle. One further piece of information is required for Pearce's method, however, namely an earth model which accounts for the upgoing and reflected legs (back down to the source depth) of pP and sP. In the case of pP, a simplifying assumption is made, namely that the event is at shallow depth, so the only effect which the layers of the earth model above the source depth have on the propagation of pP is to introduce a simple multiplicative coefficient representing the efficiency of the reflection at the free surface. In the case of sP, it is also assumed that the event is shallow, and the effect of the shallow layers is to refract the upgoing S-wave leg and reflected P-wave leg in a simple manner which can be calculated using only the seismic velocities at the source depth and at the free surface. The algorithm thus uses, in effect, a one-layer crustal model. Again, a coefficient is also introduced which represents the efficiency of the surface reflection, this time taking into account the conversion from S- to P-wave energy. We shall discuss the implications of these simplifying assumptions and the choice of the reflection coefficients later.

It can be seen immediately that one difficulty with Pearce's technique is the use of this simplistic model for the propagation and reflection of the upgoing legs of pP and sP. There are also certain practical problems in making the necessary measurements of the sought-after phases on the seismogram, as we shall point out later. It is also important to note that Pearce's technique does

not escape certain of the difficulties which beset the other extensions of the traditional fault plane solution which were discussed previously. Specifically, near-source focusing and lateral inhomogeneities along the propagation path can cause the portion of the radiation pattern sampled at a given station to be different from that which is expected on the basis of the azimuth and take-off angle which were used to plot that station on the stereonet; this problem is now compounded by similar problems for the reflected legs. Near-receiver focusing will still be a source of error, since this may fail to cancel out when the amplitude ratios are formed of phases which have reached the receiver region by even slightly different paths. Emergent signals will still contribute no useful polarity information, and it may be difficult to determine where in the wavetrains of these signals the measurements of P and of the bounds for pP and sP should be made.

We have mentioned that amplitude information for the P and S phases is introduced into the focal mechanism solution by means of inversion to determine the seismic moment tensor. By contrast, in the implementation of Pearce's technique amplitude information is introduced by means of a grid search over all possible geometrical orientations of the double couple. These orientations are defined by allowing the strike of the fault, the dip of the fault, and the rake of the slip vector within the fault to take on all possible values. In distinction to the more usual convention of defining the double-couple orientations by $0° \leq \text{strike} < 360°$, $0° \leq \text{dip} < 90°$, and $-180° \leq \text{rake} < 180°$, Pearce defines them by $0° \leq \text{strike} < 360°$, $0° \leq \text{dip} < 180°$, and $0° \leq \text{rake} < 180°$. The definitions of each of these parameters, including the sign conventions, should be inferred from Figure 1. We shall perform the grid search over strike, dip, and rake by sweeping over each of these three parameters, within the limits listed above, in increments of either 5° or 10°. In presenting graphically the results of his analysis, Pearce plots each allowed focal mechanism as an individual vector

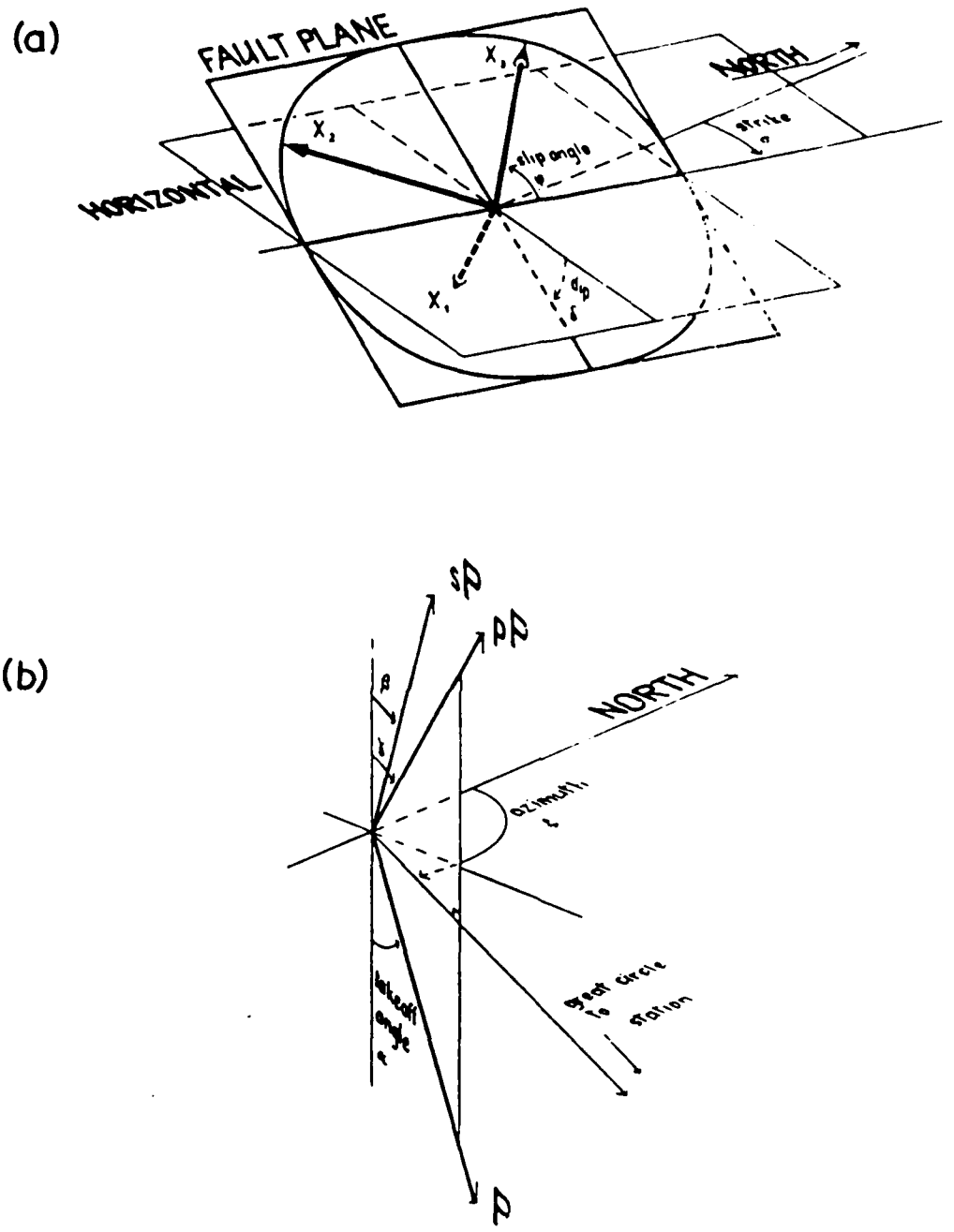

FIGURE 6. DEFINITION OF (a) SOURCE ORIENTATION AND (b) TAKEOFF DIRECTIONS

Figure 1 Figure 6 reproduced from Pearce (1979), definitions of the source parameters strike, slip, and dip for the fault plane, and the takeoff angles for P, pP, and sP.

eminating from the corresponding point within the plane spanned by the coordinates dip and rake, and having as the vector's azimuth the strike of the double couple (*cf* Figure 2).

For every point on the strike-dip-rake grid defined by the limits listed above, the ratios P/pP, P/sP, and pP/sP are computed for every station in the network. These values are then compared with the ratios of the observed amplitudes and with the observed polarities. (If no amplitude information, even upper bounds deduced from the coda amplitude, is available for a given phase at a given station, then the ratios involving that phase are simply ignored. This also applies to the polarity of each of the three phases.) Of course, the predicted amplitude ratio should not be expected to be exactly equal to the observed value, so it is necessary to specify upper and lower bounds around the observed amplitudes of each phase representing the "error bars" which take into account geophysical effects such as focusing as well as the imprecision of measurement. In the case of an unobserved pP or sP phase, the lower bound is taken to be zero, and the upper bound is taken to be the observed coda amplitude or a slightly larger value than that. Instead of forming the ratios of the observed amplitudes, then, Pearce's algorithm actually forms ratios of the amplitude *bounds*, and these are in turn used as bounds on the observed ratios. What is tested is thus whether the predicted amplitude ratios fall within the computed bounds around the observed ratios, and whether the predicted polarities agree with those which are observed. If this comparison fails for at least one station in the network, then this grid point is eliminated from the suite of possible focal mechanism solutions.

The grid search actually proceeds by testing the predicted amplitude ratios and polarities for each grid point against the observed bounded ratio and polarities of a given phase pair at a given station, and then the search over the entire grid is repeated for the next phase pair at that station or for a phase pair at the

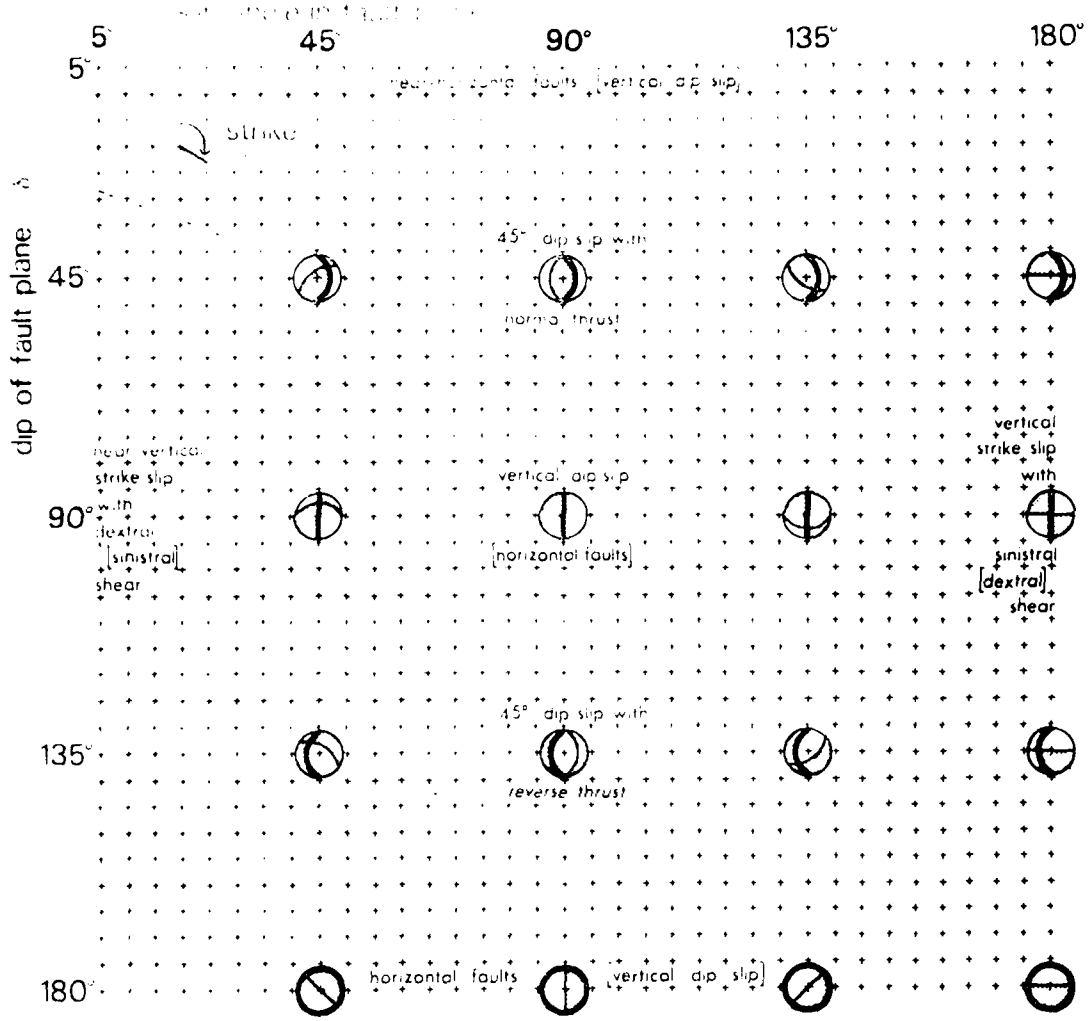

Figure 7. Method of representing acceptable fault plane orientations in terms of slip direction ω, dip δ and strike σ, as defined in Figure 6(a). Acceptable orientations are plotted as vectors from the Cartesian point defining ω and δ, in the direction of the strike σ. Lower hemisphere stereographic projections indicate the type of fault plane orientation represented by various combinations of ω and δ, and are shown oriented for strike $\sigma = 360°$ (northerly)

Figure 2 Figure 7 reproduced from Pearce (1979, showing the representation of the three dimensional closed solution space of double-couples represented by slip, dip, and strike angles used in the Pearce algorithm.

next station until all the observed data have been tested. A list of the grid points (*i.e.* the double couple mechanisms) which are consistent with the particular data point under consideration is printed out along with a cumulative list of the grid points which are consistent with all data tested so far. At the end of the process, this cumulative list contains all of the double-couple mechanisms which are considered to be acceptable solutions. Note that this list will almost always encompass a range of solutions rather than a unique value, such as is usually presented to be "the" fault plane soltuion which is found using polarities plotted on a stereonet. Note also that the range of solutions cannot always be represented as a single value with error bars around each of the three double-couple parameters, since the grid points which satisfy all the tests are not necessarily contiguous. An extension to Pearce's algorithm which we have implemented in this study is to generalize this logic to permit the retention of grid points for which the number of inconsistent observations is less than some specified limit, rather than automatically rejecting them if the number of inconsistencies exceeds zero. This revision prevents the solution from being dominated by a small number of possibly erroneous measurements. (Incidentally, we note that one common source of measurement error, namely miscalibration of the instrument gain, is inapplicable to the Pearce technique, since this error would cancel out. This is one advantage of using amplitude ratios at a given station rather than the amplitudes themselves.) In order to speed up the grid search, we have also revised the logic so that, after the maximum permitted number of inconsistencies is exceeded for a given grid point, that point is not included in any further searches over the grid. This "cascading" of acceptable solutions from one ratio test to another made the grid searching several times faster. Finally, we changed Pearce's treatment of the polarity data to consider the polarities of the phases individually rather than just their "ratio" (*i.e.*, whether the two phases had the same or opposite signs) This change permits

more P-wave polarities to be used, since usually the polarity of the other phase, whether pP or sP, cannot be observed, and therefore no test can be performed on the "ratio" of the polarities of the two phases.

So far we have described three techniques for finding the double-couple solution (or, more precisely, the range of double-couple solutions) for an earthquake : the traditional method of P-wave (and possibly S-wave) polarities, the use of amplitude data to find the seismic moment tensor, and Pearce's technique of amplitude ratios. In addition to their use for finding the focal mechanisms of earthquakes, each of these techniques may also be used as a tool for discriminating earthquakes from explosions. Since our principal interest in this study is the event identification problem, we shall now examine the use of each one of these techniques as a seismic discriminant.

The traditional technique of plotting P-wave polarities on a stereonet constitutes a simple discriminant : if an event has at least one dilatational first motion, then it is an earthquake. This straightforward method of identifying earthquakes was in fact one of the earliest discriminants, having been proposed by the Geneva "Conference of Experts" in 1958. An appealing aspect of this technique is that, unlike many other commonly used but empirically derived discriminants such as $M_s:m_b$, its physical foundation is not subject to controversy. Unfortunately, the polarity of the first motion for weak signals is usually ambiguous and sometimes misleading. The true first motion can be obscured by earth noise, causing the second swing of the seismograph to be misread as being the first motion. For this reason, the first motion discriminant is applied only to those waveforms which have a strong signal-to-noise ratio. Consequently, this technique is frequently inadequate for identifying small earthquakes. Even when the signal-to-noise ratio criterion is met, the discriminant may fail, since the P wave polarities of certain signals from explosions have been observed to be negative (Enescu *et al.*, 1973). Ignoring for the time being the possibility of

misleading first motions, we may ask whether the observation of only compressional polarities for an event means that the event is an explosion. In most cases the answer is clearly no, since a pair of orthogonal arcs representing nodal planes can usually be drawn on the stereonet which separate the stations into a pair of opposite quadrants in which compressional polarities are observed and a pair of opposite quadrants in which no polarities are reported. Only if there is extensive coverage in both azimuth and distance of those stations which report polarities can no such pair of nodal planes be found. If it does turn out through a complete grid search of all possible double-couple mechanisms that this is in fact the case, only then may the event be identified as an explosion, otherwise, an event with only compressional first motions may be either an explosion or an earthquake.

As we have explained, Pearce's technique uses a grid search over all possible double couples to find those mechanisms which are consistent with the observed bounds on the amplitude ratios and polarities. If no double couple is found which is consistent with all the data, then we conclude that either some mistake has been made or that the event is not an earthquake, so this technique too can be used as a discriminant. We shall discuss in a subsequent section of this report possible sources of error which could cause no double-couple solution to be found for an earthquake. For the moment we set aside the question of whether an earthquake might be misidentified by Pearce's technique, and ask whether an explosion will always be recognized by this method. In general, the answer to this question is no, since in analogy to the previously discussed case of a stereonet solution which involves only positive first motions, we see that usually there exists at least a narrow range of double-couple solutions which are consistent with all the data unless the network of stations provides broad azimuthal and distance coverage. Also, in analogy to the case of small events for which the first motion is usually ambiguous, for a small explosion pP and sP will

be obscured by earth noise. The "coda" amplitude which is used as an upper bound for the amplitude of the undetected surface reflections is then simply the noise level, so the ratios pP/P and sP/P are bounded by zero and by the reciprocal of the signal-to-noise ratio. This upper bound may be too large to constrain to zero the range of consistent solutions. In this study we shall examine the question of how broad the coverage of stations must be for Pearce's technique to be useful as a discriminant, and we shall briefly address the question of how small an explosion can be identified by this method.

The first-motion criterion has been used extensively as a seismic discriminant for many years. Inverting seismic measurements to solve for the moment tensor has been used more for investigating features of the source mechanism, such as the yields, of known explosions than for event identification, but some studies have employed this technique as a discriminant (*e.g.*, Stump and Johnson, 1977). Although Pearce has applied his method of amplitude ratios to the problem of determining the focal mechanisms of suites of earthquakes (Pearce *et al.*, 1980), he has used it as a discriminant for only a few specific events such as the 20 March 1976 "Semipalatinsk earthquake" (Pooley *et al.*, 1983). The purpose of this study is to investigate more fully the utility, from both a theoretical and a practical standpoint, of this technique both for studying earthquake focal mechanisms and for identifying explosions. In particular, we shall investigate whether the necessary measurements for implementing Pearce's algorithm may be made in a manner which is compatible with procedures which are currently used for routine seismic analysis.

The work which is summarized in this report is divided into three tasks. First, we shall present the results of an investigation of certain theoretical aspects of Pearce's method, such as the azimuthal coverage which is necessary to constrain tightly the range of solutions. This investigation was performed using Global Digital Seismic Network [GDSN] data at the facilities of the Center

for Seismic Studies [CSS] in Arlington, Virginia. The use of these data and facilities permitted this task to be performed in an unclassified mode. Next, we provide documentation of a package of computer software which was written to facilitate making the measurements on seismograms which are required by Pearce's algorithm. This software package constitutes a new subsystem of the Seismic Research Information System [SRIS] which was, at the time of this study, operating in a classified mode at the Alexandria Labs of Teledyne Geotech. Finally, we present results of a demonstration of this new subsystem. The demonstration was performed using a classified data base, namely the Area of Interest [AI] data set which had been used previously in the VSC Discrimination Experiment and which was used concurrently with this investigation by another study involving automated discrimination techniques. The results of this classified analysis will be presented in a separate volume of this report.

SOME DETAILED EXAMPLES OF THE PEARCE PROCESSOR

The seismologist may use the Pearce algorithm in either of two ways. In the first way, a seismologist may simply wish to test "the earthquake at depth" hypothesis of a suspected event. This test entails the estimation of P and P coda levels with acceptable tolerances. The amplitude ratio bounds of pP to P and sP to P are the result of minimum P amplitude bounds and maximum P coda bounds. Simply expressed, the pP-to-P amplitude ratio bounds are

$$-(P_{coda} / P_{minimum}) < (pP / P) < (P_{coda} / P_{minimum})$$

The first motion polarity of the P wave may or not be used for one or more of the stations. If no double-couples can be found consistent with the pP/P, sP/P bounds then the event may be indicated as an explosion. However, if double-couples can be found for a given depth, then no definite conclusion is reached and the event may be either explosion or earthquake. It may be necessary to test several depth intervals. It is not possible to rule out the *very* shallow earthquake.

As the second strategy, the seismologist may wish to find possible double-couple solutions at a given depth to test the working hypothesis that certain secondary arrivals are depth phases. There may be several alternative combinations of secondary arrivals across a network of stations resulting from coda fluctuations, or multiple earthquake sources. In the case of explosion shot arrays, there may exist well defined secondary arrivals across the entire array. In any of these circumstances the seismologist makes the necessary measurements, notes the inferred depth and estimates tolerances on the amplitude measurements. Each alternative hypothesis may be submitted to the Pearce algorithm. The processor may return a few consistent solutions, numerous acceptable solutions, or no acceptable solutions. The results *may* eliminate some of the competing hypotheses.

TABLE I

Explosions in the CSS data base used for testing the Pearce focal plane analysis algorithm. Depth (h) constrained to zero.

EV	DATE	OT	LAT	LONG	h	m_b	M_s
21	09/05/77	03:07:57.80	50.090	78.960	0	5.90	0.00
27	10/29/77	03:06:57.70	49.840	78.170	0	5.50	0.00
34	11/30/77	04:06:57.50	49.950	78.360	0	5.90	4.50
41	05/26/78	03:56:57.60	49.730	78.070	0	5.50	0.00
56	06/11/78	02:56:57.70	49.830	78.830	0	5.90	4.40
57	09/15/78	02:36:57.50	49.890	78.970	0	6.00	4.40
66	10/31/78	04:16:57.50	49.750	78.180	0	5.20	0.00
68	11/04/78	05:05:57.50	50.040	78.980	0	5.60	4.50
80	02/01/79	04:17:57.70	50.110	78.880	0	5.40	0.00
93	06/23/79	02:56:57.60	49.910	78.910	0	6.30	4.40
95	06/24/79	18:50:57.90	-21.980	-168.860	0	5.30	0.00
99	07/25/79	17:56:58.50	-21.890	-168.950	0	6.00	4.40
103	08/04/79	03:56:57.70	49.900	78.950	0	6.10	5.50
105	08/18/79	02:51:57.30	49.970	79.010	0	6.10	4.10
111	10/18/79	07:09:58.30	73.330	54.500	0	5.00	0.00
117	10/28/79	03:16:56.90	49.960	79.060	0	6.00	4.40
120	12/03/79	04:36:57.50	49.690	78.840	0	6.00	4.40
122	12/23/79	04:56:57.60	49.960	78.850	0	6.10	4.10
125	03/23/80	19:36:58.40	-21.870	-169.090	0	5.70	0.00
131	04/25/80	03:56:57.40	49.940	78.790	0	5.50	0.00
134	05/22/80	03:56:57.60	49.720	78.100	0	5.50	0.00
135	06/12/80	03:26:57.50	49.940	79.040	0	5.60	0.00
137	06/16/80	18:26:57.80	-22.020	-168.870	0	5.50	0.00
139	06/29/80	02:32:57.70	49.970	78.830	0	5.70	0.00
144	09/14/80	02:40:39.30	49.970	78.880	0	6.20	4.70
148	10/11/80	07:09:57.00	73.350	54.990	0	5.80	5.80
149	10/12/80	03:34:14.10	49.950	79.080	0	5.90	4.30
154	12/03/80	17:32:58.20	-21.930	-168.960	0	5.60	0.00
156	12/14/80	03:47:06.60	49.930	79.000	0	5.50	4.10
159	12/27/80	04:09:08.20	50.040	79.040	0	5.90	0.00
162	03/29/81	04:03:55.00	49.960	78.930	0	5.50	4.20
163	04/22/81	01:17:11.30	49.910	78.870	0	5.90	0.00
166	05/27/81	03:58:12.20	49.960	78.990	0	5.40	0.00

TABLE II

Earthquakes added to the CSS data base for testing of the Joint Epicenter Determination analysis algorithm. Depth (h_D) in km constrained and unconstrained cases.

#	DATE	OT	LAT	LONG	n	h_D	M_S
[illegible]							

In the following examples, various strategies are illustrated with examples to both verify that the Pearce processor yields consistent results with other focal mechanism methods and to explore some of the assumptions inherent in the algorithm.

Figure 3A shows the GDSN P wave signals of an East Kazahk explosion of 10/12/80, event 149 in Table I. Kaao and Zobo are complicated wavetrains due to interference of multiple arrivals and are not used in the analysis. P wave amplitude bounds are indicated by the double horizontal bar. P coda levels are also indicated by the single horizontal bars. These amplitude bounds were submitted to the Pearce algorithm as P, pP and sP bounds (except for Grfo and Gumo) The coda amplitudes were multiplied by 1.33 to give the pP and sP bounds. No first motion polarity information was used. No double-couple solutions were found to be consistent with the 20 |pP/P| and |sP/P| amplitude ratio bounds. The P wave takeoff angles for each station are shown on an equal area lower hemisphere projection in Figure 3B (P velocity of 6 km/sec at the source). A histogram of the percentage number of solutions allowed if inconsistencies are permitted is shown in Figure 3B. For example, if four observations are deleted, then 96 solutions out of 11664 (10 degree search grid) may be found. This presentation of the results does not show which observations are critical. However, if the three stations Kono, Anto, and Beao are deleted from the data set then an 180 degree azimuthal gap opens in the coverage (Figure 3B) and a great number of solutions become possible. The P coda levels are valid for a depth range of 3 to 33 km. No acceptable double-couple solutions were found for these coda levels with P wave velocities of 5, 6 or 7 km/sec at the source. It is quite clear that for this event, signal to ambient noise ratios several times worse than is apparent in Figure 3A would still discriminate as either a *very* shallow (less than 3 km deep) earthquake or an explosion. As can be seen from

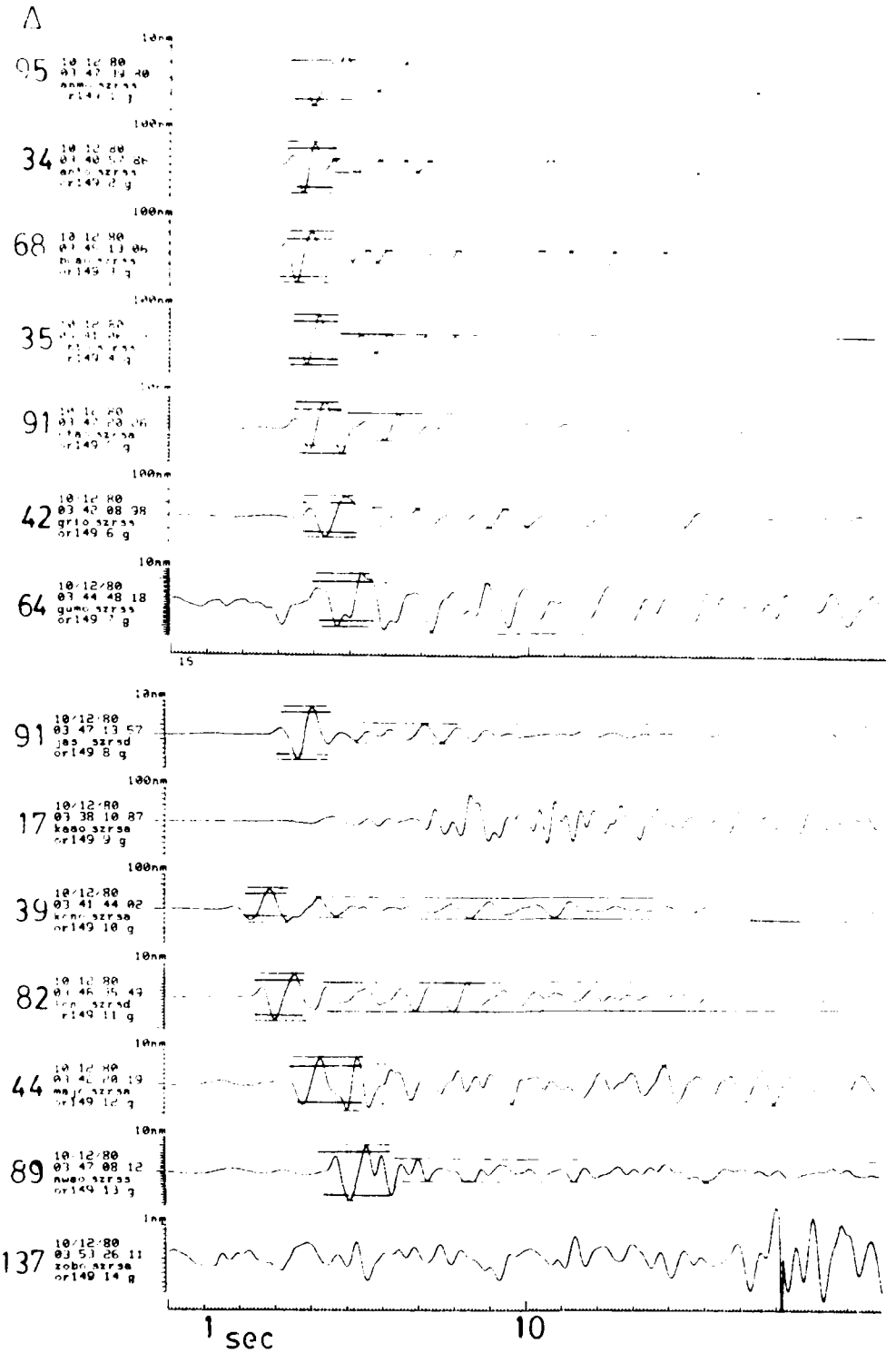

Figure 3a P wave amplitude and coda levels used as input to the focal plane algorithm as P, pP, and sP amplitude bounds are indicated with horizontal bars (event 149 Table I.)

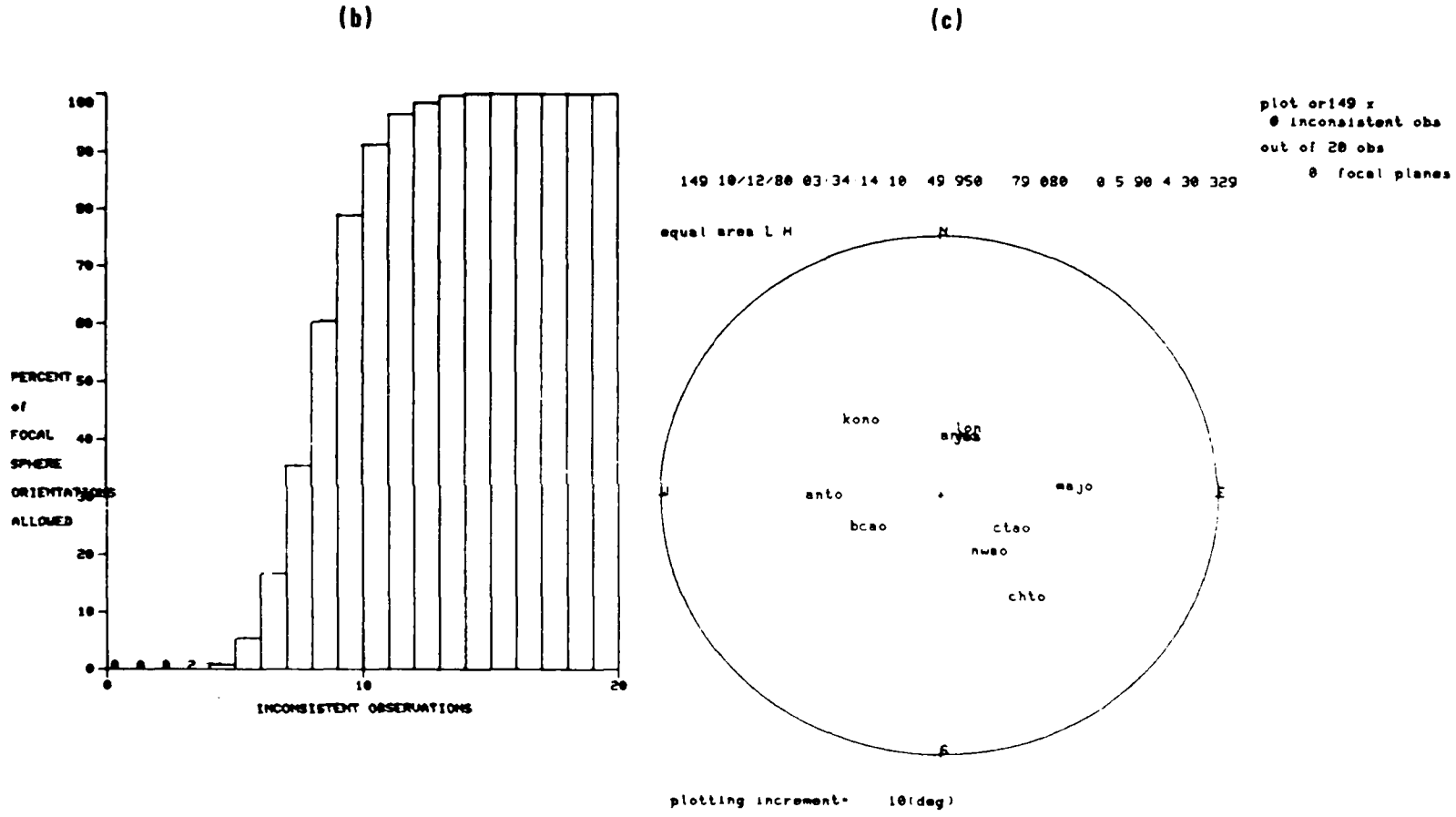

Figure 3b&c Event 149 10/12/80 03:24:14.10, 49.95N, 79.08E, 0 km, m_b 5.9 M_s 4.3. (b) A histogram of the percentage of acceptable double-couples is shown for the number of inconsistent observations tolerated. A total of 20 observations for the 10 stations; pP/P and sP/P bounds for each station. Gumo and Grfo were not used. Three of the observations must be discarded before solutions are allowed. (c) An equal area lower hemisphere projection of the P waves take off angles for each station. If Kono, Anto, and Bcao are discarded then two quadrants are open and solutions are admitted by the focal plane algorithm.

the focal sphere projection (Figure 3B), that stations Anmo, Lon, and Jas do not contribute independent information. Similarly, addition of Grfo and Gumo only provides redundant information to Kono and Majo respectively.

The New Brunswick earthquake serves as a good example of a well recorded continental earthquake with published solutions. Figure 4A (adapted from Choy et al; 1983) shows the short period GDSN seismograms and broadband deconvolved records used by Choy et al (1983) for moment tensor inversion of the New Brunswick earthquake. Amplitudes of the P wave and depth phases pP and sP are indicated on the short period records (SPZ) as they were used in the Pearce focal plane analysis program. Minimum amplitudes are measured for pP on ZOBO, BOCO, and COL. Minimum amplitudes are measured for sP on TOL, GRFO, and KONO. Maximum amplitudes are given for pP or sP on each SPZ record. The polarities were considered reliable on ZOBO, and BOCO. The P amplitude bounds were given as +/- 50% of the P amplitude measurements and submitted as input to the Pearce algorithm. Only pP/P and sP/P bounds were considered, since it was not clear that both pP and sP were indentifiable on the same record for any of the stations shown in Figure 4A. Figure 4B shows the results of a 5 degree search in slip, dip, and strike angles, given the constraints derived from the SPZ records of Figure 4A. 64 focal planes (out of 93312 possible) were found consistent with any 9 out of the 12 observations. When pP/P bounds were relaxed by use of a pP attenuation factor of 0.75 slightly expanded set of solutions was found to be consistent with all of the observations. The largest number of solutions were found for a P velocity at the source of 5 km/sec. The range of acceptable solutions can be described as having a steeply dipping tension axis and a shallow dipping compression axis. The azimuth of the compression axis is poorly constrained by the data. Figure 4C shows five of Choy et al's solutions for this event, and the Dziewonski and Woodhouse (1983), DW, best fitting double-couple.

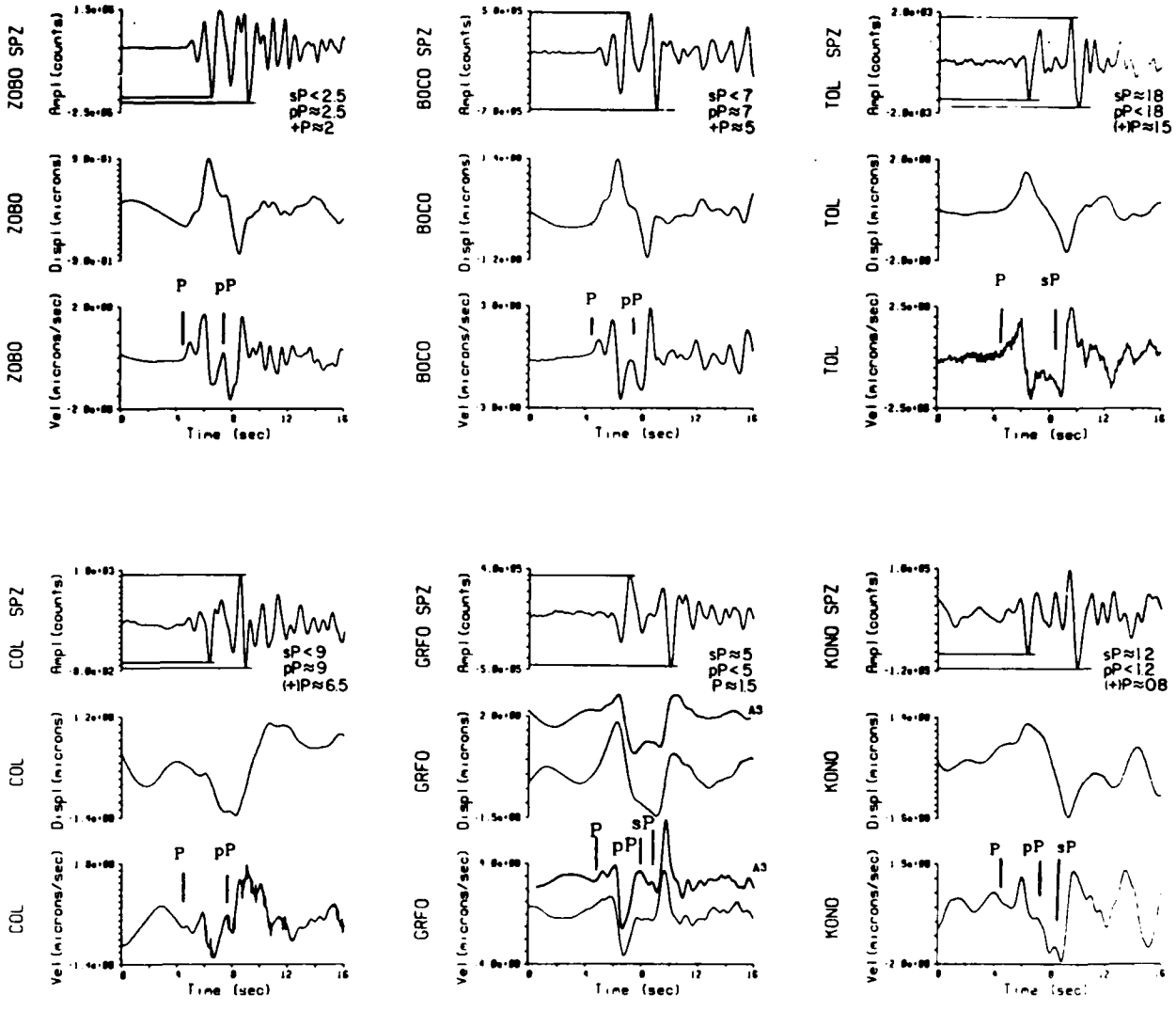

Figure 4a Seismograms for the New Brunswick earthquake adapted from Choy et al (1983). The estimated P, pP and sP amplitude bounds are indicated on the short period seismograms.

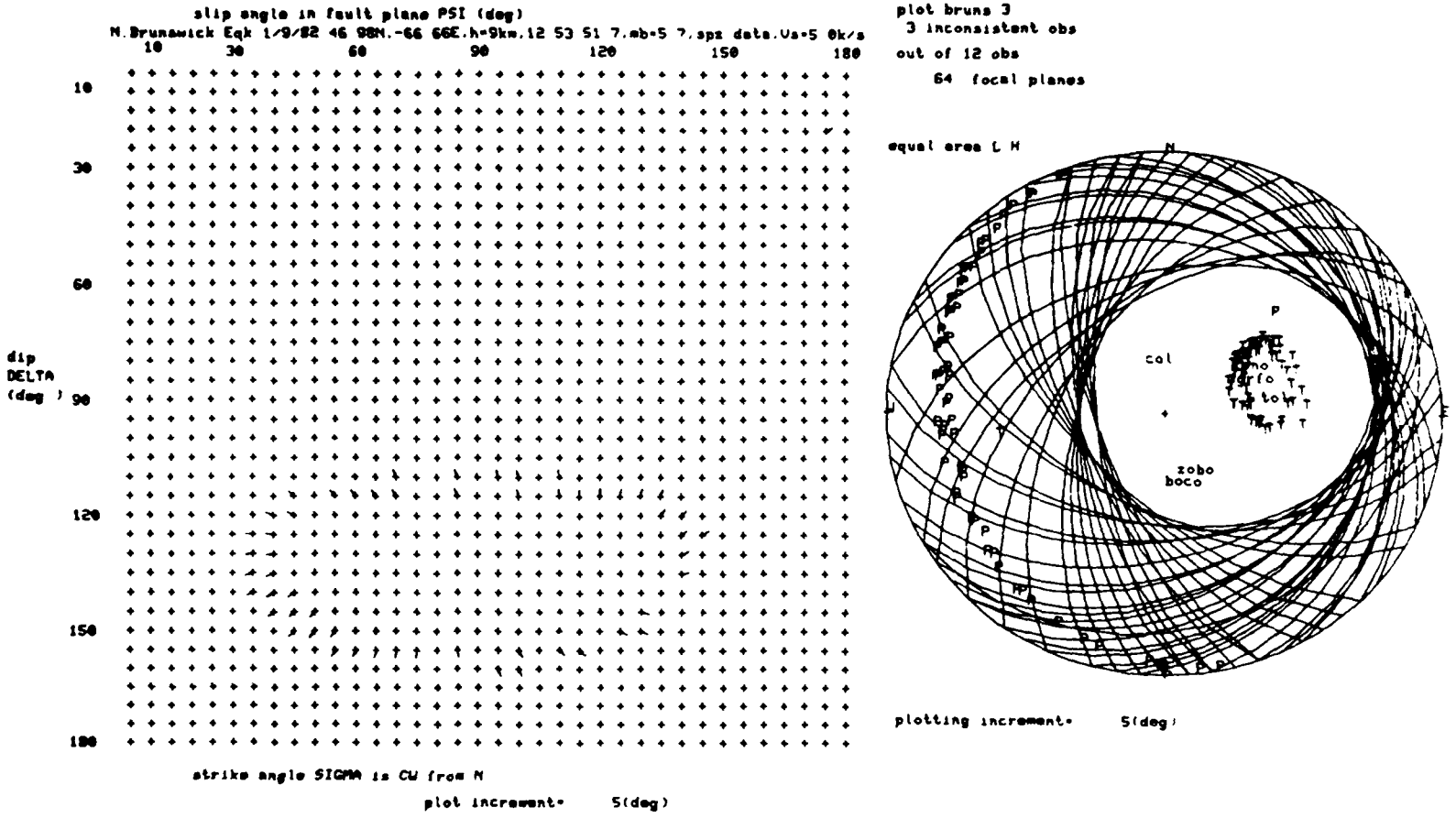

Figure 4b Acceptable focal mechanisms for the New Brunswick earthquake. Solutions span a space of double-couples with well constrained tension axis and a variable compression axis. Tension (T) and Compression (P) axis are shown on a equal area lower hemisphere focal sphere. P wave take-off analyses are plotted for each station with the station name. P wave nodal planes are shown for each acceptable solution.

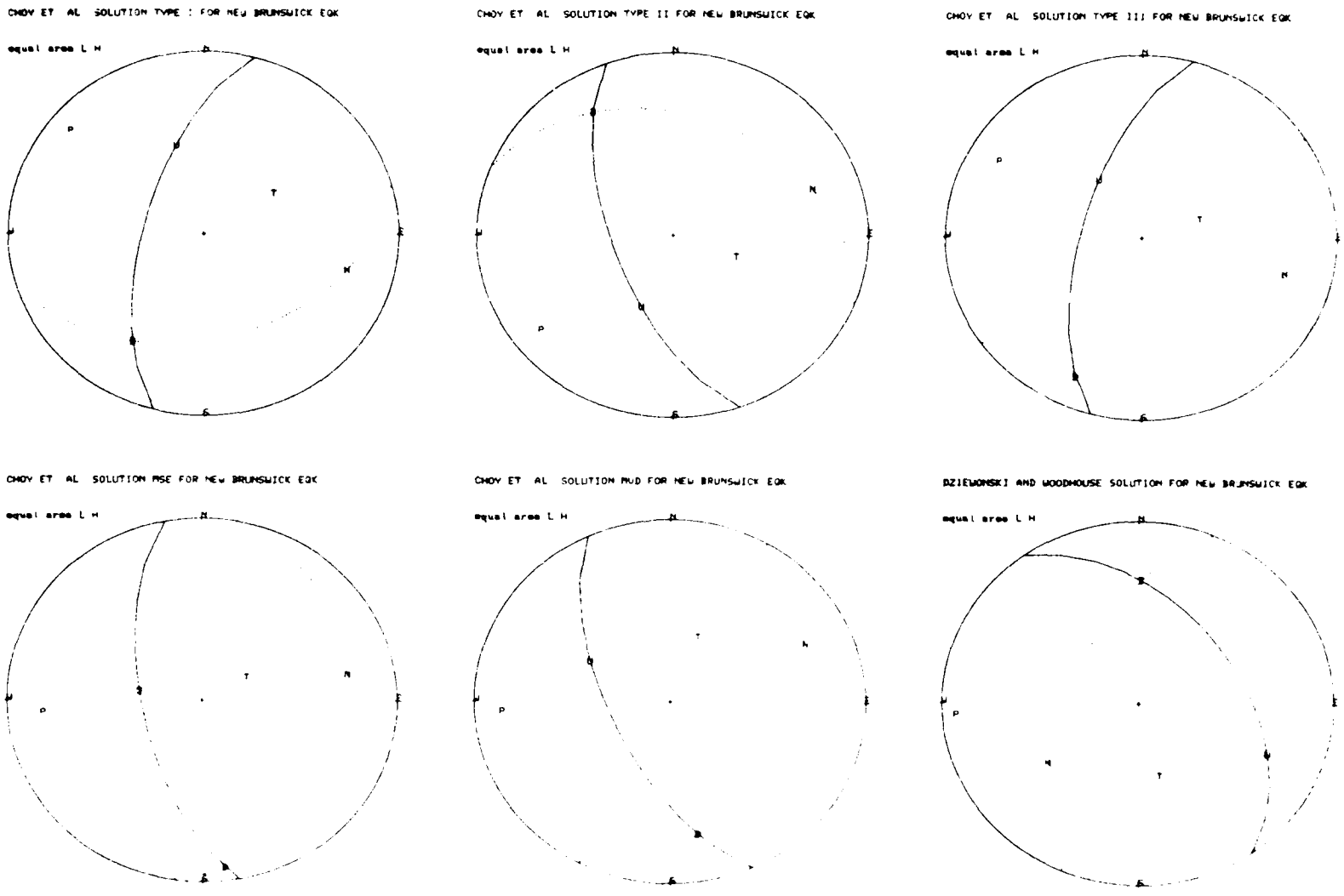

Figure 4. Several solutions from Choy et al (1983) and Dziewonski and Woodhouse (1983).

These published solutions are derived from several diff[illegible] methods. The solutions suggest that the best interpretation is a steeply dipping tens[illegible] axis and a shallow dipping East-West compression axis. All but the DW solution are contained within the solution space shown in Figure 4C. The DW solution was based on long period waveforms and was admittedly a less reliable solution. The Choy et al solutions were all based on broadband body wave data. To summarize, the amplitudes of the P, pP and sP phases apparent on six SPZ records at teleseismic distances yielded a range of focal mechanisms very close to that of much more sophisticated waveform modeling methods. The need for proper attenuation models for the pP and sP phases is apparent when the aim is to find the best fitting double-couple solution. Alternatively, the error bars on the measured P, pP, and sP amplitudes may be increased. The experience gained with this example was that increases in the error bounds simply increased the range of the acceptable solution set for a given number of inconsistencies tolerated in the observation set. The correct attenuation parameter allowed reduction in the error bounds, without an expansion of the range of acceptable solutions. The centroid of the solution space was relatively stable for a fixed set of attenuation parameters, while the volume of the solution space varied with the size of the amplitude error bounds that were used.

Two events of special interest with recently published short period records are the events of May [illegible] 1969 and March 20, 1976 near the East Kazahk test site. Using the published short period records of Pearce et al (1980), and Pooley et al (1983), we wished to verify that the previously published focal mechanisms and depths were consistent with the available data using the CSS implementation of the Pearce algorithm.

The previously published array beams for YKA, WRA, and GRA for the May [illegible], 1969 event are shown in Figure 5A along with their amplitudes and polarities.

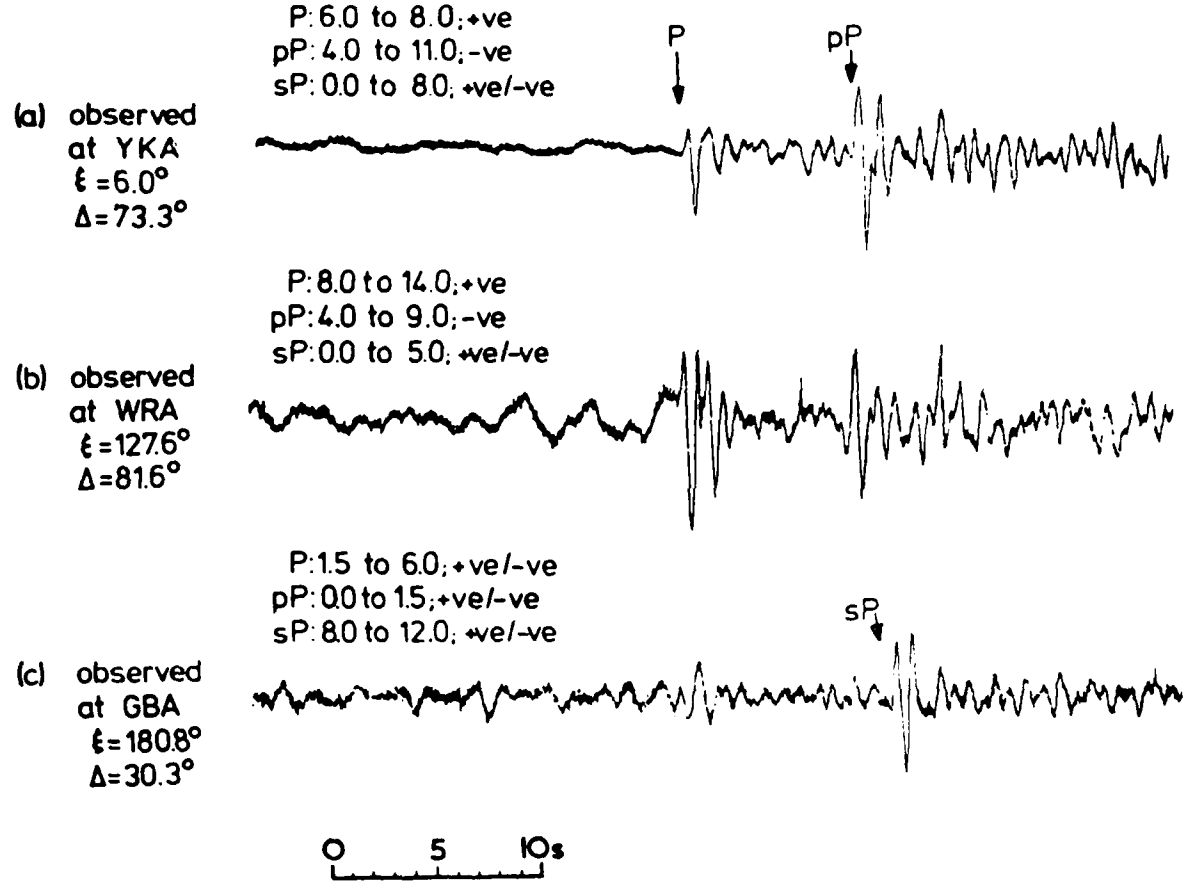

FIGURE 1. THREE TELESEISMIC SHORT PERIOD ARRAY OBSERVATIONS OF THE 1 MAY 1969 EAST KAZAKHSTAN EARTHQUAKE, ORIGIN TIME 04.00.08.7, LOCATION 43.98°N, 77.86°E AND BODY WAVE MAGNITUDE m_b = 4.9 (NEIS PARAMETERS). ξ AND Δ CORRESPOND TO AZIMUTH OF THE STATION FROM THE EARTHQUAKE AND EPICENTRAL DISTANCE RESPECTIVELY. PRESUMED PHASE IDENTIFICATIONS AND THEIR POSSIBLE AMPLITUDES (IN ARBITRARY UNITS) ARE SHOWN

Figure 5a Seismograms reproduced from Pearce (1979) for the May 1, 1969 event.

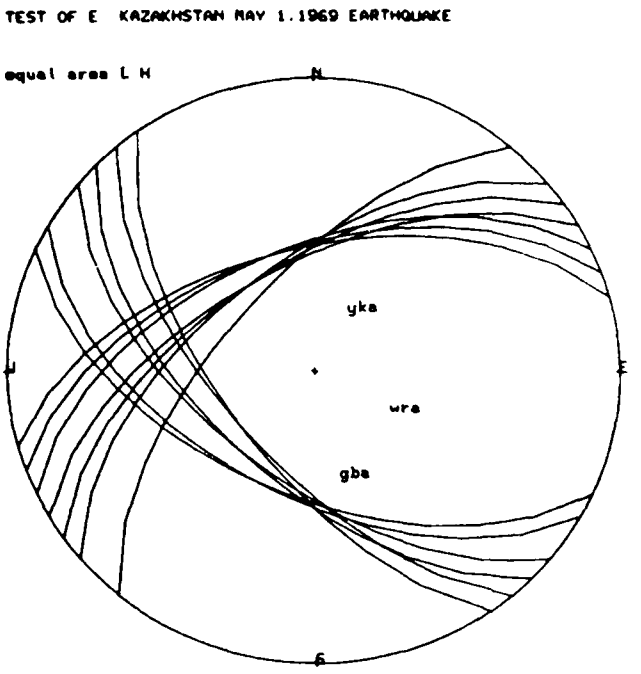

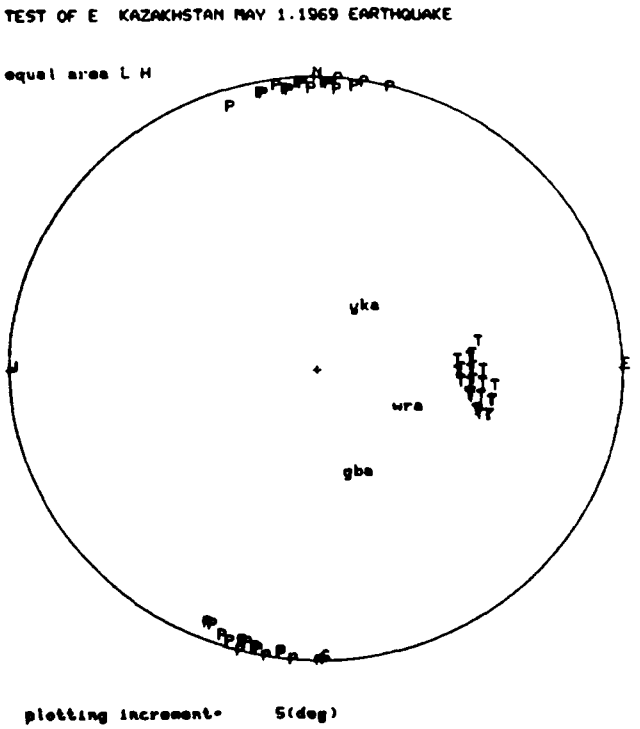

Figure 5b Acceptable solutions to the amplitude constraints shown in (A).

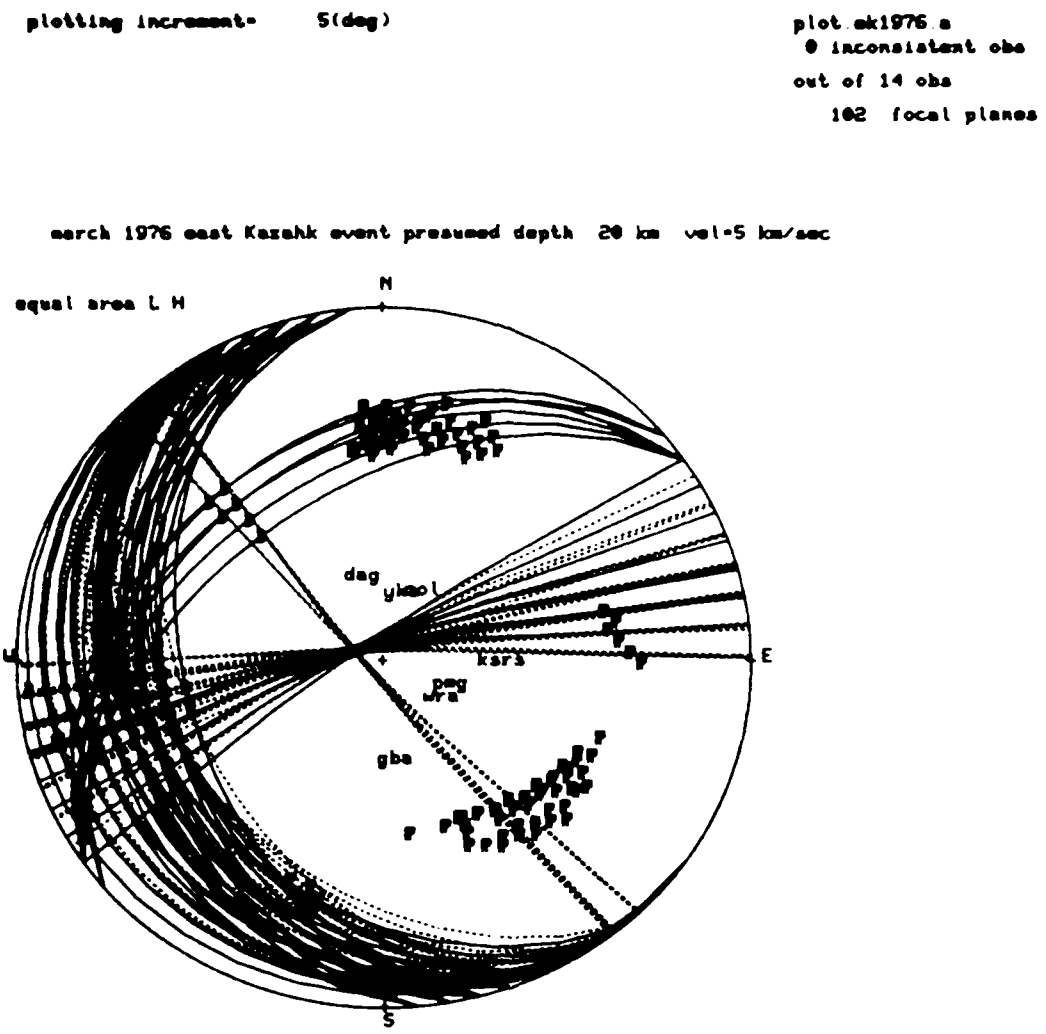

Figure 5c Acceptable solutions for the March 20, 1976 event using only pP/P and sP/P amplitude ratio constraints. Each set of P and T axis is exchanged because polarites were not considered.

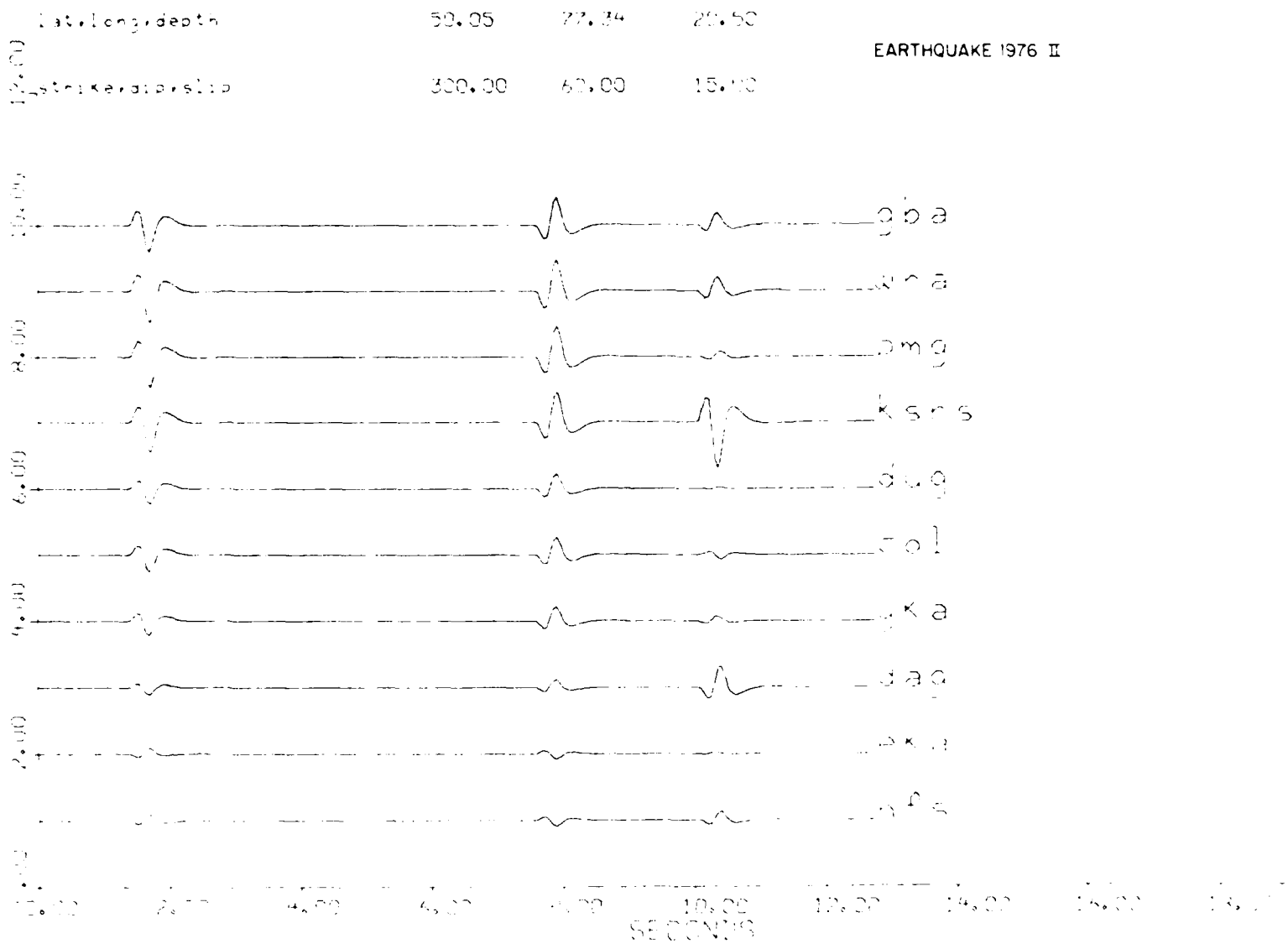

Figure 5d Simple one layer crustal model synthetics for three different possible solutions.

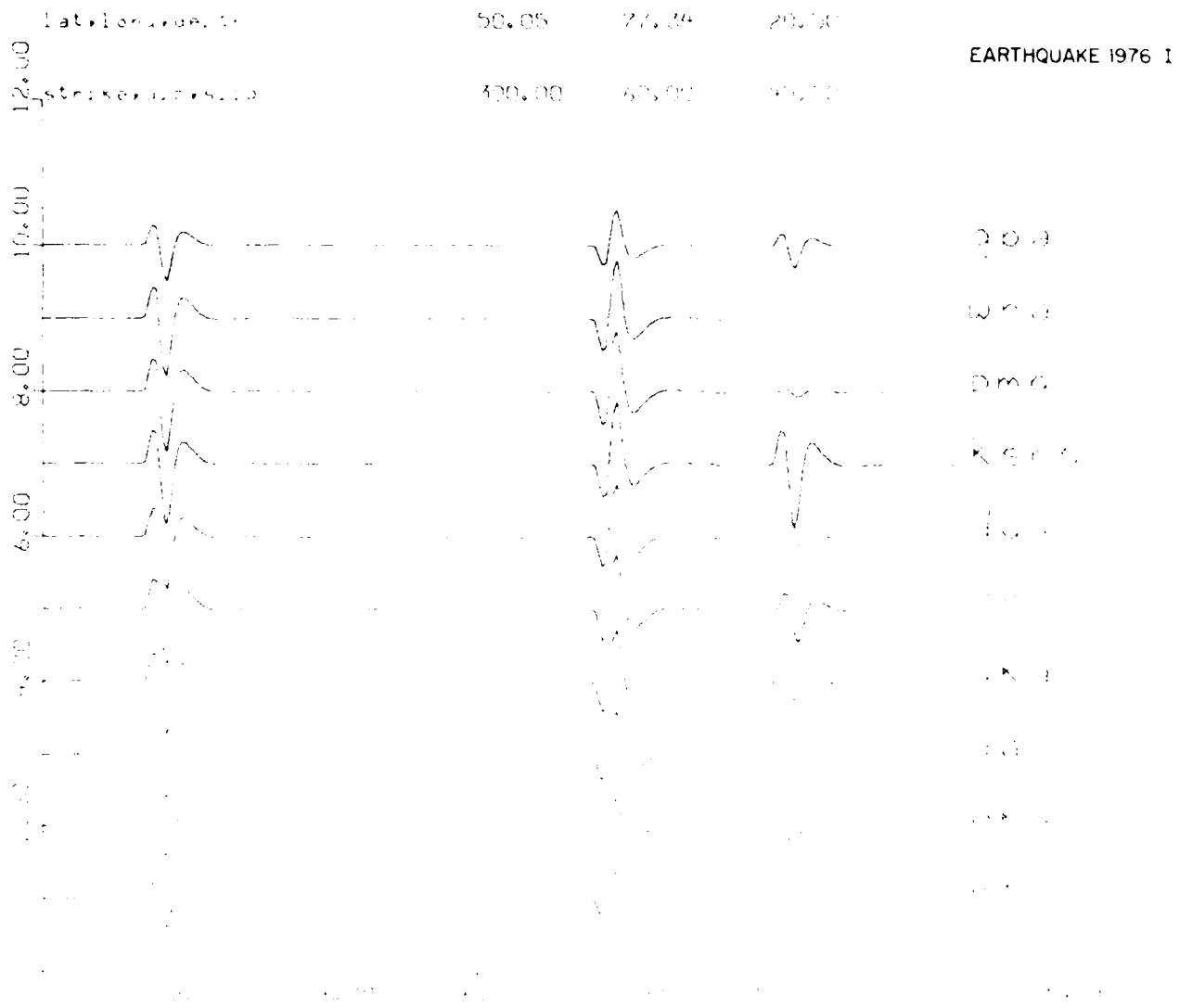

Figure 5a. Simple one layer crustal model synthetics for three different possible solutions.

Figures 5B and 5C show the range of solutions acceptable with these amplitudes using a simple one layer crustal model. The north-west striking focal planes may be compared with the Chingiz fault which strikes $N-40°-W$ with right lateral offset. The fault is visible on LANDSAT photos reproduced in Rodean (1979). Acceptable double-couple solutions to the March 10, 1976 event are shown in Figure 5D. The amplitudes were read directly from recently published seismograms in Pooley et. al. (1983). Pooley et. al. arrive at similar double-couple solutions for the March 20, 1976 event. They conclude, however, that sP amplitudes have been affected by lateral heterogeneity near the source and are less reliably fit than the P and pP amplitudes. They used a layered crust to predict pP and sP reflections as well as crustal reverberation in their simulation. Using only a simple one layer crust without reverberation, the synthetics of Figure 5E, reproduce the pP/P, sP/P and pP/sP amplitudes ratios observed in the actual data with some success. In genral sP amplitudes are at the upper limit of the tolerances submitted to the Pearce algorithm. One subset of the bimodel solution space (Figure 5D) supports near strike-slip motion upon a fault striking NW-SE. Pooley et. al.'s preferred solutions are similar to those in Figure 5D. Given the differences between a simple one layer crustal model and a layered reverberant crustal model , this exercise shows how robust the Pearce method may be to overall crustal structure. Discrepancies are most likely to occur with sP amplitudes. A north-south compressive stress system would be consistent with the inferred focal mechanisms of both the May 1, 1969 and March 20, 1976 events.

Two earthquakes near 30N, 95E (Eastern Tibet) were selected with short period GDSN recordings (events 1914 and 1716 in Table II). Earthquakes in this area were previously found to possess explosion-like M_s-m_b statistics (Der, 1973; Landers, 1972). Blandford and Gurski (1975) examined available geologic

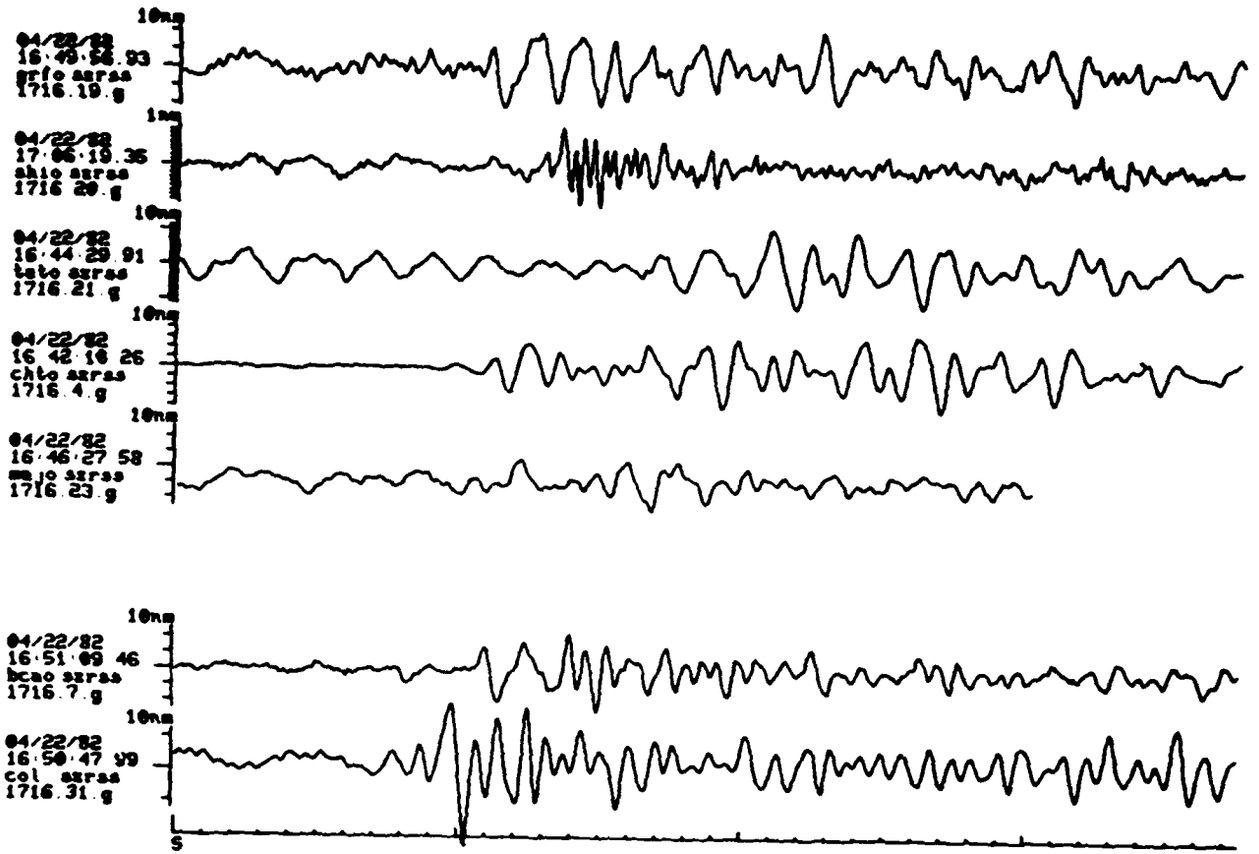

Figure 6a Unfiltered seismograms of event 1716.

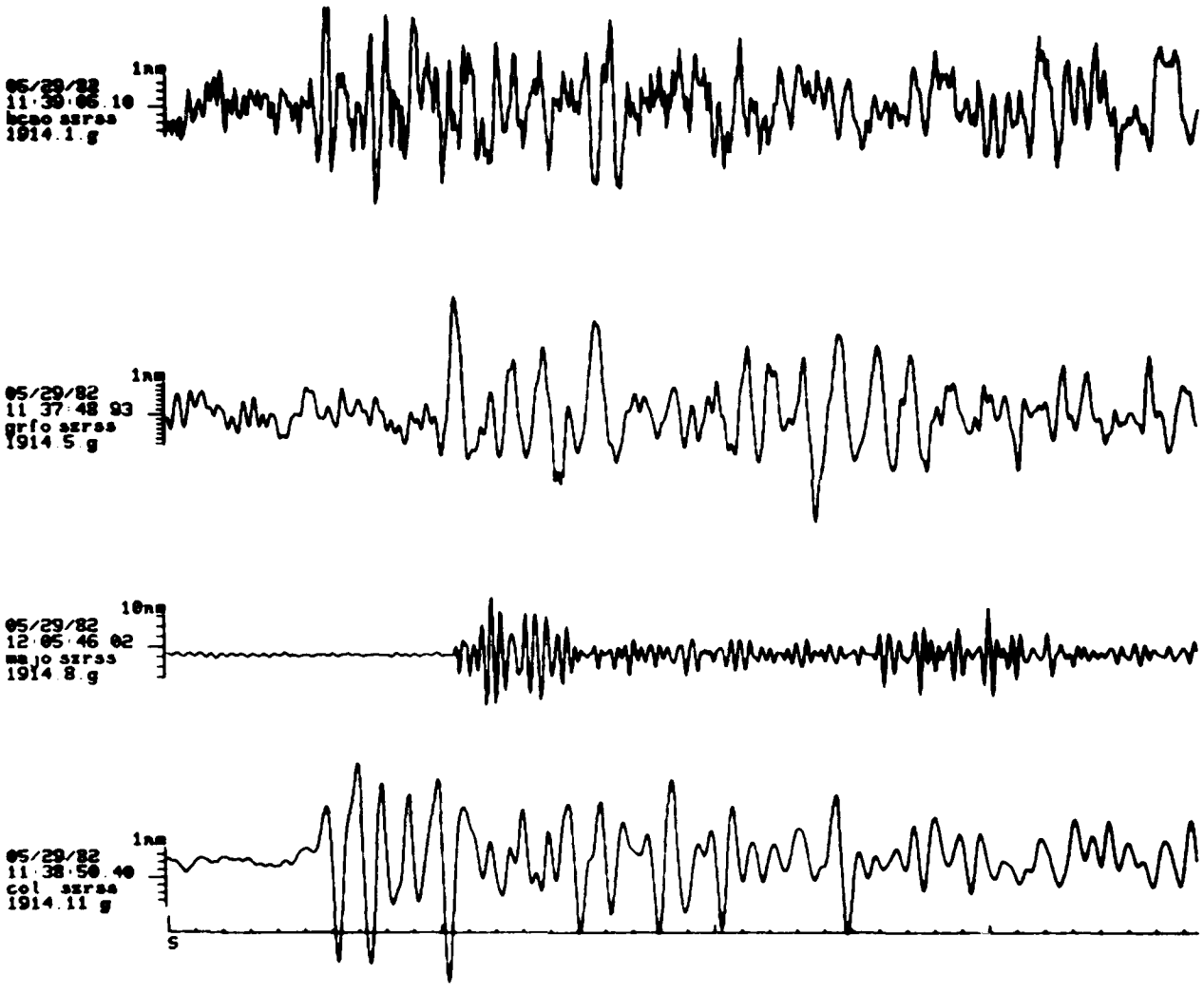

Figure 6b. Unfiltered seismograms of event 1914.

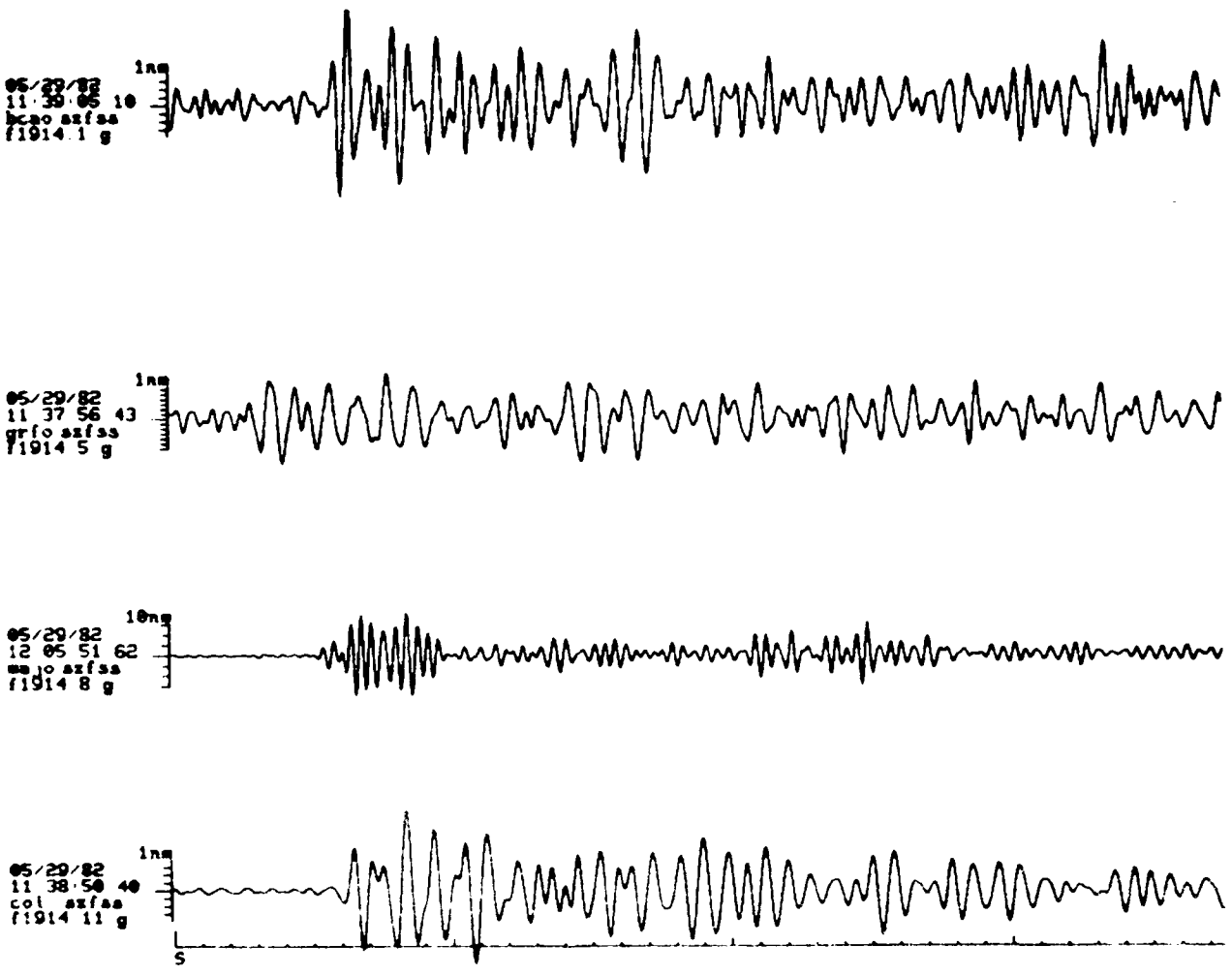

Figure 6c. Filtered seismograms of event 1914.

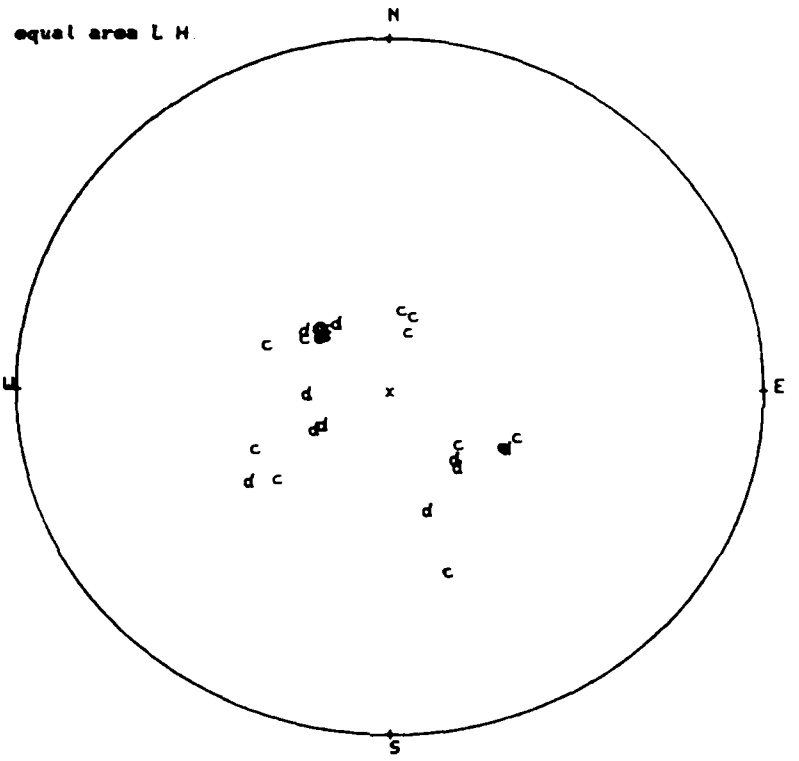

Figure 6d NEIS reported polarities for 1716.

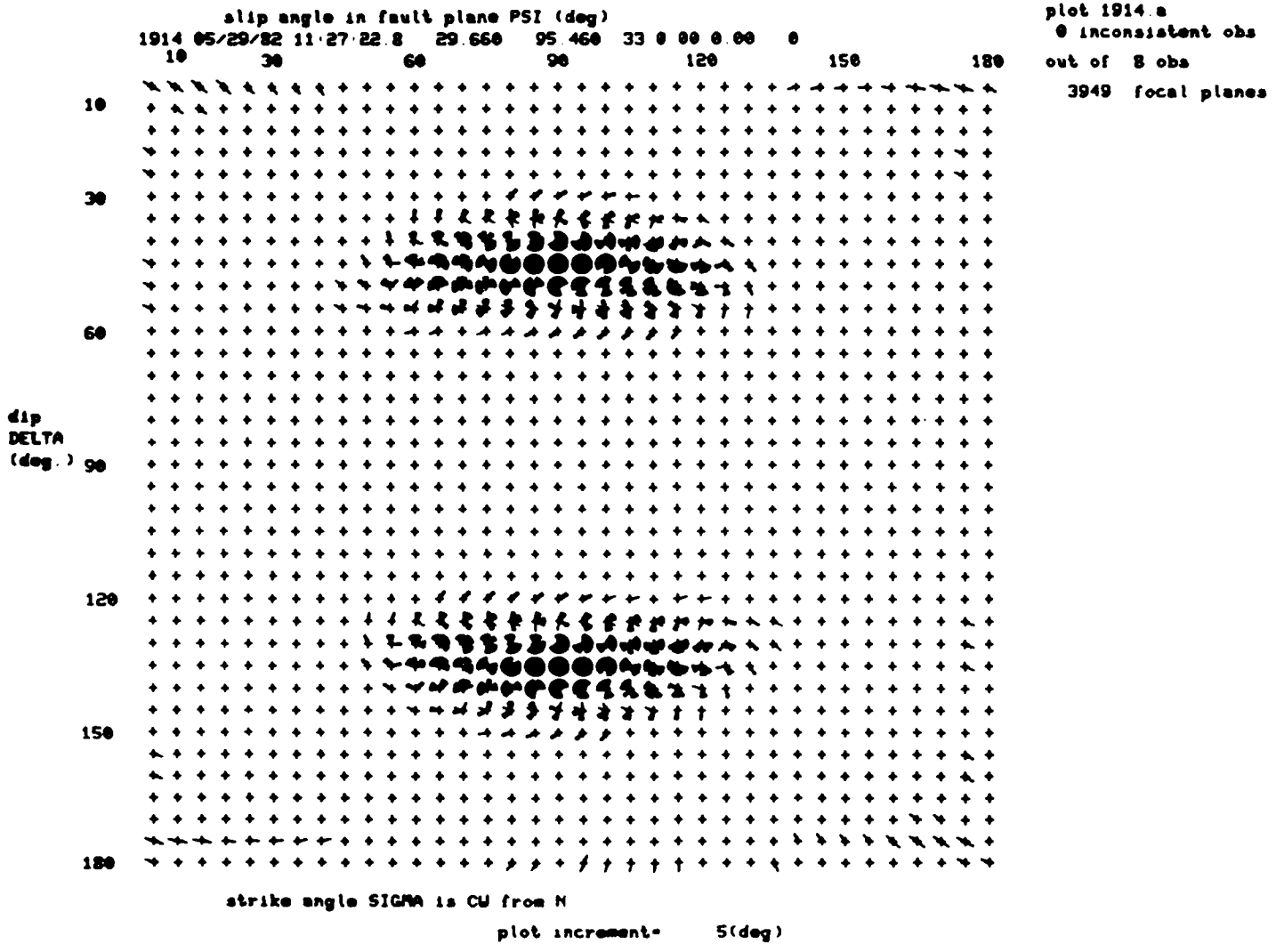

Figure 6e Acceptable focal planes for 1914 from the Pearce algorithm.

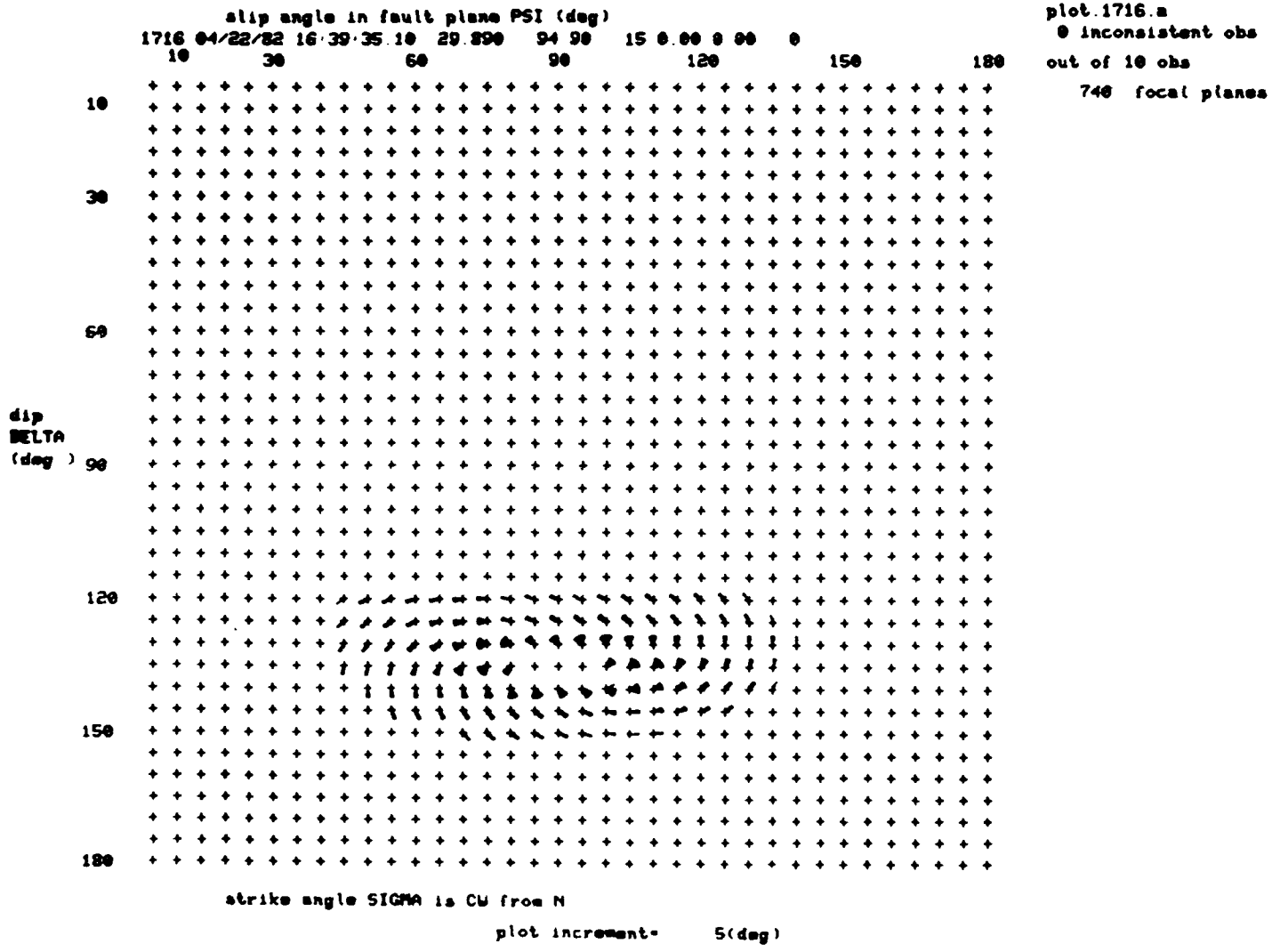

Figure 6f Acceptable focal planes for 1716 from the Pearce algorithm.

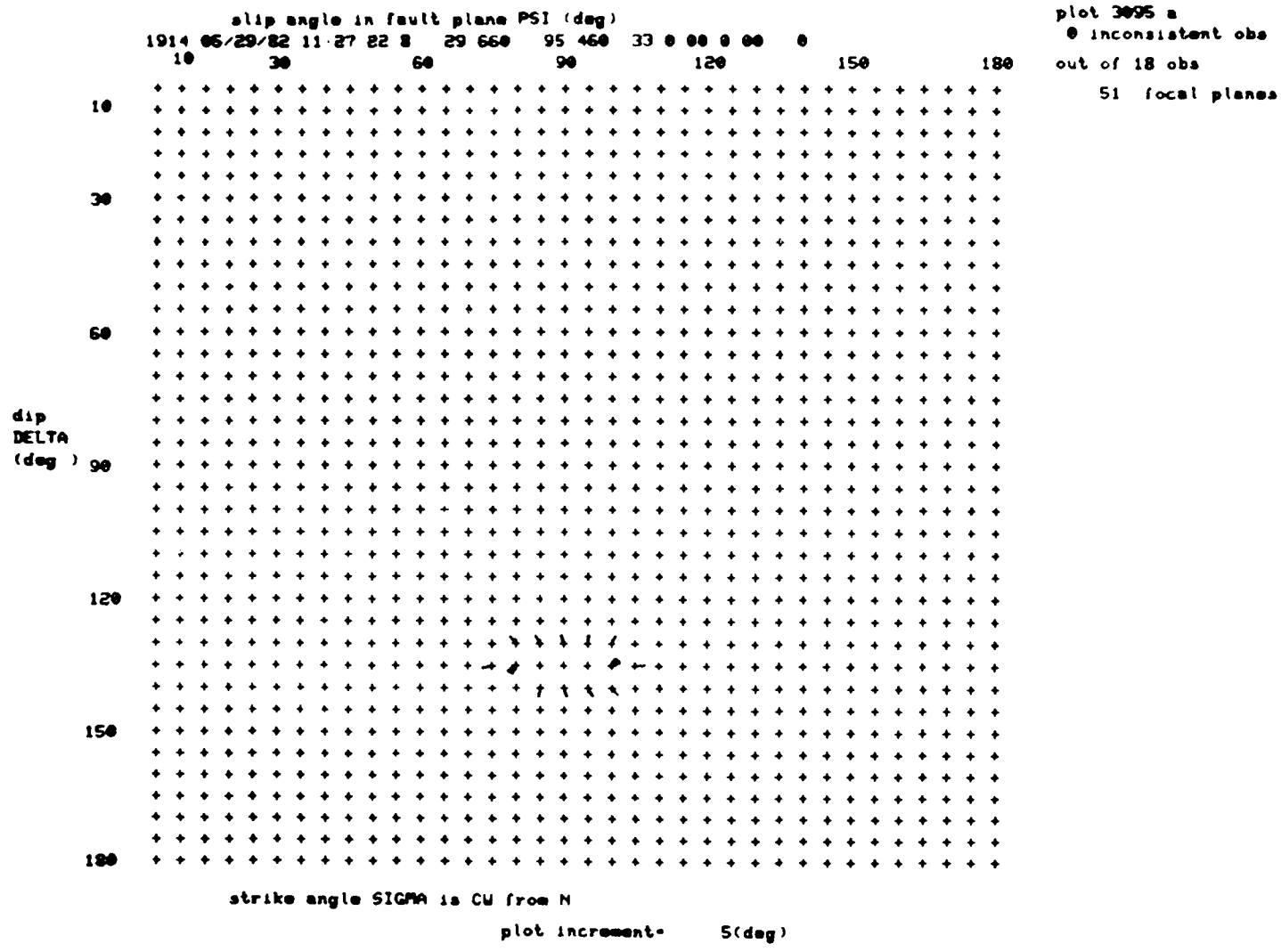

Figure 6g Acceptable focal planes for both 1716 and 1914 from the Pearce algorithm.

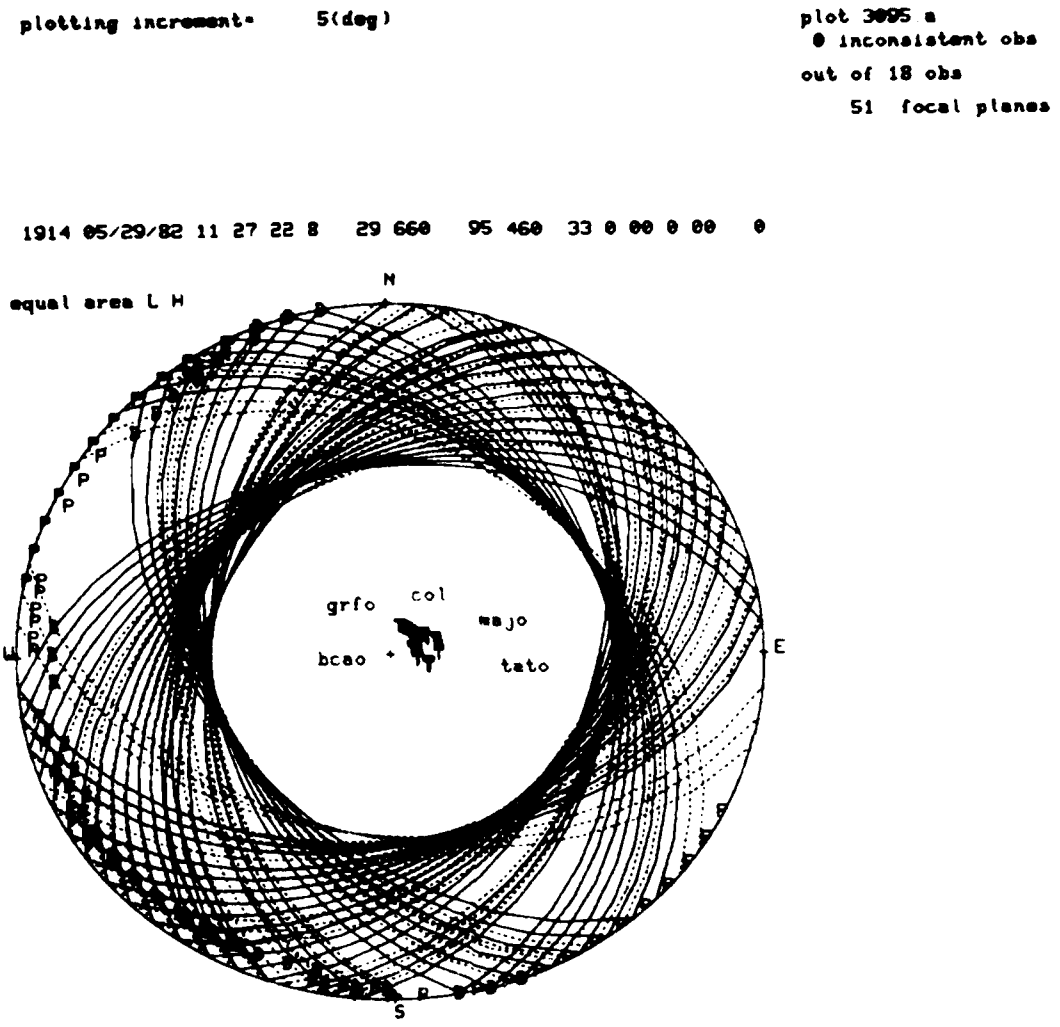

Figure 6h Acceptable focal planes for both 1716 and 1914 from the Pearce algorithm.

maps and LANDSAT images, and hypothesised that these anomalous events could be small 45° thrust events on a northwest-southeast striking fault system with shallow dip. The available seismic data has been sparse and insufficient to determine fault planes for these events. Seismograms of the two events are shown in Figures 6A,B,C. Secondary phases in the P coda of the two events were assumed to be pP, sP arrivals for depths of 15 to 20 km. Results of the Pearce algorithm are presented in Figures 6D through 6I. The pP/P and sP/P amplitude ratio bounds were found to be consistent with thrust sources. The tension axis was well constrained to the near vertical, while the azimuth of the near horizontal compression axis is unconstrained by the data. These results are consistent with the hypothesis that 45° thrust events are responsible for the low M_s measurements of the 30N by 95E events. Additional modeling would be required to test if the compressional axis is in a horizontal northeast-southwest orientation as may be inferred from LANDSAT lineaments.

Events 20 and 22 (Tabel II) are in the Lake Baikal region. Event 20 has emergent P waves and is possibly a double event (Figures 7A,B). The arrivals 10 seconds following the P wave are interpreted as pP phases. The best fit to the data is a horizontally oriented NE-SW tension axis with nearly vertical compressive axis (Figure 7C). The event is 200 km west of lake Baikal and apparently not aligned with the rift zone stress system. It was not possible to find double-couple solutions that fit the initial two P phases as P+pP. In this case the focal mechanism algorithm was used to decide between two alternative interpretations of the waveforms. The event appears to be a double earthquake with similar focal mechanisms. The sP phase is not prominent on the traces and required large amplitude constraints. The simple reflection coefficient model used was inadequate to model these sP amplitudes observed.

Event 22 (Tabel II) is located within the Baikal rift zone and decidedly shal-

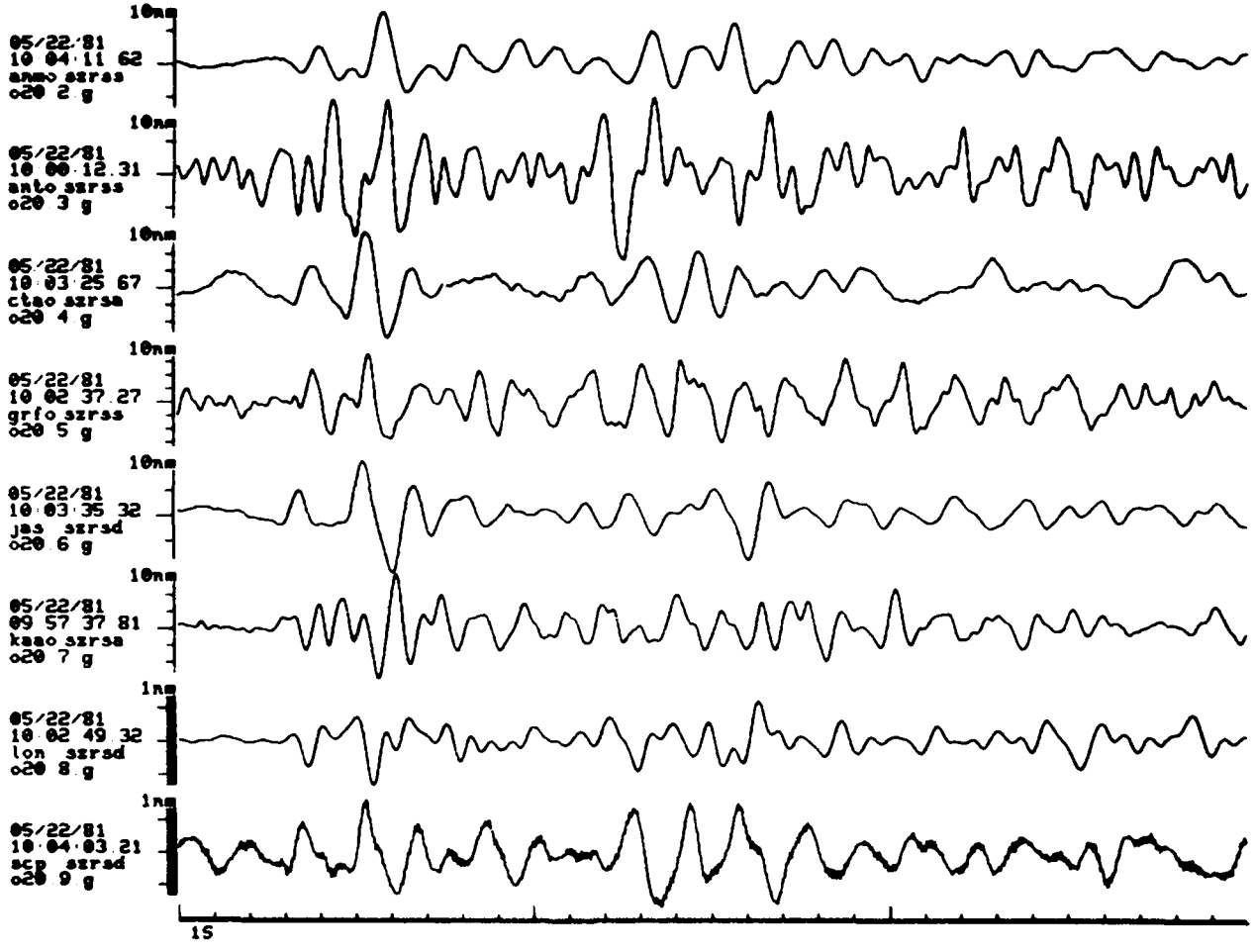

Figure 7a Unfiltered seismograms of event 20.

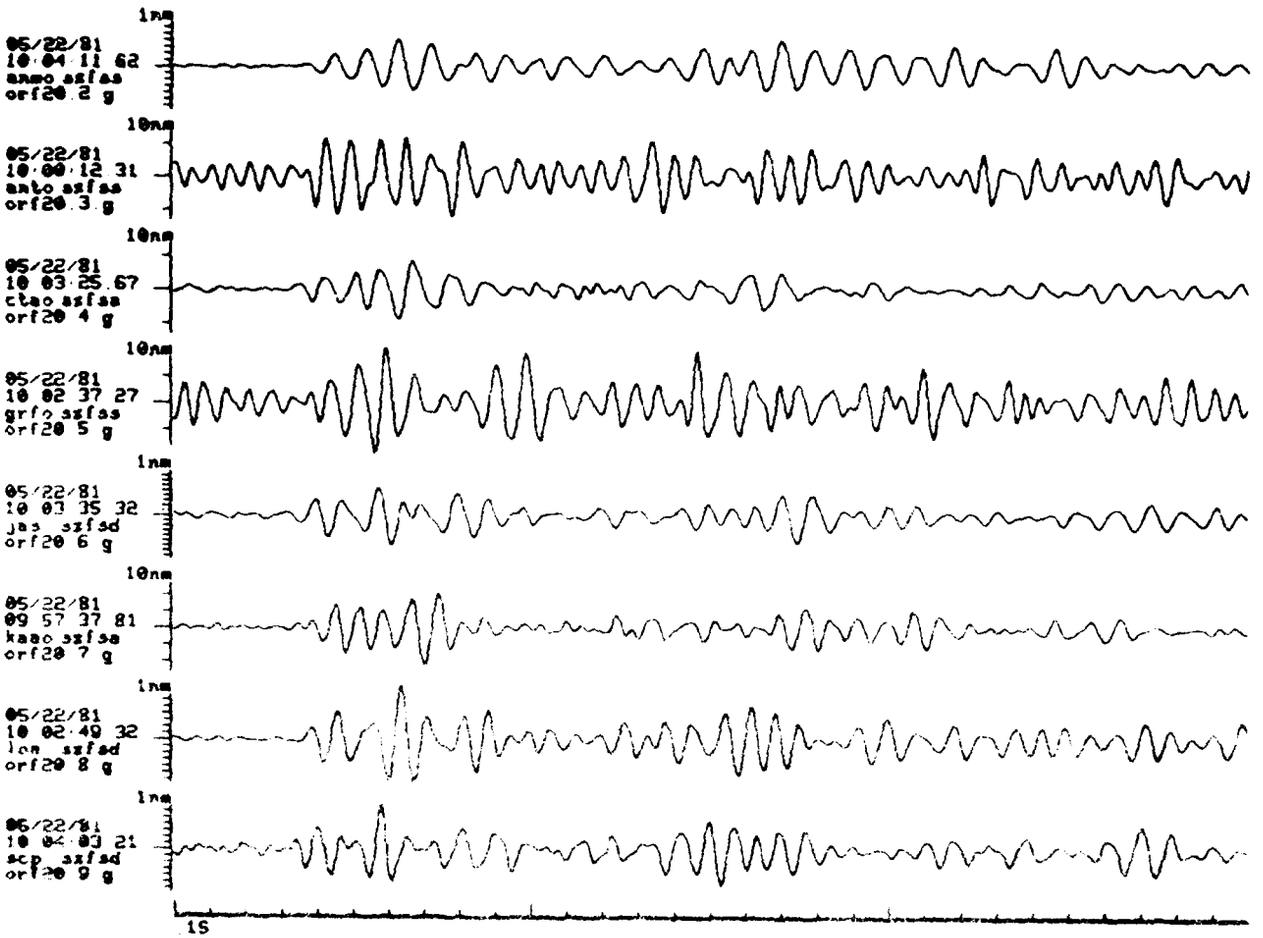
1nm
05/22/81
10 04 11 62
anmo azfas
orf20 2 g
10nm
05/22/81
10 00 12 31
anto azfas
orf20 3 g
10nm
05/22/81
10 03 25 67
ctao azfas
orf20 4 g
10nm
05/22/81
10 02 37 27
grfo azfas
orf20 5 g
1nm
05/22/81
10 03 35 32
jas azfsd
orf20 6 g
10nm
05/22/81
09 57 37 81
kaao azfsa
orf20 7 g
1nm
05/22/81
10 02 49 32
lon azfsd
orf20 8 g
1nm
06/22/81
10 04 03 21
scp azfsd
orf20 9 g
1S

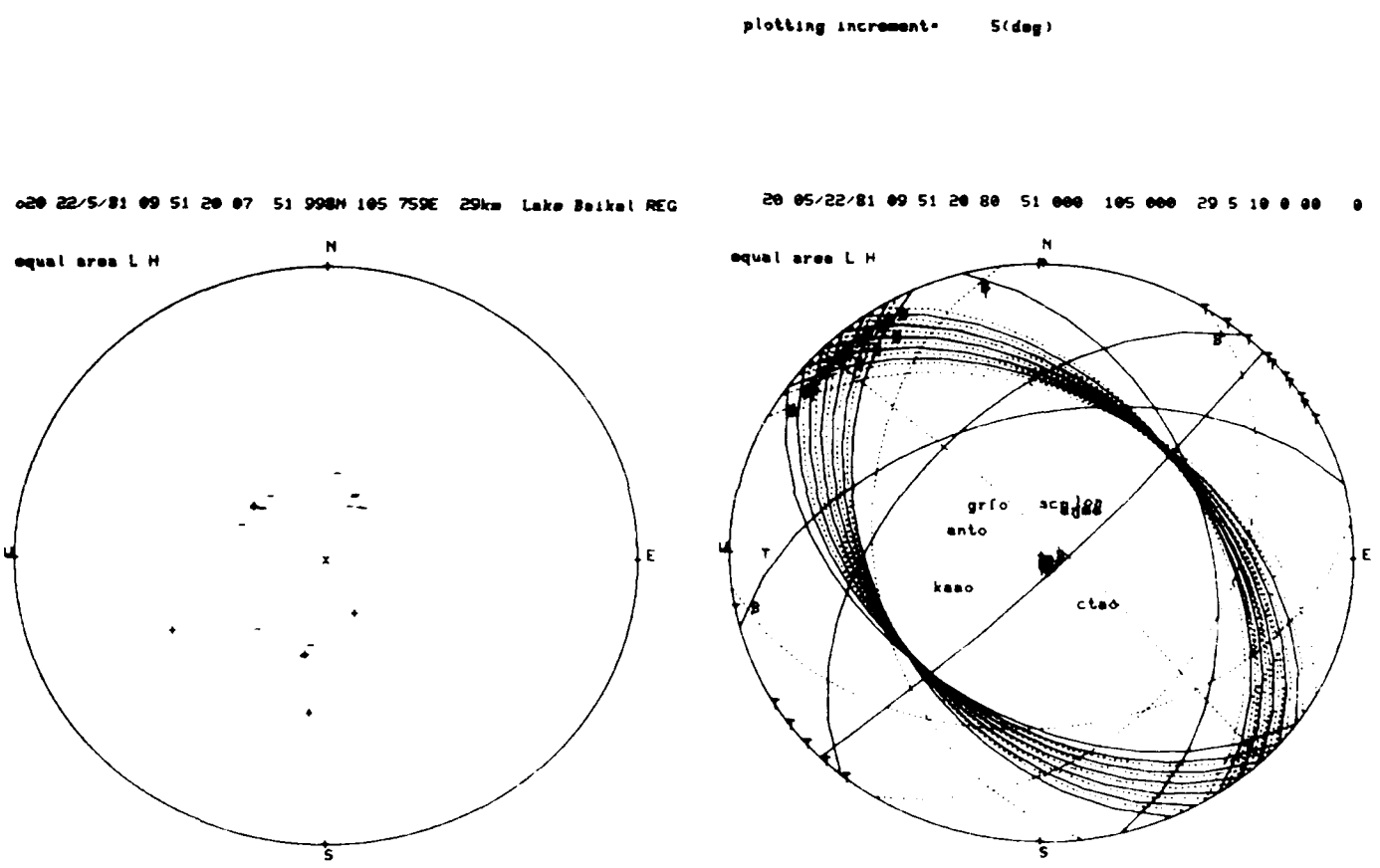

Figure 7c. USGS reported polarities, and acceptable solutions from the Pearce algorithm.

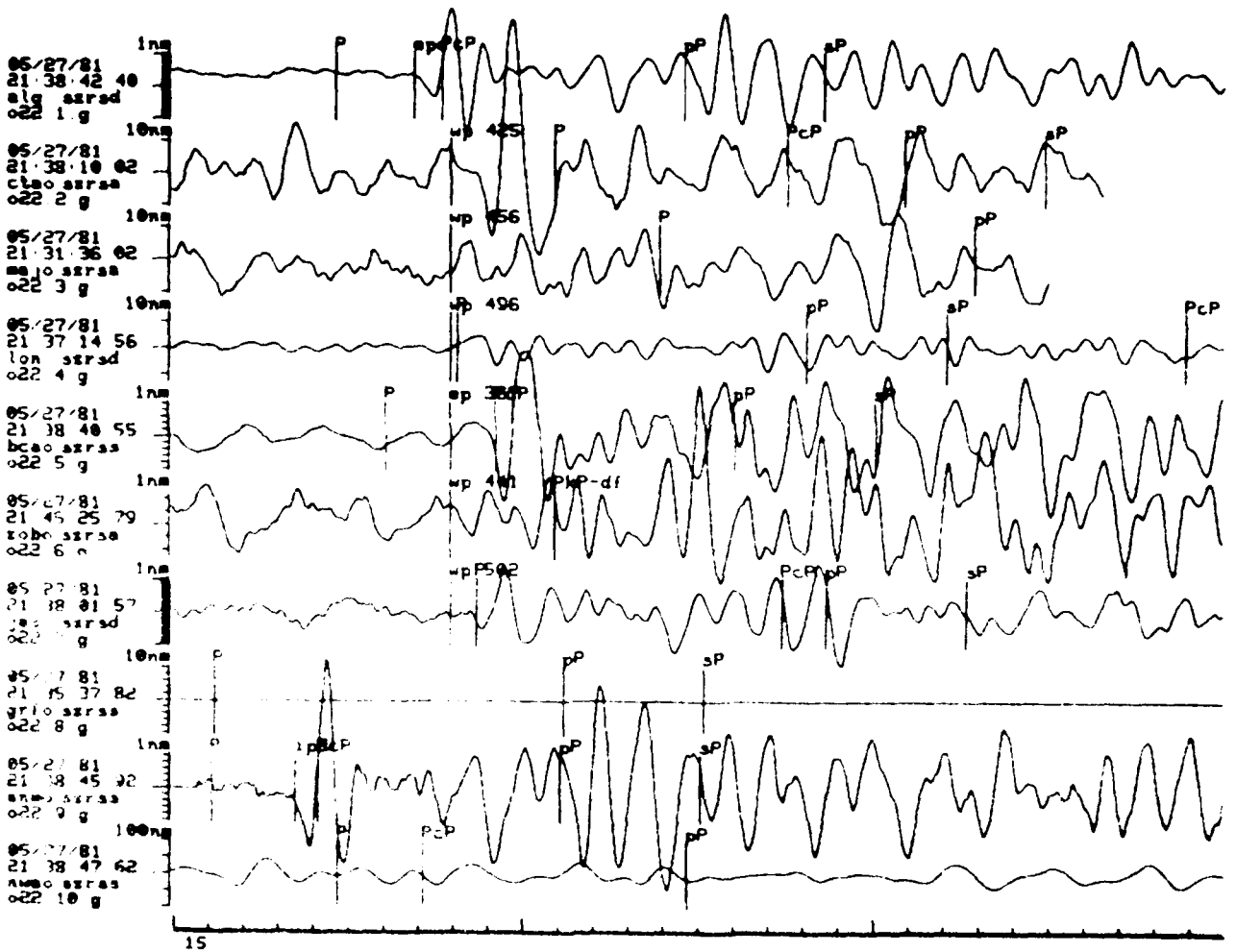

Figure [illegible] of seismograms for event 8 on the Siberian Coast.

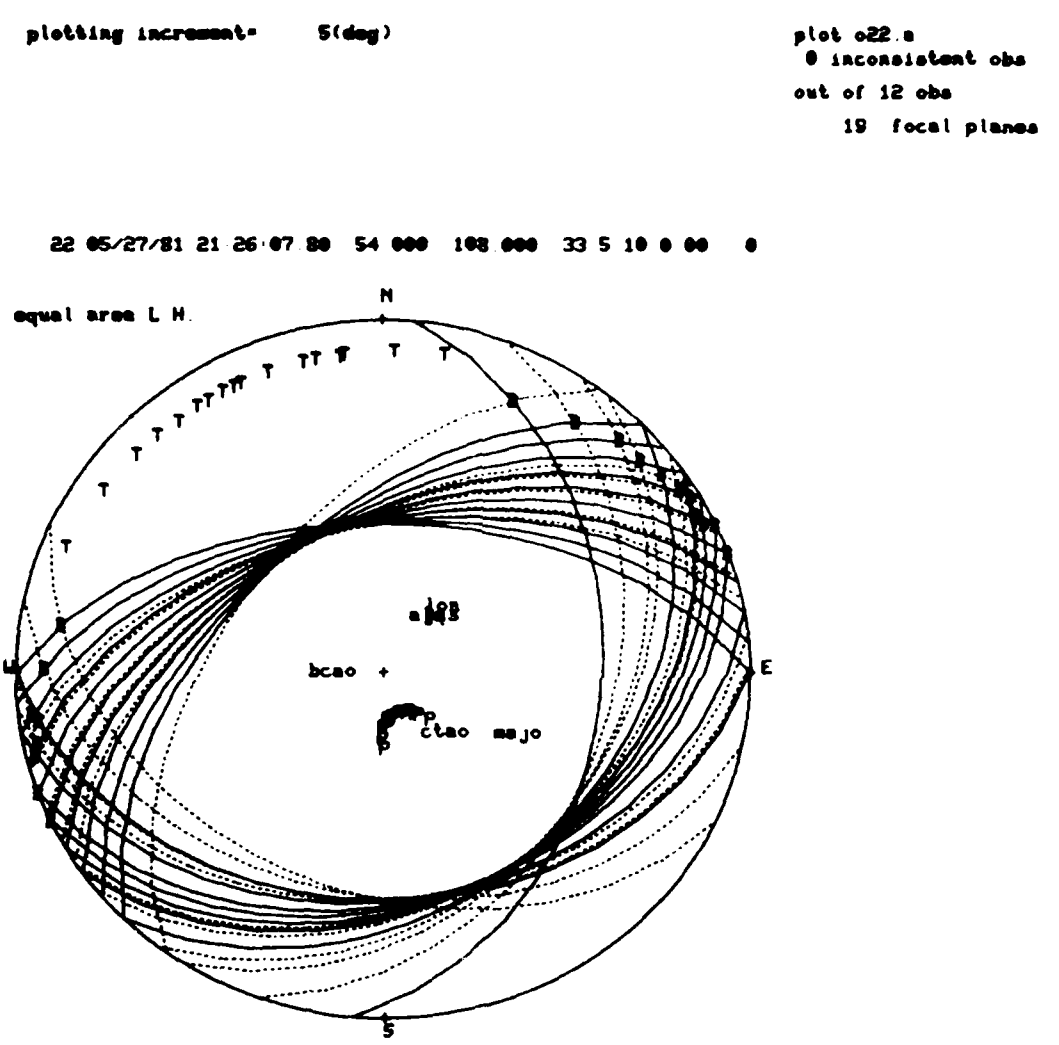

Figure 8b Acceptable double-couples for a set of tight bounds on sP, on the left. 4 observations have been ignored to generate this solution set. ISC reported polarities are plotted on the right.

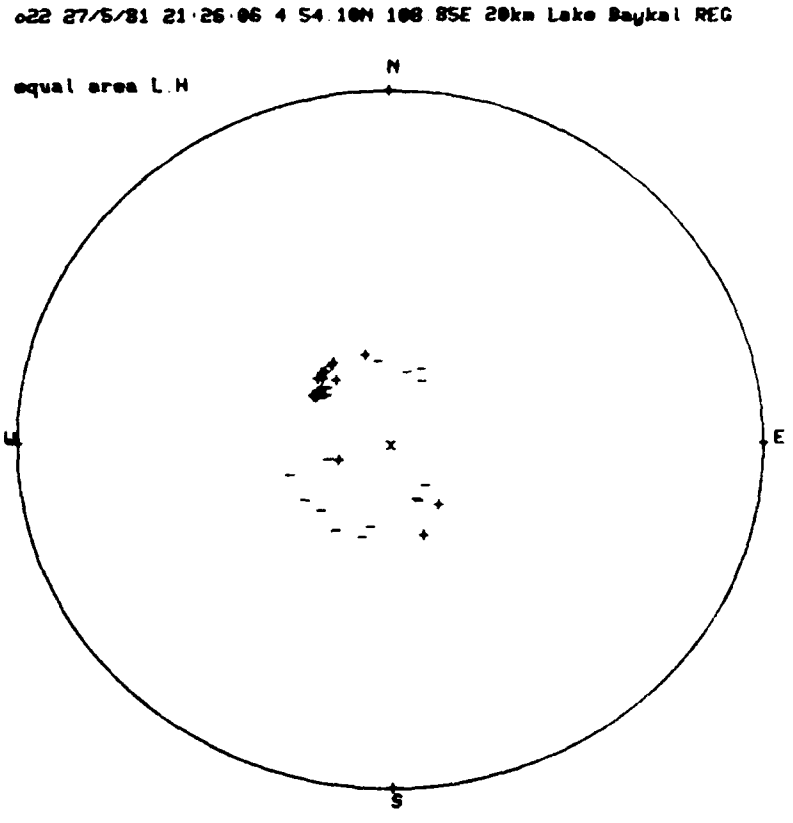

Figure 8c Polarity data for event 22. Note the cluster of compressions in the NW quadrant apparently inconsistent with the solutions in 8b.

lower than event 20 (Figure 8A). A solution set of double-couples with horizontal NW-SE tension axis and near vertical compression axis was found consistent with pP/P and sP/P bounds (Figure 8B). Polarity data from the NW azimuths (Figure 8C) suggests that adjustments may be necessary if waveform data is added in the NW quadrant. Although the focal mechanisms derived from pP/P and sP/P constraints agree with the expected tectonic stress system, it may not satisfy additional data from a missing quadrant.

Event 8 (Table II) occurred on the arctic coast of central Siberia in an area of low but detectable seismicity (Lang and Sun; 1966). Seismograms and acceptable focal mechanisms based on pP and sP bounds are shown in Figures 9A and 9B. Focal mechanisms for event 8 based on tight pP and sP bounds are consistent with nearly all the polarity data of Figure 9C. Four sP/P amplitude bounds must be violated to arrive at the solutions of Figure 9B. Scattered compressional first motions suggest that the east-west striking focal planes of Figure 9D, might be rotated to a more nearly ENE-WSW strike. If the sP bounds are relaxed, more solutions become acceptable, and it is not necessary to discard data. The enlarged solution space is the trade-off for the relaxed sP bounds. These experiments, show that the Pearce algorithm may be used in an interactive manner, to explore the robustness of the results. In this case, it is clear that the compressive axis is steeply dipping to the northwest, while the tension axis is not as well constrained. If the ISC polarity data were added to the polarities and amplitudes of the seismograms of Figure 5A, the preferred tension axis would be horizontal NE-SW. Although the location of this event is far to the southeast of the active extension of the Lomonosov ridge, the stress orientation appears to be consistent with NE-SW extensional tectonics. Also, the results indicate that the sP amplitudes predicted by the simple crustal model are too large by about a factor of 2 for this source depth and locality.

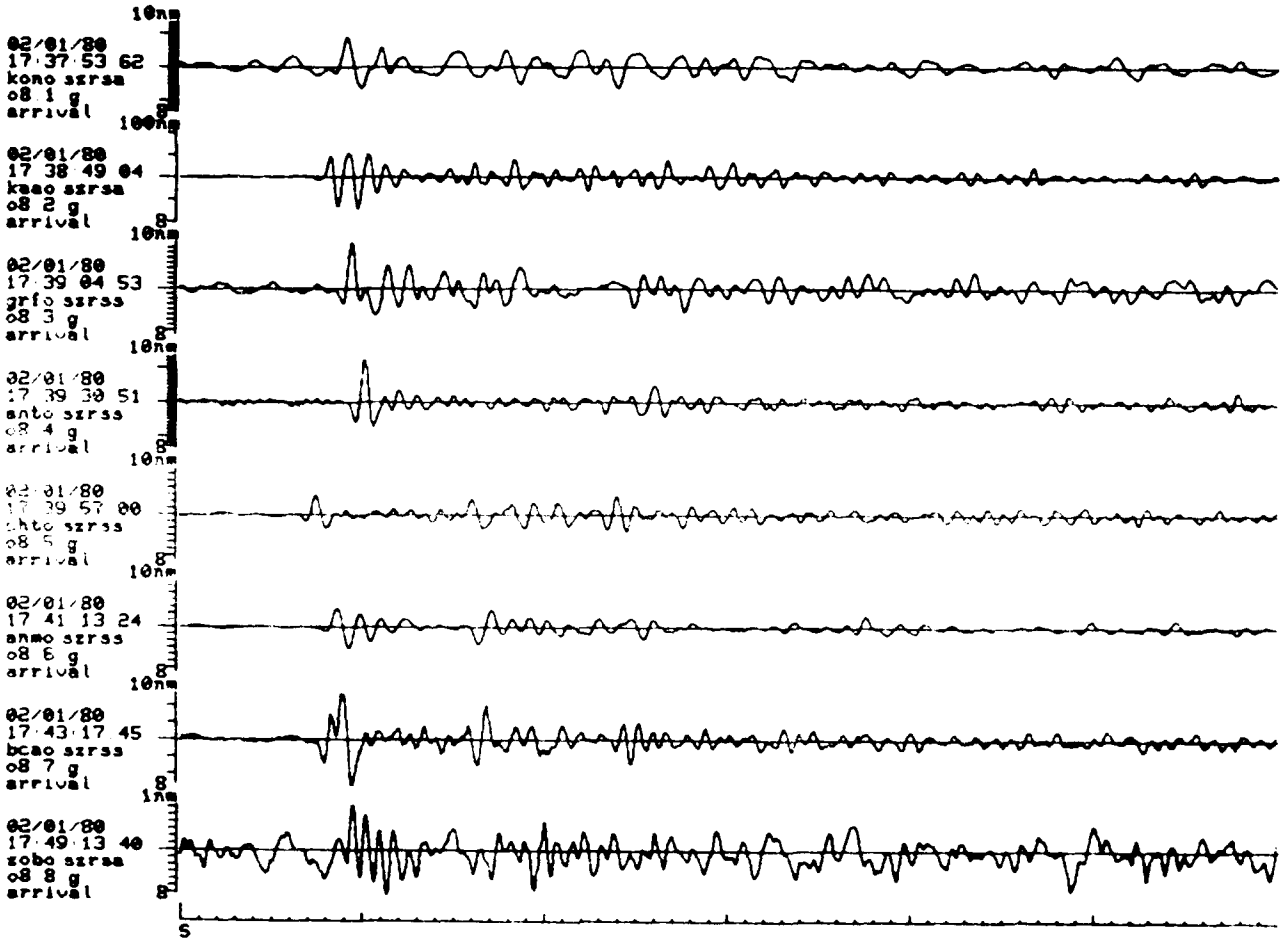

Figure 9a. Seismograms for event 8 on the Siberian Coast.

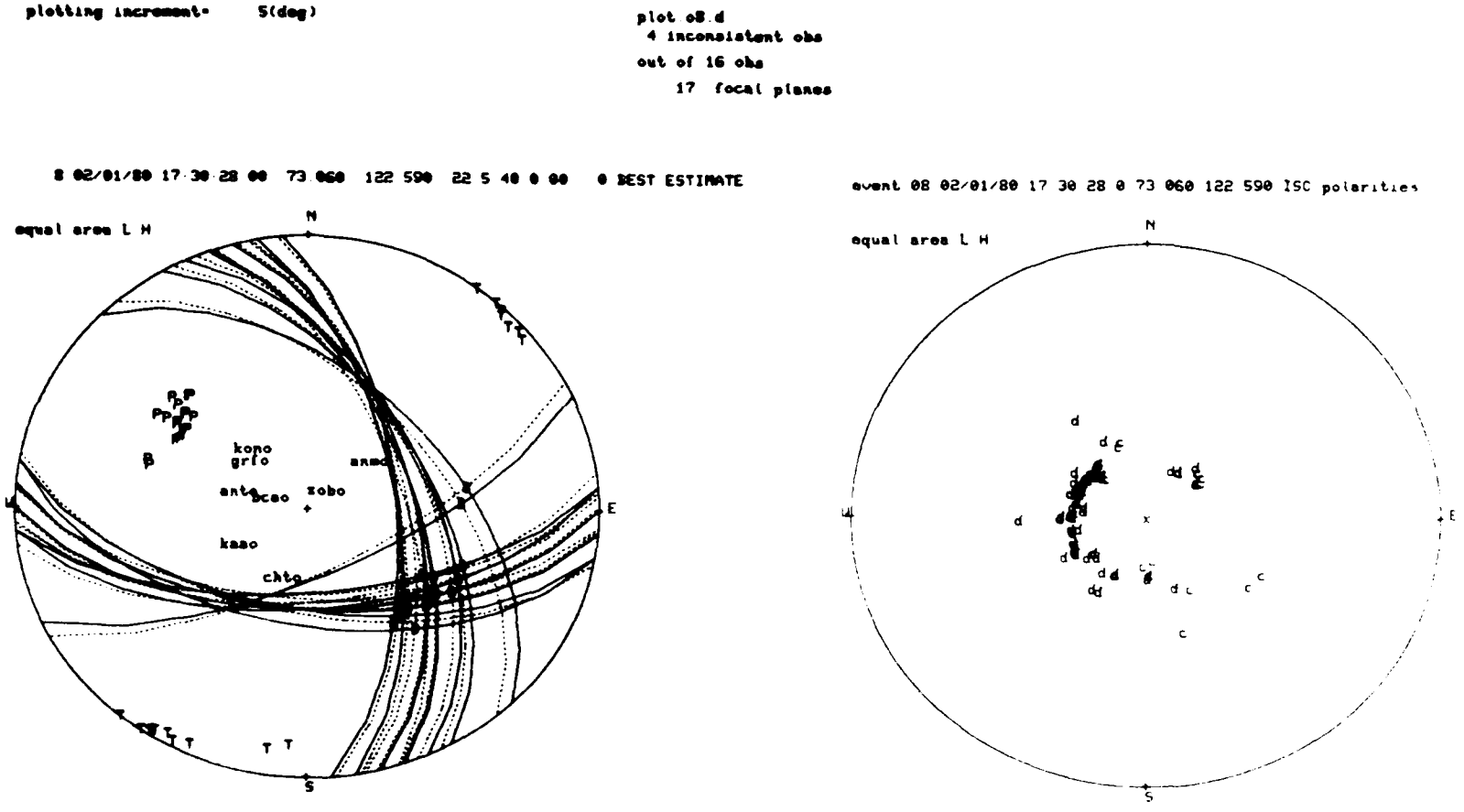

Figure 9b Acceptable double-couples for a set of tight bounds on s^P, on the left. 4 observations have been ignored to generate this solution set. ISC reported polarities are plotted on the right.

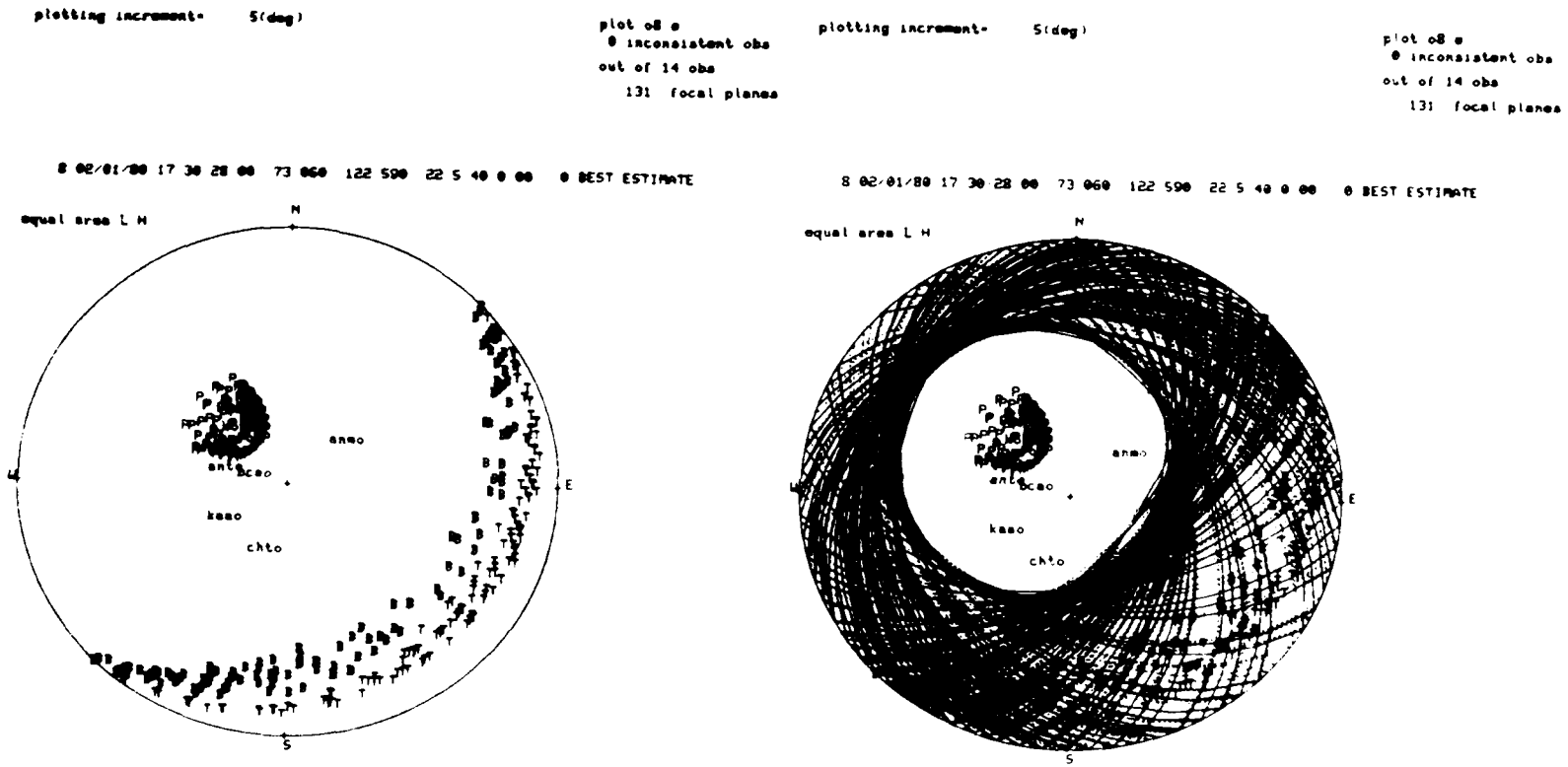

Figure 9c Double-couple solution set for a set of relaxed sP amplitude bounds. On the left, P,T, and B axis without the clutter of focal planes. On the right, the clutter of focal planes.

Event 295 (Table II) occurred near the Kunar fault in eastern Afghanistan (seismograms in Figure 10A). Prevot et al (1980) have studied the tectonics of this area and found focal mechanisms indicative of a NW-SE compressive stress system. A NEIS moment tensor solution derived from long period waves is also available for this event. Figure 10B shows the NEIS double-couple solution together with the available short period and long period first motions reported to NEIS. The NEIS double-couple solution is largely in agreement with the first motions. Crude synthetics for the NEIS double-couple solution predict large pP and sP amplitudes at Nwao, Bcao, Grfo, Kono, and Tol (Figure 10C). Unless depth phases are greatly attenuated in this source region, the NEIS double-couple solution is inconsistent with the P coda levels observed at Nwao, Bcao, Grfo, Kono, and Tol. Figures 10D and 10E are the acceptable solutions derived from the pP/P constraints on the traces shown in Figure 10A. One subset of the Pearce solution space has a nearly vertical tension axis and SE-NW compression axis, similar to the NEIS double-couple solution. The orientations of the compression axes are significantly different enough that the Pearce solutions do not predict large pP phases. The Pearce solutions still predict sizable sP phases using the simplistic crustal structure. The discrepancy is at least a factor of 2. Allowance for acceptable variations of the S-to-P velocity ratio at the source may account for some of amplitude discrepancy. However, an S wave velocity gradient between source and surface will reduce the SV component at the surface reflection point dramatically, and hence reduce the sP amplitude.

Event 516 (Table II) is located in the Tadzhik region and has an an independently determined double-couple focal mechanism from NEIS. The GDSN short period seismograms are shown in Figure 11A. The NEIS reported polarities and double-couple solution are plotted in Figure 11B. The NEIS double-couple solution is in disagreement with most of the reported polarities at southerly

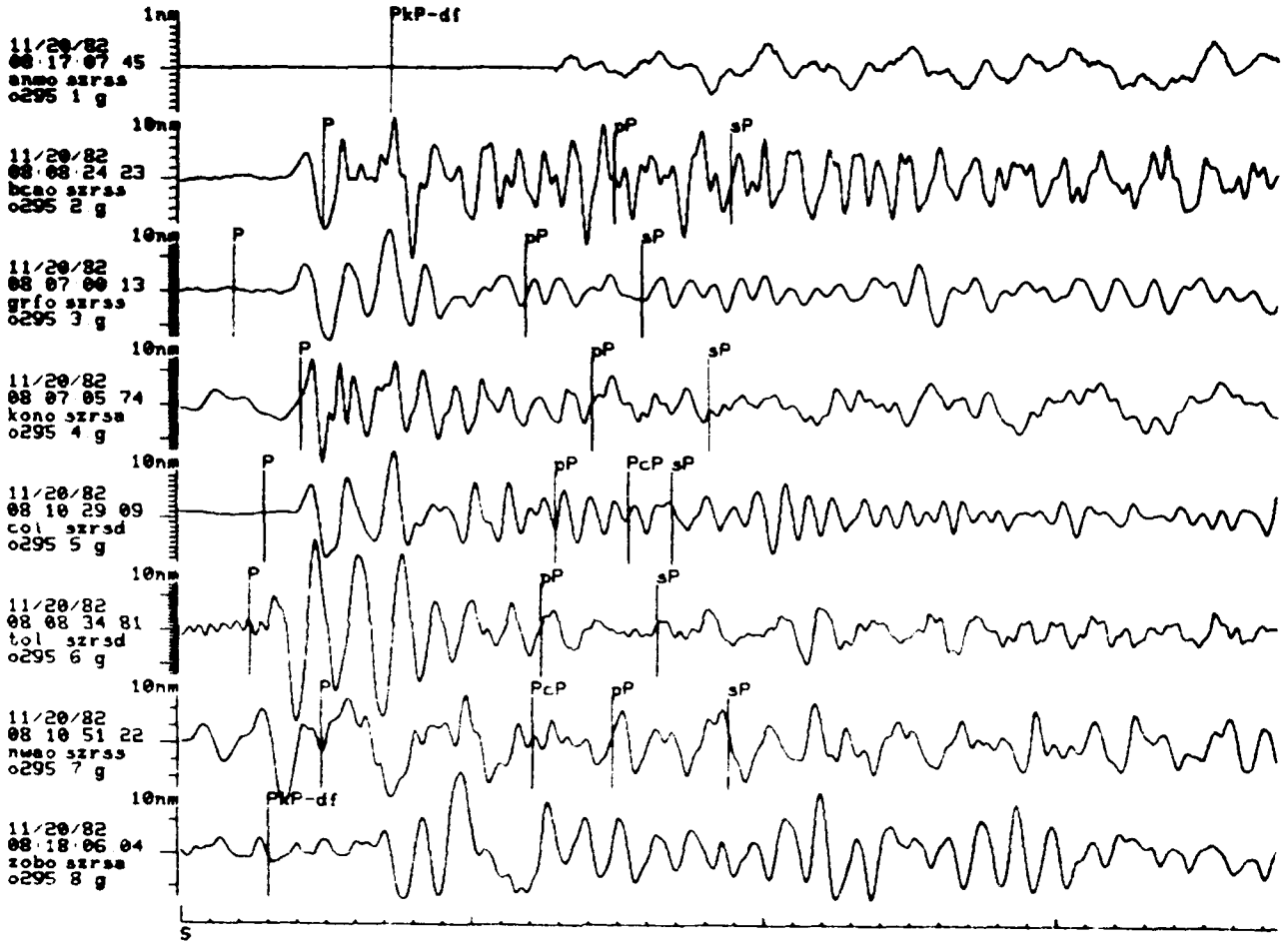

Figure 10a Seismograms for event 295. Predicted arrival times are shown for the P, PcP, pP, and sP times for the YFIS hypocentral location.

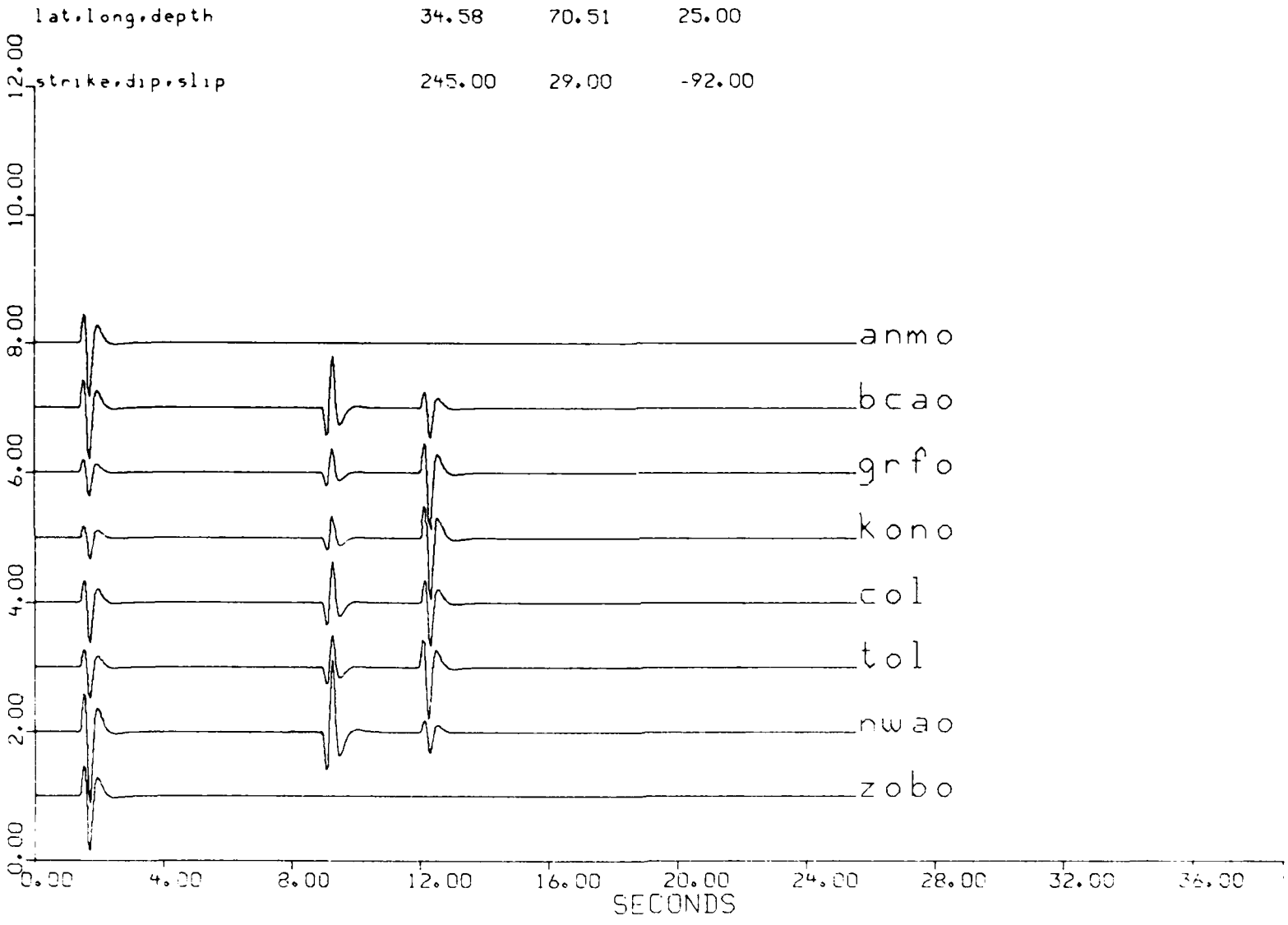

Figure 10b Synthetics using the simple crustal model. The algorithm does not properly show depth phases for the PkP arrivals at Anmo and Zobo. Amplitudes are normalized to maximum possible P amplitude from a double-couple source at that distance. Strike, slip and dip from NEIS. Note the large pP and sP arrivals with respect to the P wave amplitude.

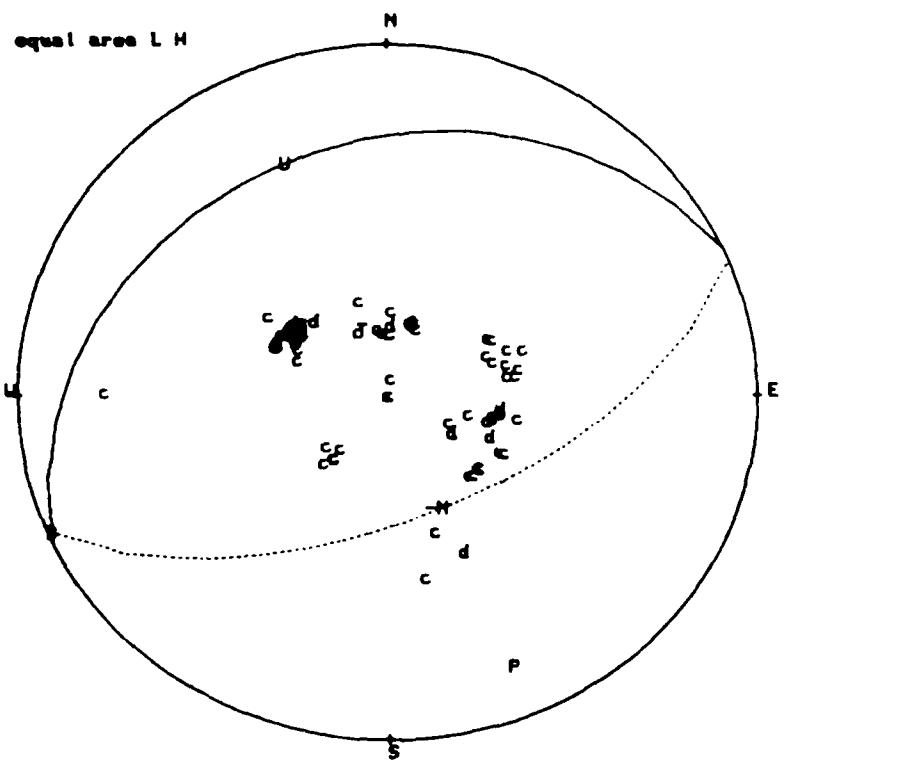

Figure 10c NEIS double-couple solution with reported NEIS polarities.

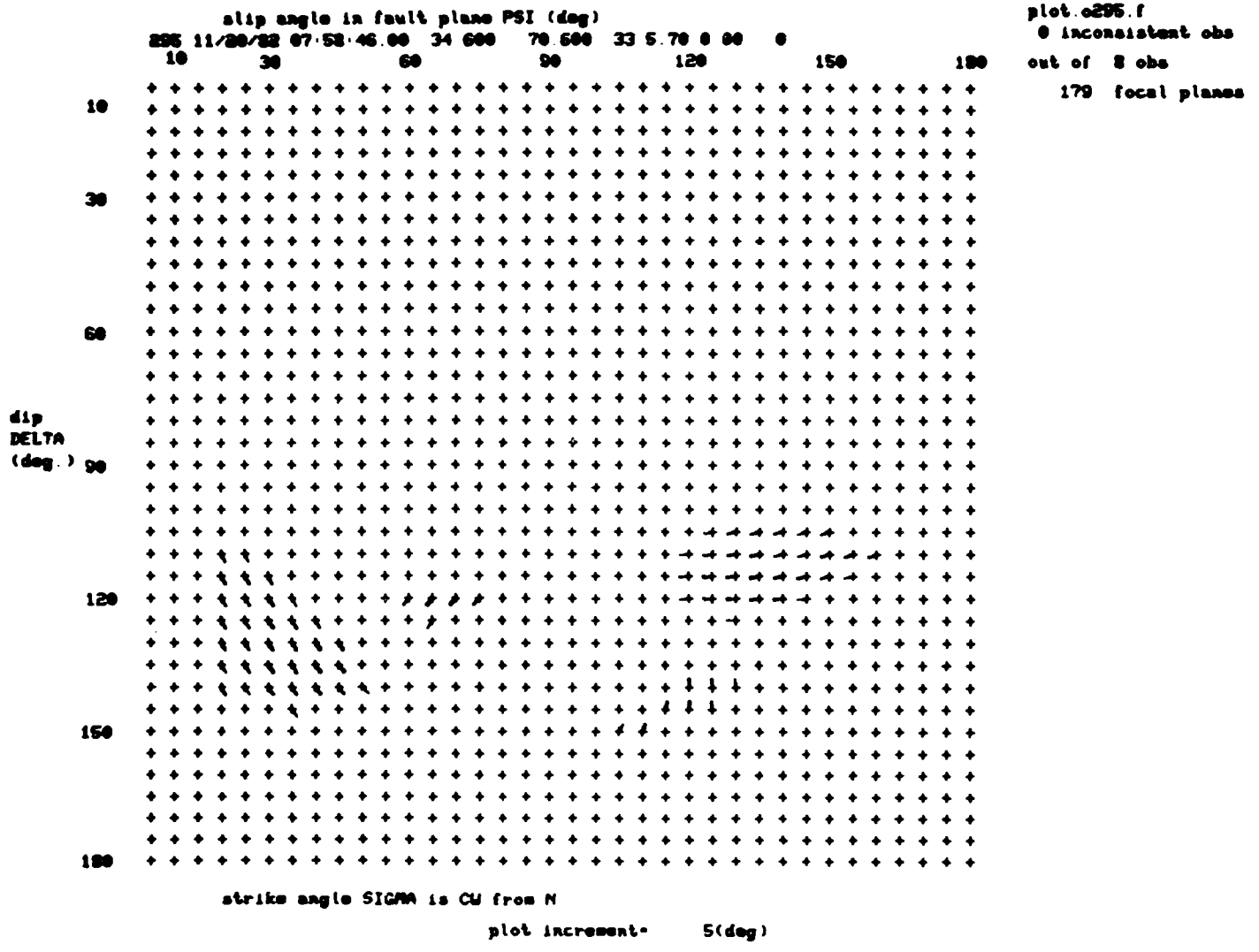

Figure 10d Acceptable solutions from the Pearce algorithm based on pP/P amplitude ratio bounds only. Two subsets of the solution space are apparent.

plotting increment= 9rdeg

plot o295.f
0 inconsistent obs
out of 8 obs
179 focal planes

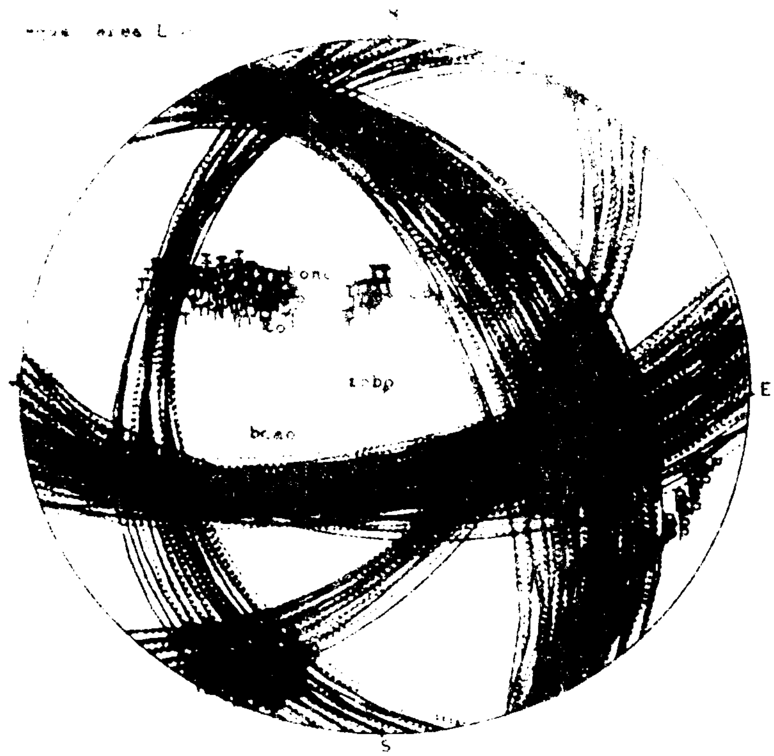

… algorithm based on …

… plots of the solution

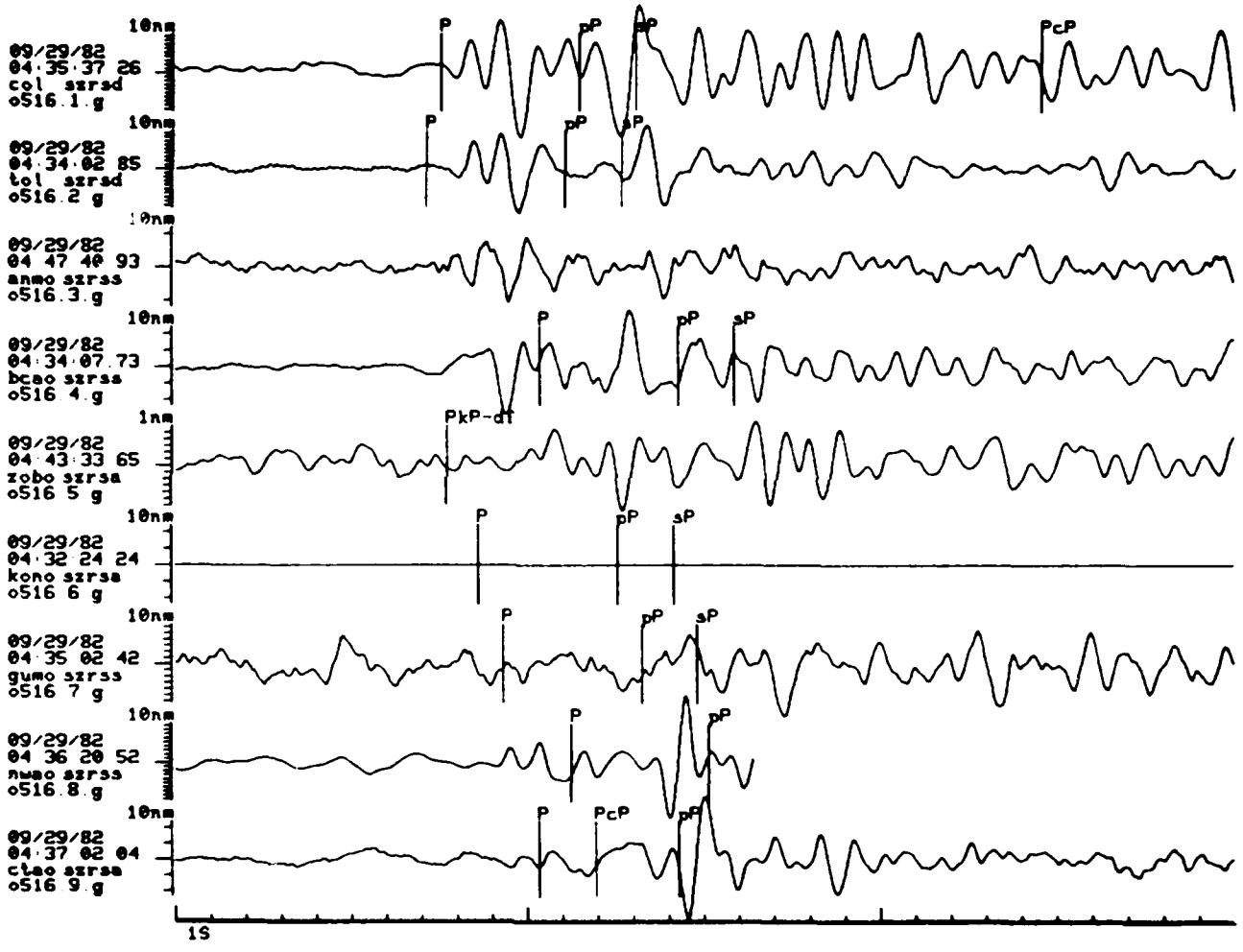

Figure 11a Seismograms for earthquake 516.

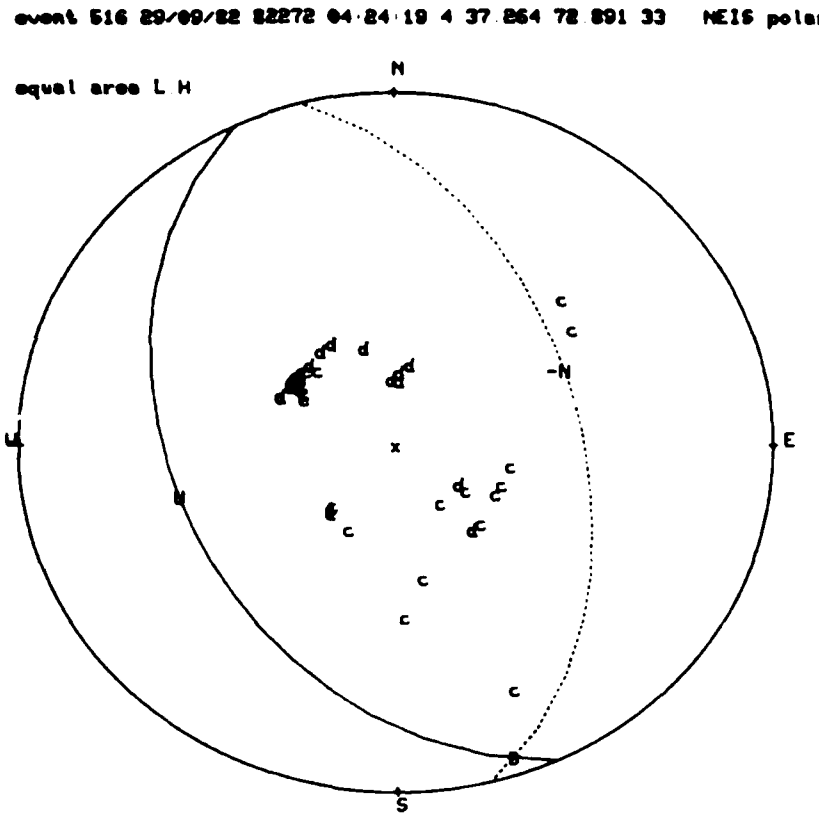

Figure 11b NEIS polarities for earthquake 516, with the NEIS double-couple. Note the large number of inconsistent polarities.

plotting increment= 5(deg)

plot.e516.d
0 inconsistent obs
out of 15 obs
3 focal planes

516 09/29/82 04:24:13.40 37.264 72.891 13 5.40 4.90 0

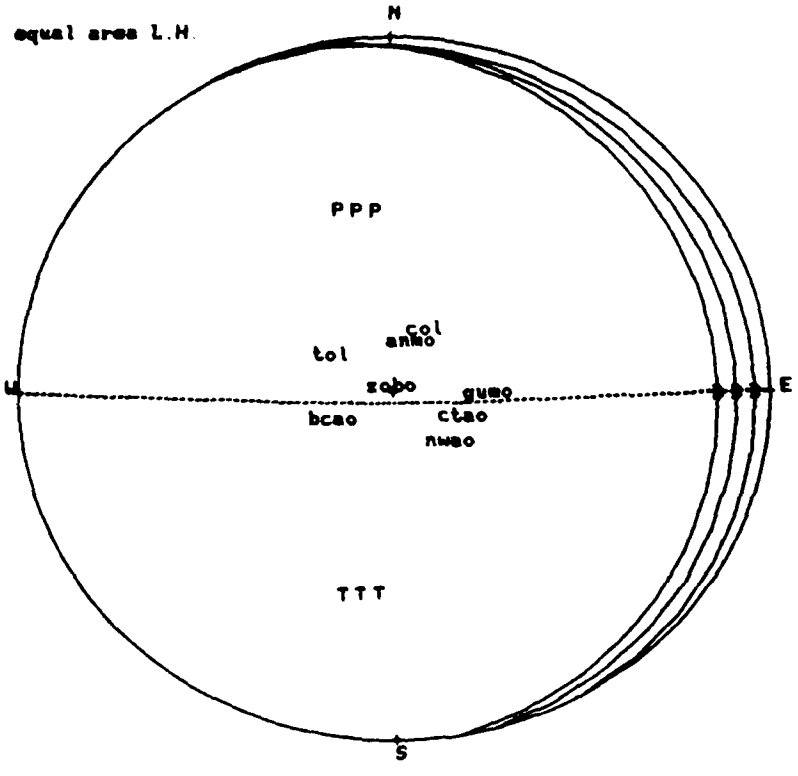

Figure 11c Acceptable solutions from the Pearce algotithm analysis of the data in (A). Polarities were only used for Col, Tol, and Nwao. Bcao, Gumo, Ctao and Zobo appear to show nodal P waves in (A).

azimuths. The first motions are largely internally consistent and indicate that the discrepancy is not do to incorrectly chosen first motions. Using pP and sP bounds from the seismograms of Figure 11A, the acceptable focal mechanisms (Figure 11C) are few and indicate a near vertical focal plane that is in much better agreement with the polarity data (Figure 11B). Also, the seismograms of Figure 11A indicate that Zobo, Ctao, Gumo, and Bcao are near nodal. Again, the NEIS double-couple solutions derived from long period data disagree with the short period data.

TESTS USING SYNTHETIC DATA

In order to better understand the power of |pP/P| and |sP/P| amplitude bounds as constraints on the allowable range of focal mechanisms, several experiments were conducted with synthetic data. These experiments were intended to explore the requirements of a network of stations to eliminate all possible focal mechanisms in the case of an explosion. In practice, maximum allowable pP, and sP amplitudes would be read directly form the coda of the explosion P wave and would be limited by the coda generation mechanisms and the ambient noise level.

Figures 12A,B and C show the fraction of allowable double-couple solutions as functions of relative depth phase amplitude and take-off angle, for various network configurations. Figure 12A shows the fraction of allowable focal mechanisms versus takeoff angle for a single station with the constraints that |pP| < |P|, |sP| < |P|, and both |pP|, and |sP| are < |P|. It is apparent that the take-off angle has little effect for the case of |pP/P| < 1, while |sP/P| < 1 is sensitive to take-off angle. However, since the pP constraint is more powerful than the sP constraint, the consideration of both gives little reduction in the possible solution space over the pP constraint alone. The observation that depth phase amplitudes are less than the initial phase amplitude at a single station eliminates roughly 50% of the allowable mechanisms. The polarities of the P or pP have not been considered.

The addition of stations at 90 degree azimuthal intervals is addressed in Figure 12B. The bounds on |pP/P| and |sP/P| were allowed to vary, and the fraction of allowable solutions was plotted for the cases of one, two, three, and four stations at 90 degree azimuthal spacing. The take-off angle was held constant at 20 degrees. The polarities of the P waves were not considered. We see that if only two stations are observed, then the coda must exhibit levels less than 0.4 of

the P wave to eliminate all possible double-couples If three or four stations are available, then coda levels of 0.95 or less are sufficient to eliminate all possible double-couples.

The results of a similar numerical experiment are summarized in Figure 12C, for a network of stations at 60 degree azimuthal intervals and 20 degree take-off angles. The results are somewhat similar to the previous experiment, in that four or more stations with coda levels slightly less than the P wave are sufficient to eliminate all possible double-couple solutions. The differences between the two results indicate that the network's azimuthal coverage may be important to the inherent capability of the network to discriminate between earthquakes and explosions. To simulate something closer to the azimuthal coverage that may be available in practice, additional simulations were conducted with a random distribution of azimuths and teleseismic take-off angles. Furthermore, since the coda levels experienced in practice are not the same at all stations, a random model of the |pP/P| levels was used.

A Monte Carlo simulation of a random network with random pP/P amplitude ratios was performed. Five or more realizations of 20 stations was generated for each set of statistics. The station azimuths were evenly distributed in 360 degrees of azimuth and take-off angles were evenly distributed between 10 and 35 degrees. The |pP/P| amplitude ratio bounds were given by a normal distribution with means of 1.0, 0.75 and 0.5, and standard deviations of 0.25 and 0.5. The number of stations required to eliminate all double-couples was counted for each realization. A survey of the simulations indicates that explosions will be inconsistent with double-couples when three out of four azimuthal quadrants are represented with coda amplitude levels below the P amplitude level. Since 270 degree azimuthal coverage will require four or more stations, the simulations came down to the probability that four stations would be "drawn out of the hat"

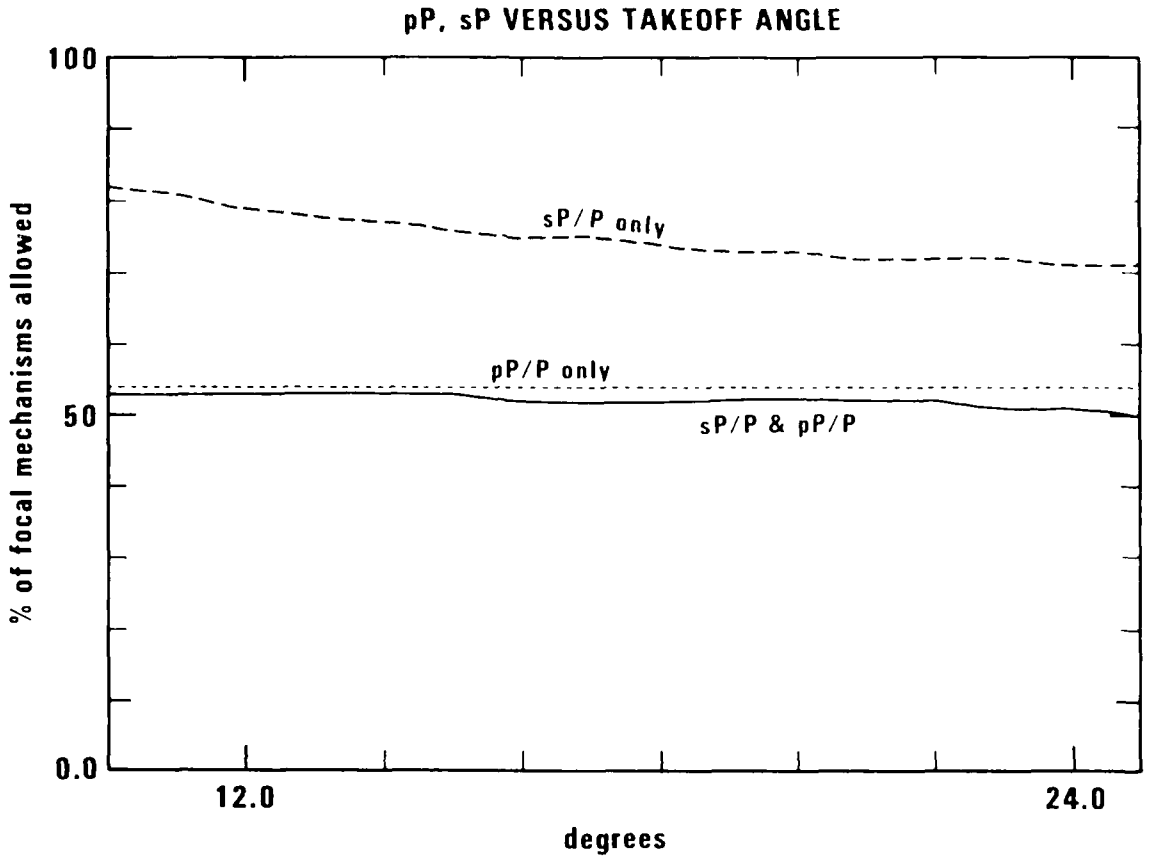

Figure 12a The percentage of all possible double-couples eliminated by the constraint of $|pP/P| < 1$, and $|sP/P| < 1$ at a single station. Constraints are considered together and separately. The teleseismic takeoff angle is varied from 10 to 25 degrees. The observation that $|pP/P| < 1$ eliminates nearly 50% of all double-couples at any teleseismic takeoff angle. The implications that sP P are less significant and slightly dependent on takeoff angle. The observation that both pP and sP are smaller than P implies that slightly fewer solutions are acceptable the observation the pP < P alone.

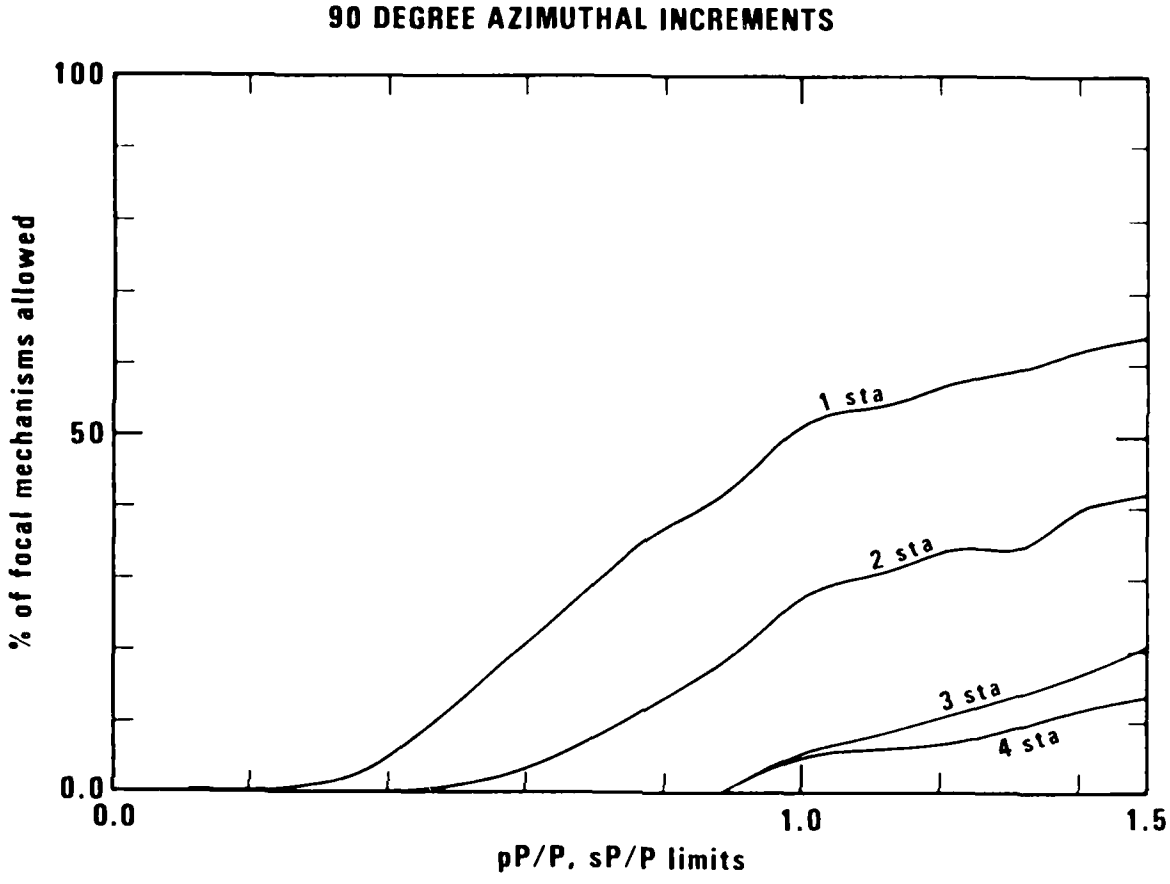

Figure 12b The percentage of all possible double-couples eliminated by one, two, three, or four stations at 90 degree azimuthal increments varies as a function of the absolute limit of the pP and sP amplitudes. All takeoff angles are assumed to be 20 degrees.

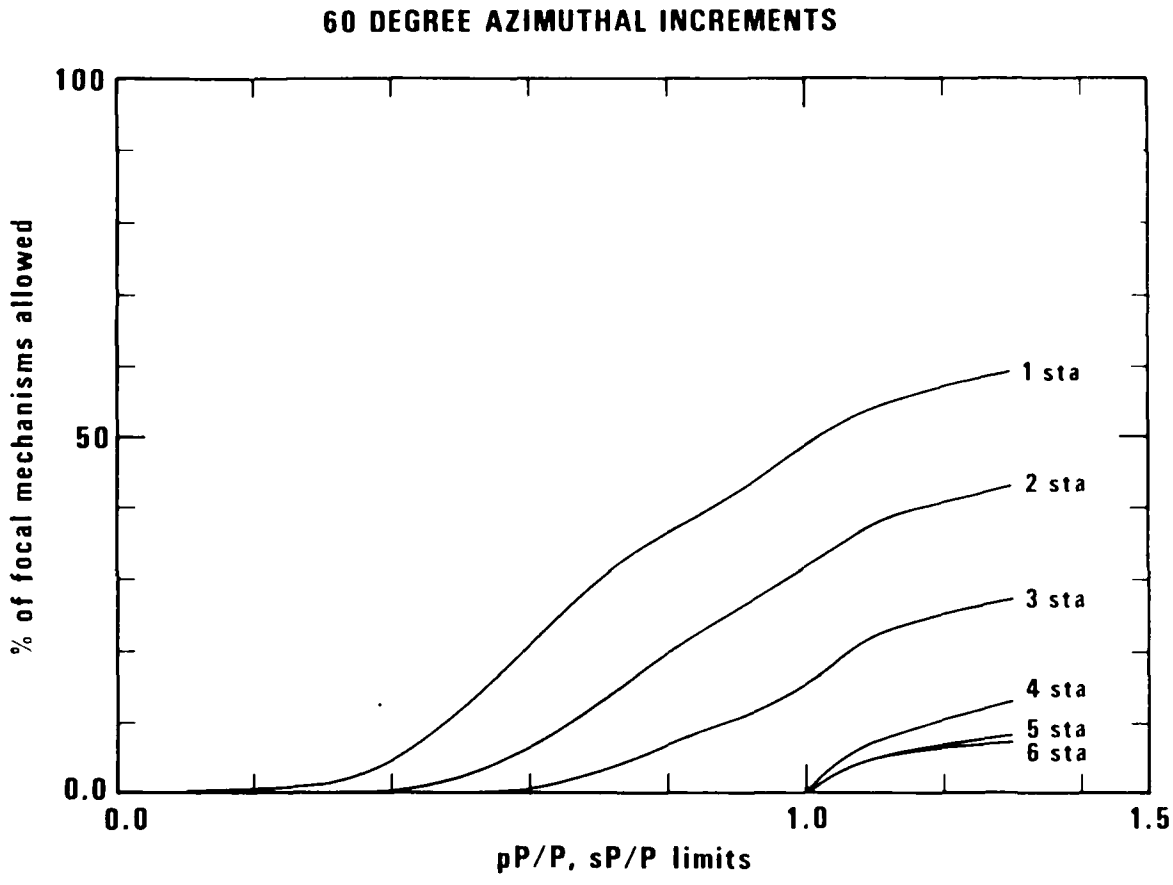

Figure 12c The percentage of all possible double-couples eliminated by a network of stations at 60 degree azimuthal increments. Four or more stations are required with $|pP/P|$ and $|sP/P| < 1$ to eliminate all possible focal mechanisms from consideration.

with sufficiently small coda amplitudes. The stochastic variation in teleseismic take-off angles did not seem to be a significant factor. The average number of stations required to eliminate all double-couples for a mean |pP/P| of 0.75 with 0.25 standard deviation was 8 stations. The average number of stations required to eliminate all double-couples for a mean |pP/P| of 0.5 with 0.25 standard deviation was 6 stations. For |pP/P| = 0.75 with a standard deviation of 0.5 an average of 11 stations was required and the results were highly variable. Values of |pP/P| > 1.0 were of little use in eliminating double-couple solutions.

As one last set of tests, a series of hypothetical shot arrays were investigated with a nine station network appropriate to the east Kazahk test site. Four hypothetical shot ratios were considered; the first shot equal in magnitude to the second shot, ie shot1/shot2=1.0, as well as the ratios shot1/shot2=0.5, shot1/shot2=.66, shot1/shot2=1.5, and shot1/shot2=2.0 The extremal bounds on the two arrivals were assumed to be +/- 25 percent. The only shot ratio that allowed solutions was shot1/shot2=1. The nine station test array together with the solution set for (1+/-0.25)/(1+/-0.25) is shown in Figures 13A and B. These solutions would be easily removed if polarity information was available on the first shot since the double-couple solutions all possess vertical nodal planes, and would be eliminated by any three stations with the same polarity separated by 90 degrees of azimuth. Results for the other shot ratios are robust with respect to deletion of one or two stations from the network. The Pearce algorithm would appear to have some potential for discrimination of shot arrays designed to simulate P+pP if the two shots were of greatly different magnitude, or if the two shots were of comparable magnitude and polarities were available for two or more quadrants.

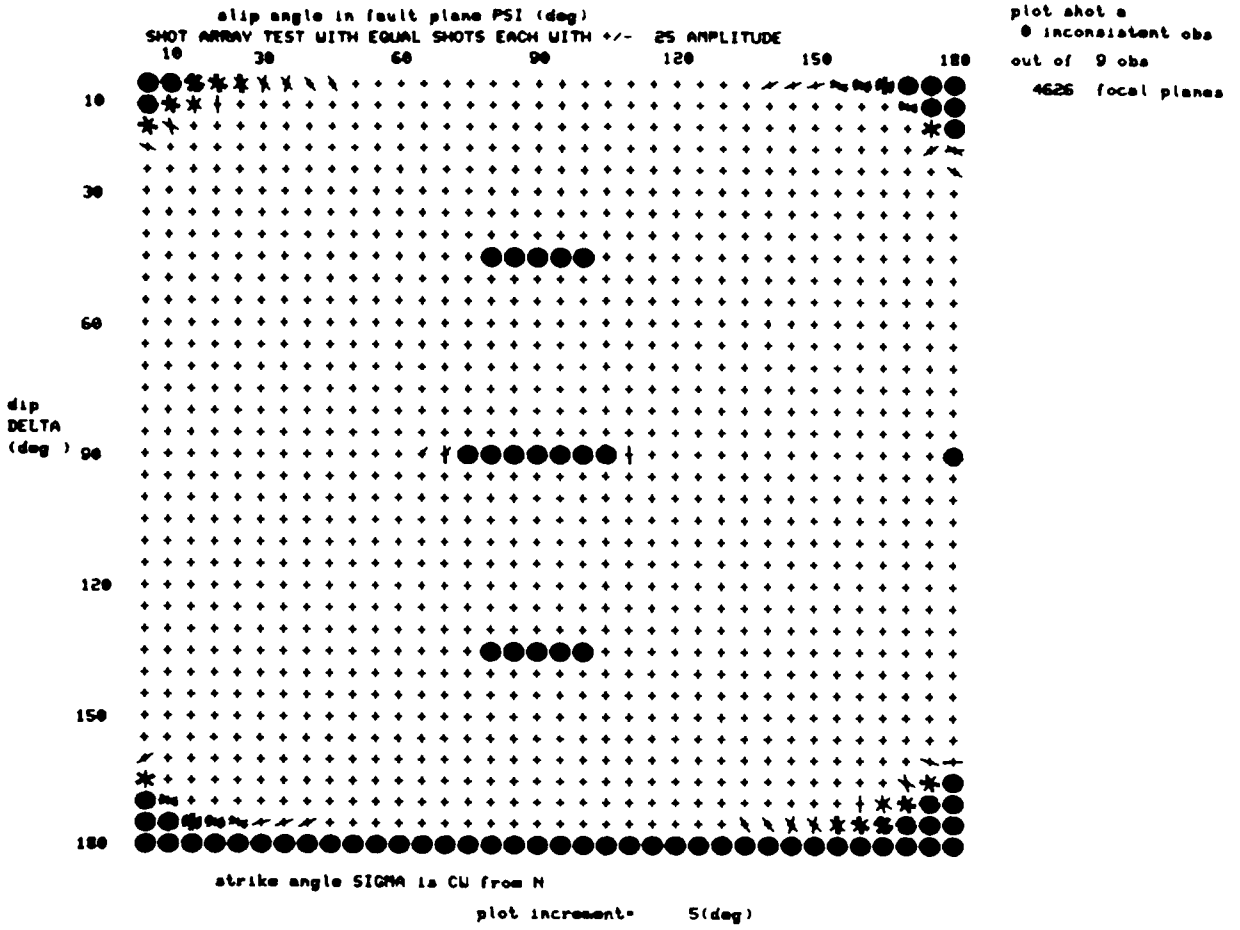

Figure 13a Results of a hypothetical nine station network with two arrivals of nearly equal amplitude. Both P and the prospective pP are given 25% amplitude tolerances. 4626 possible focal planes out of 93312 are found. No polarity information is used. Solutions are either of dip-slip with normal thrust, dip-slip with reverse thrust, vertical dip-slip, or horizontal faults with horizontal slip.

plotting increment= 10(deg)

plot shot a
0 inconsistent obs
out of 9 obs
708 focal planes

new file ?

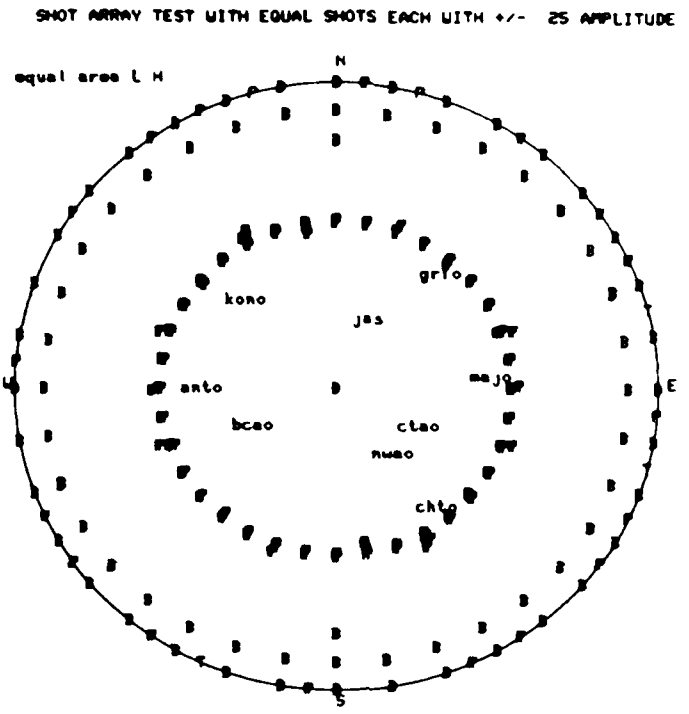

Figure 13b Results of a hypothetical nine station network with two arrivals of nearly equal amplitude. Both P and the prospective pP are given 25% amplitude tolerances. 4626 possible focal planes out of 93312 are found. No polarity information is used. Solutions are either of dip-slip with normal thrust, dip-slip with reverse thrust, vertical dip-slip, or horizontal faults with horizontal slip.

DATA PROCESSING AT THE CSS

Procedures and software were developed at the CSS to input amplitude measurements of P arrivals and prospective depth phases into the Pearce algorithm and to analyze the results in graphical form. Software documentation in the form of manual pages is reproduced in the appendix. A flow chart of the typical seismic analysis is shown in Figure 14. The hypocentral location may be preliminary, or poorly constrained (33 km). The process of depth estimation and depth phase identification may be an interactive process where the seismologist 1) selects prospective depth phases, 2) infers a depth, 3) estimates the amplitude bounds of P, pP, and sP, 4) runs the Pearce algorithm, and 5) analyzes the output. The seismologist may decide that either the depth phases are incorrectly selected, that the amplitude estimates may be improved, or that the results are satisfactory.

For the purpose of discrimination, amplitudes are read from the network of stations at selected time windows following the P onset. Each time window implies a depth range, and the Pearce processor is run as a batch job for each depth interval in consideration. The output was analyzed at a later time.

Although the UNIX operating environment at the CSS was satisfactory for the interactive aspects of focal plane analysis, such as amplitude measurements, or graphics display, the Pearce processor was too slow to run in ***real time***. The processor was typically used in a "quasi-batch" mode as an overnight process. Restructuring of the Pearce algorithm may reduce computation slightly. However, the major computational task of calculating nearly 100,000 radiation patterns for each observation (5 degree search increments), is central to the algorithm and not easily avoided. An option to reduce computation was added to eliminate consideration of solutions that have already been found inconsistent with more than a set number of observations. This option reduces

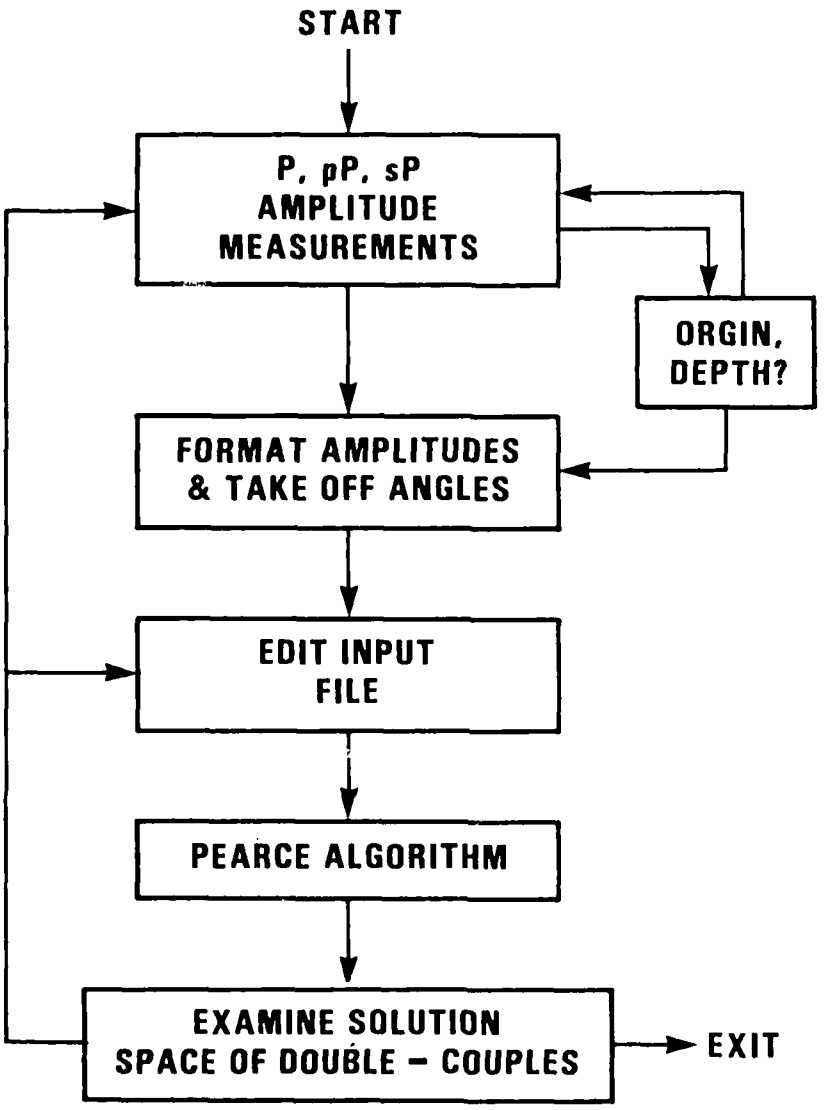

Figure 14 Flow chart of data analysis.

execution time at the expense of complete statistics for each possible solution

For the purpose of this preliminary study, the individual seismograms were interpreted with an interactive graphics display program. The amplitude measurements were made manually by control of a cross-hair terminal-host computer interface. In the case of most explosions and a few earthquakes where prospective depth phases are not obvious, an automated processor could be developed that gives the bounds on pP/P for given set of depth intervals at each station. The output would then reviewed by the seismologist before submission to the Pearce processor. Such an automated procedure would speed-up the procedure as a discrimination tool. If such a processor is developed, it should allow for uncertainties in the P arrival time, and use both seismologist provided P picks as well as predicted arrival times based on hypocentral parameters.

Two waveform data bases were used to evaluate the Pearce focal plane analysis algorithm at the Center for seismic studies. The first data base consisted of explosions recorded at SRO, ASRO, and DWWSSN stations. The underground explosions were located in East Kazahk, Novalya Zmelya, and Tuamoto test sites. The majority were located in the East Kazahk test sites. The second data base consisted of Eurasian earthquakes recorded on the same network of stations available from GDSN day tapes. Pertinent information for these two sets of events are presented in Tables I and II. The waveforms for each event were displayed and measurements of the P wave and P wave coda were made with two objectives. The first objective was to test if a simple measure of the P coda maximum would discriminate explosions form earthquakes when normalized to the P wave amplitude and used as a maximum bound on pP/P amplitude ratios across the network of stations. P coda was defined for the purpose of these measurements as that portion of the seismogram more than 3 seconds after the P wave onset. This corresponds to minimum pP-P times of 3 seconds

or depths of about 5 km or greater. Since the time of the prospective pP arrivals on each seismogram were not necessarily consistent with some fixed depth, this simplistic estimate of the maximum |pP/P| and |sP/P| ratios is considered conservative. Because more stringent bounds on |pP/P| and |sP/P| ratios are derived from forcing some consistency with a fixed depth, a second set of experiments were performed to find the best estimates of depth and source mechanism that satisfied the prospective depth phase arrivals of the earthquakes and explosion waveforms. For the earthquakes and explosions, a time window following the P wave was selected with a large excursion in the coda on one or more seismograms. Each waveform amplitude was measured within 5 seconds of the prospective depth phase arrival time. The focal plane solutions for the earthquakes were compared with available published source mechanisms in the the same region and with polarity data reported to ISC, and NEIS. Selected earthquakes are discussed in the section on *SOME DETAILED EXAMPLES OF THE PEARCE PROCESSOR*

Ideally, each event should be recorded at five or more stations at distances between 30 and 90 degrees with uniform azimuthal coverage. Given such a situation it would be possible to test the hypothesis that each event was an earthquake. Stations clustered at specific azimuths from the epicentral location do not give independent information and may give redundant information. Because of the non-uniform teleseismic coverage of the Eurasian continent by the SRO, ASRO network, and numerous down-time exhibited by these stations, the addition of DWWSSN stations to the digital network day tape in 1982 strongly enhanced the data coverage. Regional distances were not used because depth phase arrival times are more sensitive to the regional velocity structure and because the upper mantle P wave travel time triplications complicate the selection of depth phases. For the same reason, some PkP observations were not

used when PkP triplications produced interfering secondary arrivals. Available CSS software was used to display the P+Pcoda waveforms with predicted P, pP, sP, PcP, and PkP(df)(bc)(ab) arrival times. The software was not capable of predicting pPcP, sPcP, pPkP, or sPkP arrival times. Nor were the travel time tables adequate for shallow events (less than 33 km). Differential sP-pP times were usually incorrect for shallow events and the pP times systematically late. Because hypocentral coordinates were usually preliminary and because of local station travel time biases, the predicted P and depth phase times were often incorrect. The available software did not permit an interactive relocation.

As a first pass experiment, explosions and earthquakes were tested with depth phase amplitude bounds of the form; $|pP| < C$. The value of C was read from the maximum P coda amplitudes following the P arrival. The explosion amplitudes were submitted to the Pearce processor for takeoff angles with source velocities of 5.0, and 6.0 km/sec. The earthquake amplitudes were submitted to the processor with velocities appropriate for the best guess depths. None of the earthquakes failed to yield some solution set of double-couples. Out of the 41 explosions in Table I, 12 were consistent with double-couple solutions in the crust. Only two of these 12 events had 5 or more stations. All of the other 10 events were only recorded on four or less stations. All of these remaining 10 events were not recorded in one or more quadrants. Six of these 10 events were recorded in only 2 quadrants (stations located only in Europe and North America). Of the two events with 5 or more stations recorded; event 72 was located in the Tuamato islands with recordings in only 2 quadrants, and event 115 was also recorded in only 2 quadrants. These 12 explosions spanned the magnitude range of 5.2 to 6.0 m_b. Bandpass filtering was used on seismograms from 10 of the 41 explosions. With one or two exceptions, bandpass filtering did not reduce significantly depth phase amplitude constraints. The early P coda did not pos-

sess significantly different frequency bandwidth than the P wave, and only where ambient noise was high did filtering significantly affect the amplitude bounds.

Several of the earthquakes with well constrained focal mechanisms are discussed in a previous section. The minimum amplitude bounds for pP and sP were considered as well as the maximum amplitude bounds, P polarities, and more stringent bounds on depth phases were interactively varied to attain a best estimate of the solution set of focal mechanisms. Those of special interest, with independent estimates of the focal mechanism, or illustrated some aspects of algorithm are treated with detail in a previous section.

PEARCE ANALYSIS SUBSYSTEM OF THE SRIS

In the previous section of this report we described a system for performing Pearce's analysis using the VAX 11/780 computers which run under the UNIX operating system at the CSS. In this section we shall describe another system for performing Pearce's analysis which has important operational differences from the system at the CSS. This system also uses a VAX 11/780 computer, but it runs at a different facility, the Seismic Research Center [SRC] in Alexandria, Virginia, and it uses a different operating system, namely VMS [Virtual Memory System]. The system at the SRC is a subsystem of a larger seismic analysis system, whereas the CSS system operates in a stand-alone mode. The two systems also differ in two respects with regard to their databases. At the time of this study, the facilities at the CSS were restricted to the use of only unclassified data, but the SRC system was run in a classified mode. Also, the CSS system uses waveforms copied to disk from the GDSN tapes, whereas the SRC system employs a highly structured file system consisting of event records and waveform files which are accessed using the Record Management System [RMS] "indexed file" I/O features of VMS.

The contractual task which was fulfilled by the construction of this second system was that of adding the capability of performing Pearce's analysis to the Seismic Research Information System [SRIS] (formerly known as the Regional Event Location System [RELS]), a large software package for seismic analysis which runs on the VAX at the SRC. Documentation of SRIS has been published elsewhere (Teledyne Geotech, 1982), and we shall herein assume familiarity on the part of the reader with the design and operation of this system. In its original formulation, SRIS contained one subsystem devoted to the discrimination task, namely the Discrimination and Identification of Seismic Events [DISE] subsystem (von Seggern, 1981), commonly known as the "interactive" discrimination subsystem. The performance of that subsystem has been tested by Blandford *et al.* (1983) using measurements which were made on continuous

waveforms by a new SRIS subsystem, the Automatic Seismic Discrimination System [ASDIS] (Farrell, 1981). In the final formulation of SRIS, this new "automatic" discrimination subsystem was extended to handle the segmented waveforms of the AI data set, and a third discrimination subsystem was added so that Pearce's technique could be implemented on the system. We shall refer to this last subsystem simply as the "Pearce" subsystem. In order to provide results which could be compared with previous studies and with the concurrent testing of the automatic discrimination subsystem, the Pearce subsystem was designed to operate on segmented data files so that it too could be applied to the AI data set. In its final configuration, then, SRIS contained three discrimination subsystems : an interactive discrimination subsystem, which operated on alphanumeric data files; an automatic discrimination subsystem, which originally operated only on continuous waveform data but later on segmented waveform files as well, and which generated the input for the interactive discrimination subsystem; and the Pearce discrimination subsystem, which operated on segmented waveform files. (As we shall discuss, provision was also made for the Pearce subsystem to access continuous waveform data, but this feature of the design was not implemented.) In this section we shall present certain documentation pertaining to the design and operation of the SRIS Pearce discrimination subsystem.

The Pearce analysis at the SRC consists of three separate stages of data processing. First, the interactive graphics capabilities of the SRIS are used to access the desired waveforms and to make the amplitude and polarity measurements which are needed by the Pearce algorithm. Next, this algorithm itself is run as a batch job on VMS. As we have described in the previous section, the grid searching which is performed by this algorithm can be a time-consuming process, particularly when the focal-mechanism parameters are searched in increments of 5°. Cascading the grid search from one amplitude test to another in the manner which we have described speeds up this process, but it also loses information about which stations most strongly restrict the range of allowed solutions (this information may be valuable for identifying

critical, or perhaps erroneous, measurements), and even with "cascading" it is still slow enough that running it on-line would cause a troublesome delay before the SRIS would be free again for further waveform processing. Making the Pearce algorithm a batch job gives the SRIS operator the option of either deferring this analysis until sometime after he has finished using SRIS (in which case he may submit the job from a "dumb" terminal not connected to SRIS) or of submitting the job interactively from the SRIS keyboard and monitoring its output on the raster screen while it runs. We anticipate that the operator will select this second option if the Pearce analysis is the only processing which remains to be performed during a given SRIS session; in this case, the operator will want to know while he is still at the SRIS analysis station whether the Pearce algorithm was unsuccessful and whether he should repeat any of the waveform measurements. Finally, the range of solutions allowed by the Pearce algorithm, which is stored on the system as a binary file so that it can be accessed at any time in the future, is input to an interactive job which displays these solutions graphically. Two versions of this graphics job exist : one uses the Tektronix storage tube, which is not connected with SRIS, and the other uses the Graphicus-80 [G-80] refresh screen which is a part of the SRIS analysis station. The Tektronix version would be used for off-line processing, such as for displaying the results of the Pearce analysis which had been run as a batch job or for re-displaying the results of analysis which had been performed sometime in the past. The G-80 version would be used for on-line processing, so that the SRIS operator could examine the results of a Pearce algorithm job which he had just finished running.

We shall now describe the features of the new SRIS subsystem which permits the operator to make the waveform measurements which are to be used by the Pearce algorithm. This new subsystem is an extension of the Interactive Analysis Station [IAS] subsystem, which is described in the SRIS documentation volumes (Teledyne Geotech, 1982). This new subsystem is invoked by requesting the SUBMENU feature from among the other options which are offered to the operator on the "main menu" of the IAS,

Table III

SUBMENU Options of the Pearce Measurement Subsystem

Option	Function Performed
GETCONWF	Retrieve continuous waveform data
GETSEGWF	Retrieve segmented waveform data
AMPLIM	Make measurements of maximum or minimum bounds on the amplitude of signals (or of coda)
POLARITY	Make picks of signal polarity (+, -, or 0)
SCRSAVE	Save results measured so far into scratch file
T-PICK	Display time corresponding to cursor position on waveform
DEPTH	Choose a trial value of the event depth; for this depth, mark the predicted arrivals of *pP*, *sP*, and *PcP*
TAKEOFF	Compute the takeoff angle of the *P* phase of the waveform being measured
DISPLAY	Display the retrieved waveforms and mark the predicted *P* arrivals
P-PICK	Replace the predicted *P* marker with an observed pick
MAINMENU	Return to the main menu of the IAS to perform waveform processing
IDLE	Submenu element which cannot be picked but which blinks as a prompt whenever the system is waiting for a submenu pick

which is displayed on the G-80 screen. Requesting the SUBMENU clears the main menu from the screen and replaces it with a new menu of options, all of which pertain to the Pearce measurements. These options are listed and defined in Table III. Strictly speaking, the IDLE element is not a submenu option; it merely blinks when the system is in a state in which it can accept and process a submenu pick. We shall now describe how an analyst can use these options to make the waveform measurements which are required by the Pearce algorithm.

The operator will first need to access the waveform data pertaining to the event under analysis. He may retrieve continuous waveform data using submenu option GETCONWF or segmented data using option GETSEGWF. The GETCONWF option, however, was never implemented in this design, since we were tasked to demonstrate the system using the AI (segmented) dataset rather than continuous waveform data. This menu option was thus included only as a stub, so that it could be added to the system at a later time if it was desired to do so. This option, if it were to be implemented, would use much of the same software for accessing the continuous waveform files which is used by the IAS and by the on-line Detection Processing [DP] SRIS subsystem. That this existing software may in fact be used successfully for retrieving continuous waveform data has been demonstrated by Blandford *et al.* (1983). We shall therefore desribe only the option GETSEGWF, which employs a newly developed software package for retrieving segmented waveform files such as those of the AI dataset.

The GETSEGWF option employs two types of data files which are described in the Data Base Specification [DS] volume of the SRIS documentation (Teledyne Geotech, 1982) : Event Arrival Files [EAF] and Segmented Data Files [SDF]. The operator directs the system to read the proper EAF record by replying to its prompt, which appears on the raster screen, to enter the year, Julian day within the year, and event number within the day of the desired event. The event arrivals for each day constitute a single EAF, so the first two items entered are sufficient to cause the system to open the proper VMS/RMS "indexed" file. (It is also necessary for the system to know on what

disk and within what directory the EAF resides; this information is hard-coded within subroutine RDSEG.) All three of the items entered are concatenated to form the "key" which enables the RMS feature of VMS to find the correct record in the indexed file. The system reads the "type 0" EAF record for the sought-after event, which includes such information as the event hypocenter and origin time. Information about the individual signal arrivals from this event as recorded at stations throughout the network are contained in the "type 1" records which follow this type 0 record in the EAF. The system reads through these records (by reading the first one with a keyed read and then using sequential reads after that) in order to find out what waveforms are available. Before reading the EAF type 1 records, the system prompts for the desired phase (for our purposes, *P*), and it opens the SDF for the same Julian day as that of the EAF. Consequently, when it finds an EAF type 1 record of a phase of the designated type (*i.e.*, short-period *P*), it can perform a keyed read of the corresponding SDF record to retrieve the waveform containing that arrival. The EAF thus functions as a pointer to the waveforms in the SDF. Having the system search through the archived data in this manner rather than having the analyst locate and load the desired waveforms is perhaps the principal difference between the SRIS Pearce subsystem which is documented in this section and the CSS system which was described in the previous section. The header for each waveform which is retrieved from the SDF is displayed on the raster screen, and, if the analyst chooses, the waveform itself is plotted on the screen of the G-80. The system then prompts the analyst either to add this new waveform to the database which will be measured or to reject it. If the waveform is accepted, then the system transfers the waveform to a memory buffer, and it retains certain information from the SDF header, such as the epicenter-to-station distance, forward azimuth, and back azimuth. The system asks the operator whether he wants to examine more waveforms, and if he does, then it continues reading the EAF and retrieves the SDF record corresponding to the next desired (*i.e.*, *P*) arrival in the list. This process continues until there are no more type 1 EAF records for this event or until a maximum of

30 waveforms have been added to the memory buffer. (If more than 30 waveforms exist, the operator can process them all by performing the analysis on the first 30 and then using the submenu option GETSEGWF again to access the next 30, and so on.)

The GETSEGWF option automatically calls the functions of the DISPLAY submenu option to plot any combination of up to 16 waveforms, chosen from the memory buffer, simultaneously on the screen. (It should be noted, however, that displaying more than 8 to 10 waveforms, depending on the number of points per waveform, usually causes an objectionable amount of flicker, and it greatly reduces the vertical resolution of each waveform.) The operator can subsequently use the DISPLAY option, independently of the GETSEGWF option, any time the IDLE element is blinking. This will permit him to change the combination of waveforms which is shown on the screen so that, for example, he can examine the next set of 8 or 10 waveforms out of the maximum of 30 which he has chosen. DISPLAY also allows the operator to choose how many points of the waveforms are to be plotted. He will usually select the entire waveform, since the *P* arrival, and hence also the *pP* and *sP* arrivals, are close to the end of some of the segmented data windows. The chosen waveforms are then plotted on the G-80. The traces are labelled by a reference trace number which will be used in further operator/machine interactive commands, by the station name, and by the source-to-receiver distance and forward azimuth. Pointers are drawn on the traces marking the arrival times for the *P* phase, which are calculated using the Herrin (1968) travel-time tables, the source-to-receiver distances taken from the SDF, and the source depth taken from the EAF (unfortunately, this value was always set to zero for the AI events). The software for accessing the travel-time tables and for computing the predicted *P* arrival times using them is the same as is used by the Event Location System [ELS] subsystem (Teledyne Geotech, 1982), so we shall not describe it herein. In order to examine the waveforms, and particularly the predicted *P* arrivals, more carefully, the analyst may choose to invoke the MAINMENU option to return control to the IAS. From the IAS subsystem, he can use the main menu of that subsystem to expand or

compress the plotted trace horizontally, magnify or demagnify it vertically, or filter it. When he is satisfied with the adjustments which he has made to the trace, he can then return to the Pearce subsystem by again selecting the SUBMENU option on the main menu.

The markers which have been drawn on the waveforms using the event location taken from the EAF will, of course, be only approximate markers to the true *P* arrival times. The discrepancy between the predicted and actual arrival times will be particularly pronounced if the depth which is listed in the EAF is incorrect (as we have pointed out, this is the case for the AI dataset, which lists default depths of zero for all 133 events). The operator is therefore meant to use these markers only as a guide in searching for the *P* arrivals visually. When he believes he has found a true signal onset on a given trace, he will invoke the P-PICKS option of the submenu, and then he will move a cursor across the G-80 screen until it coincides with the observed signal onset on that waveform trace. (Cursor control on the G-80 is provided by a pen attached to a data tablet.) He will then depress the pen on the tablet, transmitting a "hit" to the system, and a new *P* marker with the associated time will be displayed. The analyst may make up to 32 picks to adjust and readjust the *P* phase markers on all of the traces until he is satisfied that they are correct. He will then press the "FNI" button on the G-80 keyboard, and the predicted *P* markers will disappear from the screen. They will be replaced by new ones drawn at those points on each of the waveforms which were last selected by the operator as being the true signal start points. The time corresponding to this point on each trace is retained in memory as the corrected *P* arrival time. The operator may choose the P-PICKS option repeatedly until he is satisified with the positions of all the *P*-markers. As a further guide in making the selection of the *P* onset, the operator may invoke the T-PICK option, which writes on the screen the time corresponding to any "hit" made on the waveform trace using the pen and data tablet without changing the value of the chosen *P* arrival time.

The operator will next wish to exercise the DEPTH option on the submenu. This option first draws a horizontal axis on the bottom of the screen, marked off in increments of 10 km and labelled in increments of 50 km from 0 to 600 km. This axis will be referred to as the depth axis. (Note that it has no logical connection with the waveform traces which are displayed on the screen above it.) The operator will then use the pen and data tablet to position a cursor on this axis and "hit" a trial depth. Using the event epicenter and origin time taken from the EAF and the depth which was chosen on the axis, the system then computes *pP*-*P*, *sP*-*P*, and *PcP*-*P* delay times for each of the stations corresponding to the displayed waveforms. Once again, the *P* travel times are computed using the Herrin (1968) tables, but now the travel times for *pP* and *sP* are computed using polynomial formulas taken from the ADAPS system (Teledyne Geotech, 1968), and those for *PcP* are computed using the Jeffreys-Bullen (1940) tables. The software for accessing the travel-time tables and tables of polynomial coefficients and for computing the travel times from them is the same as that which is used in the ELS subsystem of SRIS (Teledyne Geotech, 1982).

Two points ought to be noted about the computation of these delay times. First, mixing travel-time tables in this manner will obviously bias the results since different earth models are being used to compute the travel times of the different phases. We also point out that the polynomial fit which is used for the *sP* travel times is inappropriate for depths shallower than about 30 km. Second, it is obviously inaccurate to choose an arbitrary trial depth for the event while leaving the epicenter fixed to the value which is listed in the EAF. The latitude, longitude, and depth variables are not independent, so changing one of them would affect the other two in the location algorithm and hence in the computation of the travel times. In spite of these two objections, the computation of the delay times for the three reflected phases is adequate for the purposes for which it is used, as we shall now describe. The calculated delay times are added to the *P* arrival times which were selected using P-PICKS, and markers are then drawn on each waveform trace corresponding to the predicted *pP*, *sP*, and *PcP*

arrivals. As with the initial P markers which were drawn by the system but were then replaced by analyst picks, these markers are meant simply to assist the analyst in finding the phases visually. The advantage of having these markers is that they provide a means for relating the individual traces on the display to one another. That is, the markers serve to account for the rollout with distance of the reflected phase arrival times in a manner which is at least consistent, if not strictly accurate. It is this rollout which we wish to illustrate with these markers. As Goncz and Barker (1978) have demonstrated, it is easier to make pP picks on a screenfull of traces simultaneously than on each one of those traces individually. If an analyst searches for pP on each trace independently of the other traces, he may end up picking coda arrivals with short delay times, indicating a shallow source depth, on some traces while picking arrivals with long delay times, indicating a deep focus, on other traces. This problem can be alleviated if it can be demonstrated that the pP pick which the analyst makes on one trace is consistent with the picks which he makes on the traces for the other stations. The markers which are drawn by the DEPTH option are a means for illustrating this inter-station consistency graphically. The analyst will use this feature by choosing a trial depth on the depth axis and noting the positions of the pP, sP, and PcP markers which are drawn on each trace. If the depth which he chose is the right one, a consistent pattern will appear of arrivals in the codas occurring at increasing delay times with increasing source-to-receiver distance in the same manner as do the markers drawn on the traces. If no such pattern is apparent, the operator may then "hit" another depth on the axis to draw a new set of markers. He will continue choosing trial depths either until he is satisfied that no reflected phases can be detected on any of the traces or until he finds a depth for which the pattern of markers seems to match certain observed arrivals in the codas for at least some of the traces. Again, we emphasize that this match will be only approximate, but the positions of the markers may be adequate to guide the analyst to note visually the true onsets of the reflected phases. In particular, on those traces on which he would not otherwise note pP, he

AD-A145 215 PEARCE FOCAL SPHERE ANALYSIS OF EXPLOSION AND EARTHQUAKE MECHANISMS(U) TELEDYNE GEOTECH ALEXANDRIA VA ALEXANDRIA LABS K L MCLAUGHLIN ET AL. 10 NOV 83 2/2

UNCLASSIFIED TGAL-IR-83-4 F08606-79-C-0007 F/G 8/11 NL

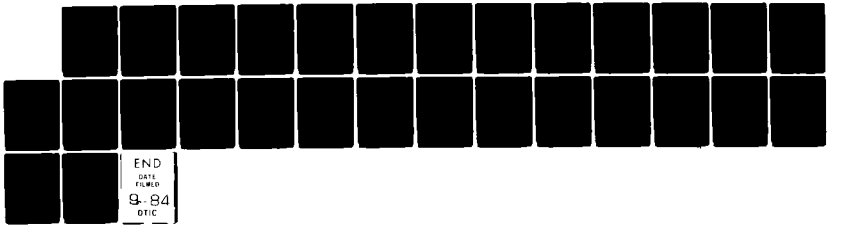

END
DATE FILMED
9-84
DTIC

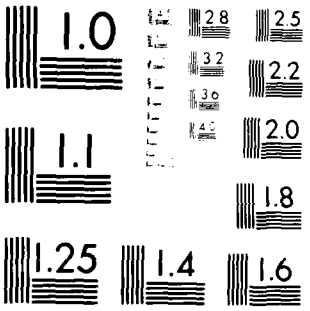

may now be able to detect it by examining closely that portion of the wavetrain surrounding the marker, since this is the time window within which pP would arrive if the event were at that same source depth for which the predicted pP delay time does in fact agree with the observed delay at those stations for which he was able to identify the pP arrival. If he nevertheless is still unable to find pP on some traces, the analyst will use the marker to show him where within the coda he should measure the coda amplitude level which will then be used as an upper bound on the amplitude of the undetected pP phase.

Once the analyst either has identified the pP and sP phases or has decided, on the basis of the cursor positions, where within the P-wave coda he will make measurements bounding these undetected phases, he will next use the POLARITY submenu option to make picks of the first motion direction of P, pP, and sP. He will enter the reference number of the trace on the screen for which he wishes to make the picks, and, in response to a prompt appearing on the screen, he will enter a code of "1", "2", or "3" to denote which phase he is picking. He then will enter a code of "+", "-", or "0" as the polarity pick. The system will substitute default values of "0" for the polarities of all phases which the analyst does not explicitly pick. The analyst thus need pick only those phases with clear first motions (usually only P phases, and only those at certain stations). The polarity picks can be made in any order, and they can be repeated if the analyst recognizes that he has made a mistake. As a guide to error detection, the "+", "-", or "0" code which the analyst enters is echoed on the graphics screen.

The final set of measurements is made using the submenu option AMPLIM. As he did for the polarity picks, the analyst will enter information defining which trace he is about to measure. In response to a prompt appearing on the screen, he will also enter a numeric code telling the system whether he is about to measure the amplitude bounds P_{max}, P_{min}, pP_{max}, pP_{min}, sP_{max}, or sP_{min}. These six measurements may be made in any order, and they may be repeated any number of times. Default values of zero are supplied by the system for any measurements not made by the analyst; these

default values would be used, in particular, for the minimum amplitude bounds of undetected phases. The analyst will then use the pen and data tablet to position a horizontal cursor on the screen somewhat above (if he is measuring the maximum bound) or below (if he is measuring the minimum bound) the maximum excursion of the upswing peak of the phase. When the cursor is where he wants it, it will register a "hit" by depressing the pen on the data tablet. He will then move the cursor to a position somewhat below (for the maximum bound) or above (for the minimum bound) the maximum excursion of the downswing peak, and register a second "hit". The system then computes the amplitude bound as being the difference between the cursor positions for the "hits" on the upswing and downswing peaks. If the analyst wishes, he may instead measure first the downswing and then the upswing peaks, since the system uses the absolute value of the difference between the cursor positions.

In any event, the analyst will use AMPLIM to take the difference between the upswing and the downswing "hits" to compute P_{max}, and he will use it to compute P_{min} in the same way. Note that the system does *not* compute the difference $P_{max} - P_{min}$; rather, both of these values are written into the output file along with the maximum and minimum bounds for pP and sP. Both the maximum and minimum bounds are required, since the Pearce algorithm uses the bounds on the ratios P/pP and P/sP. The minimum bound for the ratio P/pP is given by P_{min}/pP_{max}, and the maximum bound is given by P_{max}/pP_{min}, with similar ratios bounding the ratio P/sP. (Actually, in order to avoid computational difficulties with large numbers, the algorithm will instead use the reciprocal ratios pP/P and sP/P if the original ratios are too large. This would of course happen when the P-wave coda is measured in place of undetected surface reflections; in this case, $pP_{min} = sP_{min} = 0$.) The P-wave measurements which the analyst makes using the AMPLIM option are shown in Figure 15. Similar measurements would be made for pP and sP, if they are detected, or for the coda maximum if these phases are undetected. The amplitude bounds which are measured in this manner are reflected on the raster screen so that the analyst can review them and can

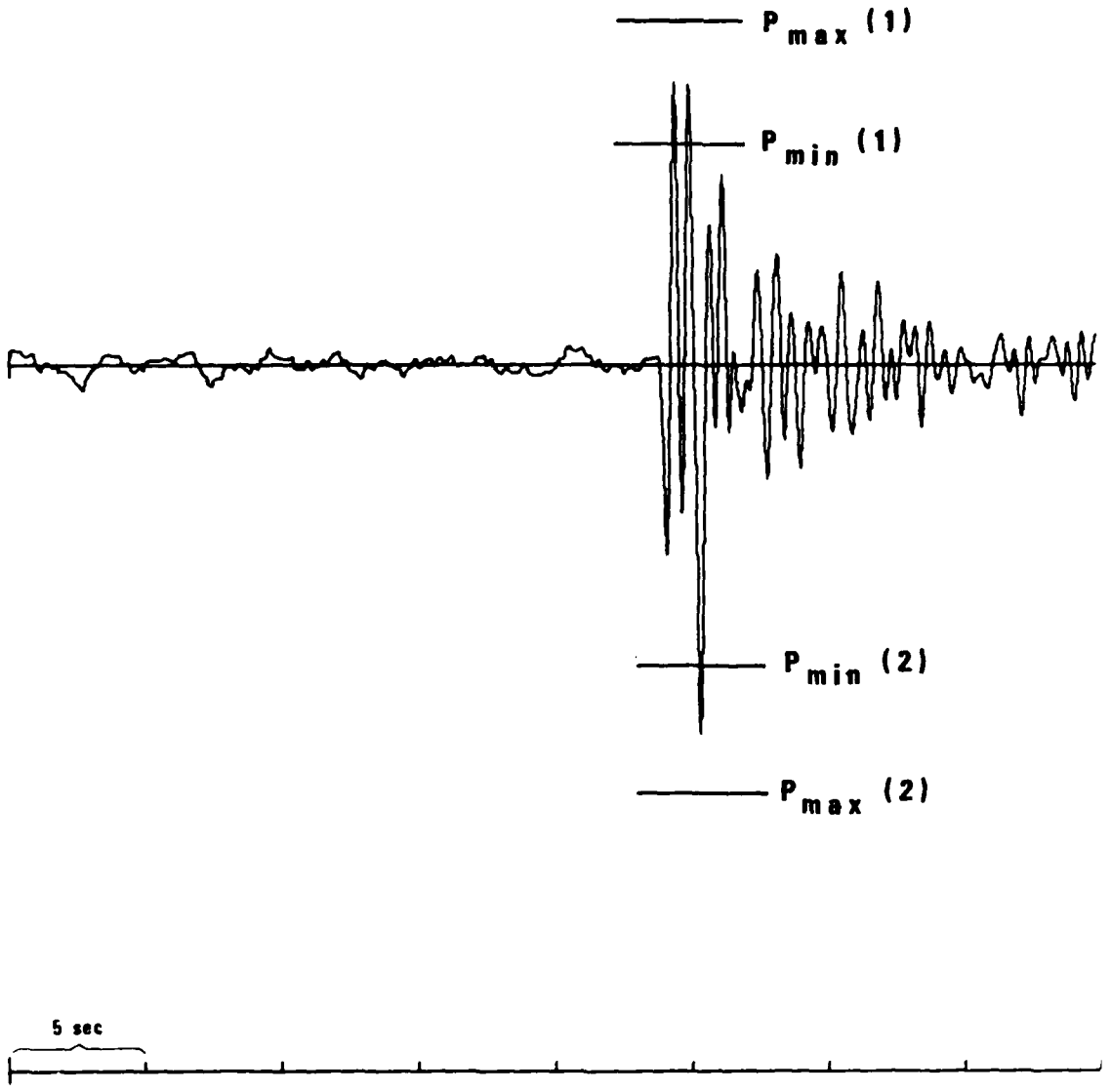

Figure 15 P-wave amplitude bounds measured using the AMPLIM options.

repeat the measurements if he considers them to be unsatisfactory.

The amplitude information is converted by the system from inches on the G-80 screen to nanometers on the seismogram using the scale factor in the SDF header. This information in turn is taken from the gain factor for data tapes which is listed in the SENSOR.DAT file for that station (*cf*. DS documentation volume, Teledyne Geotech, 1982). It also uses whatever scaling factors were applied by the DISPLAY submenu option and by the IAS main menu features for waveform trace magnification. It should be mentioned that for the seismograms from certain stations, the gain factors in the SENSOR.DAT files were in error by a factor of 1000 since they were scaled to microns rather than to millimicrons; as we have pointed out, the Pearce analysis is unaffected by calibration problems of this sort, since the gain factors cancel out when the P/pP and P/sP ratios are taken. No correction for instrument response is applied in order to convert the measured amplitudes on the seismogram to amplitudes of ground displacement; a feature for making this correction can be added to the AMPLIM option at a later time if it is concluded that the difference between the period of the P phase and that of the pP and sP phases is large enough to cause a significant difference between the instrument gain factors which should be applied to the measurements of those phases. As it stands now, we consider the period-related difference in gain factors to be one of the many sources of amplitude variation for which we wish to compensate manually by placing the horizontal cursors far enough above and below the amplitude peaks that the difference $P_{max} - P_{min}$ would represent sufficiently large "error bars" for the measurement of the P-wave amplitude, and similarly for the other two phases. In the next section of this report we shall discuss how large these error bars should be.

It will be noted that the submenu option DEPTH draws markers for pP, sP, and PcP, but options POLARITY and AMPLIM both ignore the PcP phase. The reason that this phase is marked by DEPTH is simply to assist the analyst so that he does not mistake this core reflection for one of the surface reflections.

When the analyst has finished making all the required measurements on the waveforms displayed on the screen, he will invoke submenu option TAKEOFF to compute the takeoff angles from the event's hypocenter to the stations corresponding to each of the displayed traces. Input to this computation consists of the epicenter-to-station distances taken from the SDF header and the event depth corresponding to the last "hit" made during the DEPTH analysis. The computation employs a fourth-order polynomial fit which was made to the tables of *P*-wave take-off angles of Pho and Behe (1972). These tables in turn were derived from the Herrin (1968) travel-time tables. The coefficients of the polynomial fit are listed in Table IV. Linear interpolation was used to compute the take-off angles for depths intermediate between those which are listed in the table. As is shown in Table IV, we assume that the source-to-receiver distance Δ lies within the range $20^\circ \leq \Delta \leq 100^\circ$. We are unable to extend this lower limit on Δ since the codas of regional *P* phases are contaminated with a variety of triplicated arrivals and since it would require detailed ray-tracing, rather than just an average earth model, to calculate the take-off angle of the *P* phase at regional distances. It would actually be better to use 30° as a cut-off, but we shall allow the lower limit to be 20° and leave it to the discretion of the analyst whether measurements made in the distance range $20^\circ \leq \Delta \leq 30^\circ$ ought to be retained or deleted in each individual case.

Use of this SRIS subsystem concludes with submenu option SCRSAVE, which writes into a file the station name, event-to-station forward azimuth, takeoff angle, polarity, and maximum and minimum amplitude bounds for the data analyzed thus far. This output file is organized so that each record contains all the information pertaining to one of the three phase pairs *P*:*pP*, *P*:*sP*, or *pP*:*sP*. Measurements made for stations at distances of less than 20° or more than 100° are deleted by SCRSAVE, as are measurements in which the maximum amplitude bound of some phase is zero (indicating that the phase was not measured) or for which the minimum amplitude bounds of both phases are zero (as is frequently the case for the phase pair *pP*:*sP*). Default values of unity, which can be overridden by the analyst in response to a prompt from the

Table IV

Polynomial Fit to the Tables of P-wave Take-off Angles

Takeoff angle = $A_4\,\Delta^4 + A_3\,\Delta^3 + A_2\,\Delta^2 + A_1\,\Delta + A_0$ where :

$20^\circ \le \Delta \le 30^\circ$					
depth (km)	A_4	A_3	A_2	A_1	A_0
0	-8.9961×10^{-4}	0.088244	-3.1096	45.407	-188.74
15	-9.9971×10^{-4}	0.097157	-3.3786	48.217	-188.12
40	-1.0342×10^{-3}	0.097221	-3.2019	41.208	-101.49
100	-1.5370×10^{-3}	0.14629	-5.0034	70.899	-287.83
150	-1.7324×10^{-3}	0.16475	-5.6646	81.710	-356.31
200	-1.6357×10^{-3}	0.15310	-5.1682	72.834	-299.44
250	-1.4115×10^{-3}	0.12897	-4.2170	56.630	-198.14
300	-1.3592×10^{-4}	-1.4688×10^{-3}	0.73169	-25.825	311.84
350	-3.6024×10^{-4}	0.020701	-0.095277	-11.947	224.68
400	4.2282×10^{-4}	-0.057965	2.8319	-59.673	513.84
450	1.2112×10^{-3}	-0.13608	5.6935	-105.52	786.59
500	1.9307×10^{-3}	-0.20600	8.1988	-144.65	1013.3
550	1.9975×10^{-3}	-0.20784	8.0600	-138.51	952.43
600	1.4360×10^{-3}	-0.14637	5.5508	-93.342	653.70

$30^\circ \le \Delta \le 85^\circ$					
depth (km)	A_4	A_3	A_2	A_1	A_0
0	-1.3478×10^{-6}	3.0859×10^{-4}	-0.025787	0.69203	23.882
15	-1.5862×10^{-6}	3.6270×10^{-4}	-0.030168	0.80422	27.251
40	-1.8867×10^{-6}	4.3052×10^{-4}	-0.035485	0.89992	35.170
100	-1.8528×10^{-6}	4.2264×10^{-4}	-0.034783	0.86392	36.543
150	-1.7764×10^{-6}	4.0319×10^{-4}	-0.032953	0.78147	38.643
200	-1.6109×10^{-6}	3.6568×10^{-4}	-0.029809	0.65428	41.627
250	-1.3332×10^{-6}	3.0505×10^{-4}	-0.025089	0.48568	45.199
300	-1.5685×10^{-6}	3.5118×10^{-4}	-0.027981	0.52881	47.045
350	-1.4794×10^{-6}	3.2904×10^{-4}	-0.025856	0.41824	50.795
400	-1.1750×10^{-6}	2.5625×10^{-4}	-0.019411	0.14766	56.892
450	-9.9141×10^{-7}	2.1119×10^{-4}	-0.015206	-0.051250	62.402
500	-7.6472×10^{-7}	1.5393×10^{-4}	-9.7699×10^{-3}	-0.30480	68.961
550	-4.0815×10^{-7}	6.8354×10^{-5}	-2.0155×10^{-3}	-0.64711	76.984
600	6.2078×10^{-8}	-4.8654×10^{-5}	8.9045×10^{-3}	-1.1284	87.341

Table IV
(cont.)

$85^\circ < \Delta \leq 100^\circ$					
depth (km)	A_4	A_3	A_2	A_1	A_0
0	0.0	-7.8222×10^{-4}	0.22419	-21.429	697.66
15	0.0	-8.8889×10^{-4}	0.25482	-24.362	793.18
40	0.0	-9.9552×10^{-4}	0.28656	-27.515	900.94
100	0.0	-1.0134×10^{-3}	0.29098	-27.870	910.44
150	0.0	-9.4224×10^{-4}	0.27153	-26.106	857.75
200	0.0	-1.0667×10^{-3}	0.30530	-29.144	948.92
250	0.0	-9.4222×10^{-4}	0.27112	-26.029	855.16
300	0.0	-9.9558×10^{-4}	0.28570	-27.352	895.79
350	0.0	-1.0311×10^{-3}	0.29534	-28.220	922.50
400	0.0	-1.0844×10^{-3}	0.30985	-29.532	962.82
450	0.0	-9.9599×10^{-4}	0.27567	-26.418	869.50
500	0.0	-9.7778×10^{-4}	0.28032	-26.820	881.95
550	0.0	-1.0311×10^{-3}	0.29487	-28.139	922.72
600	0.0	-8.7112×10^{-4}	0.25084	-24.116	801.63

system, are also written into this file for the pP and sP reflection coefficients and for the ratio of the seismic velocities at the source depth to those at the surface. (If the analyst allows the default values to be used, he will change them to more realistic values at a later time simply by editing this output file in the same manner as he would any other formatted file consisting of alphanumeric data.) He may then request more waveforms via submenu option GETSEGWF, or he may return to the main menu of the IAS and then terminate SRIS execution.

In the second (classified) volume of this report, we shall describe the application of the SRIS Pearce analysis subsystem to the segmented waveforms of the Al dataset.

CONCLUSIONS AND RECOMMENDATIONS

For explosions with mb > 5, pP amplitude constraints are sufficient to eliminate the possibility of an earthquake at depths ≥ 3-5 km , provided adequate azimuthal coverage exists. The CSS data set was inadequate to test explosions for mb < 5. Explosions consistently produced P coda of small enough amplitude over a network of stations, that they could not be mistaken for crustal earthquakes at depths greater than 3 to 5 km. Those earthquakes that failed the discrimination test were inadequately recored in at least two teleseismic azimuthal quadrants. One station, MAJO, exhibited poor performance with respect to other stations in this regard. MAJO short period waveforms from East Kazahk were characterized by an emergent P wave and a large second arrival. This behavior is most likely due to local anomalous structure at Matsushiro, Japan.

Synthetic tests indicate that the Pearce algorithm will likely eliminate the *earthquake at depth* hypothesis if 4 to 5 stations can be found with pP/P amplitude ratios of 1.0 or less, and the stations provide 270 degree azimuthal coverage. Because of detection thresholds of the GDSN network, it was not possible to operationally test whether the method would continue to work at signal-to-noise ratios closer to 1.

Earthquakes produced coda levels and secondary phases consistent with double-couple solutions at depths greater than 3 km. Often "constrained" focal mechanisms could be inferred. Some of these mechanisms were found to contradict focal mechanisms based on long-period data. It is possible that short period data are sensitive to different and more local stress systems than long period seismic data. A concerted effort to incorporate more polarity data would be helpful when waveform data is sparse in a particular quadrant.

sP amplitudes were found to be less reliable than pP amplitudes. Both uncertainties in SV-to-P surface reflection and S wave attenuation above the

source may be responsible. Detailed crustal models may improve the SV-to-P reflection modeling, but the results of Pooley et al (1983) indicate that near source heterogeneity is also responsible for deflection of SV energy near the focal planes. Shorter wavelength S waves should be more sensitive to any lateral velocity gradients than the longer wavelength P waves at the same frequency.

Bandpass filtering of digital waveforms was found to be useful for reduction of noise while measuring time-domain amplitudes. Filtering did not greatly increase the detection of depth phases. Both P coda and depth phases have similar frequency bandwidths. Consequently, the depth phases are not likely to be separated from the coda by simple filtering. Three component polarization filtering and beam-forming should be expected to improve depth phase detection when local coda generation is important. It was not possible to test this supposition with this limited study. RSTN short period three component data should offer a suitable test of whether polarization filtering can improve depth phase detection by a reduction in locally generated P coda signal.

The Pearce algorithm was found to be too slow to run interactively under the present CSS Unix operating environment. Furthermore, batch operation of the processor on the multitude of measurements made during a day's analysis of waveform data may take several hours to complete. This mode of operation makes it difficult for the operator to recall all the detailed logic that may have been involved in the selection of specific secondary arrivals from one day to the next. Also, the seismologist may submit more than one alternative set of amplitude bounds to the processor for later analysis. Access to a mainframe computer operating in a batch mode would shorten turn around time, and eliminate confusion for the seismologist attempting to examine the many possibilities. Some gains in efficiency in the Pearce algorithm are possible with changes in the code.

In an operational environment, where the Pearce algorithm may be used to test the hypothesis of a double-couple mechanism at depth, it will be necessary to quickly and automatically generate the amplitude bounds from the seismograms for each depth range of interest. Such an algorithm should allow for the uncertainties in the initial P arrivals, and estimate noise prior to the P arrival for comparison with the P coda. The seismologist should be able to quickly estimate the P arrival times for use by the processor. The use of predicted P times based on a preliminary origin should also be available. The depth interval, and set of amplitude bounds could be quickly stored as an alternative hypothesis for the Pearce processor. Such an automated "pP prospector" would allow the seismologist to review the prospects of several hypotheses and select the most likely alternative.

ACKNOWLEDGEMENT

Raymond Kimmel made the measurements on the SRI Pearce subsystem which are reported in Volume 2 of this report. David von Seggern performed the initial implementation of Pearce's algorithm on the SRI

REFERENCES

Armbruster, J., L. Seeber, and K. H. Jacob (1978). The northwestern termination of the Himalayan Mountain Front : Active tectonics from microearthquakes, *J Geophys Res*., *83*, 269 - 282.

Barley, B. J., and R. G. Pearce (1977). A fault plane solution using theoretical *P* seismograms, *Geophys. J. R. Astr. Soc.*, *51*, 653 - 668.

Blandford, R. R., and J. Gurski (1975). Use of earth resources technology satellite (ERTS) to determine tectonic characteristics near low M_s:m_b earthquakes in Tibet, *SDAC-TR-75-13*, Teledyne Geotech, Alexandria, Virginia.

Blandford, R. R., D. H. von Seggern, W. Rivers, J. Goncz, J. Burnetti, A. Hill, F. Maas, and B. Carroll (1983). Analysis of two days of AEDS data using the Seismic Research Information System [SRIS] : automatic detection, post-detection, and automatic association; interactive location and discrimination (U), *SDAC-TR-83-2*, Teledyne Geotech, Alexandria, Virginia. (S)

Chatelain, J. L., S. W. Roecker, D. Hatzfeld, and P. Molnar (1980). Microearthquake seismicity and fault plane solutions in the Hindu Kush region and their tectonic implications, *J. Geophys. Res.*, *85*, 1365 - 1387.

Chen, W. P., J. L. Nabelek, T. J. Fitch, and P. Molnar (1981). An intermediate depth earthquake beneath Tibet : Source characteristics of the event of September 14, 1976, *J. Geophys. Res.*, *86*, 2863 - 2876.

Choy, G. L., J. Boatwright, J. W. Dewey, and S. A. Sipkin (1983). A teleseismic analysis of the New Brunswick Earthquake of January 9, 1982, *J. Geophys. Res.*, *88*, 2199 - 2212.

Der, Z. A. (1973). M_s:m_b characteristics of earthquakes in the eastern Himalayan regions, *SDL 296*, Teledyne Geotech, Alexandria, Virginia.

Douglas, A., P. D. Marshall, J. B. Young, and J. A. Hudson (1974). Seismic source in East Kazakhstan, *Nature*, *248*, 743 - 745.

Dziewonski, A.M., and J.H. Woodhouse (1983). An experiment in systematic study of global seismicity: Centroid-moment tensor solutions for 201 moderate and large earthquakes of 1981. *J. Geophys. Res.*, *88*, 3247 - 3271.

Enescu, D., A. Georgescu, D. Jianu, and I. Zamarca (1973). Theoretical model for the process of underground explosions. Contributions to the problem of the separation of large explosions from earthquakes, *Bull. Seism. Soc. Amer.*, *63*, 765 - 786.

Farrell, W. E. (1981). Automatic Seismic Discrimination System (ASDIS), *VSC-TR-82-26*, S-CUBED, La Jolla, California.

Goncz, J. H., and B. W. Barker (1978). Detection of depth phases using computer graphics, *SDAC-TR-78-8*, Teledyne Geotech, Alexandria, Virginia.

Hartell, S. (1980). Faulting process of the May 17, 1976, Gazli, USSR, Earthquake, *Bull. Seism. Soc. Amer.*, *70*, 1715 - 1736.

Herrin, E. (1968). Seismological tables for *P*, *Bull. Seism. Soc. Am.*, *58*, 1196 - 1219.

Honda, H., (1957). The mechanism of earthquakes, *Scientific Reports, Tohoku University, Series 5, Geophysics, 9*, 1 - 46.

Jefferys, H., and K. E. Bullen (1940). *Seismological Tables*, Brit. Assn. Gray-Milne Trust.

Landers, J. E. (1972). Some interesting central Asian events on the M_s m_b diagram, *Geophys. J. R. Astr. Soc., 31*, 329 - 339.

Lang, W.J., and R.J. Sun (1966). Atlas of the Sino-Soviet Bloc to support detection of underground nuclear testing, Volume III. Seismicity.

Pearce, R. G., (1977). Fault plane solutions using relative amplitudes of pP and P, *Geophys. J. R. Astr. Soc., 50*, 381 - 394.

Pearce, R. G. (1979). Earthquake focal mechanisms from relative amplitude of P, pP, and sP : Method and computer program, *Report no. 0-41/79*, United Kingdom Atomic Energy Authority, AWRE, Aldermaston.

Pearce, R. G., (1980). Fault plane solutions using relative amplitudes of P and surface reflections : further studies, *Geophys. J. R. Astr. Soc., 60*, 459 - 487.

Pearce, R. G., H. Bainbridge, P. F. Key, and J. B. Young (1980). The 1976 earthquake sequence in Uzbekistan - focal mechanisms determined using the relative amplitude method, *Report no. 0-27/80*, United Kingdom Atomic Energy Authority, AWRE, Aldermaston.

Pho, H.-T., and L. Behe (1972). Extended distances and angles of incidence of P waves, *Bull. Seism. Soc. Amer., 62*, 885 - 902.

Pooley, C. I., A. Douglas, and R. G. Pearce (1983). The seismic disturbance of 1976 March 20, east Kazakhstan : earthquake or explosions ?, *Geophys. J. R. Astr. Soc., 74*, 621 - 631.

Prevot, R., D. Hatzfeld, S. W. Roecker, and P. Molnar (1980). Shallow earthquakes and active tectonics in Eastern Afghanistan, *J. Geophys. Res., 88*, 2199 - 2212.

Rodean, H. C. (1979). ISC events from 1964 to 1976 at and near the nuclear testing ground in eastern Kazakhstan, *UCRL-52856*, Lawrence Livermore Laboratory, Livermore, California.

Stauder, W., and W. M. Adams (1961). A comparison of some *S*-wave studies of earthquake mechanisms, *Bull. Seism. Soc. Am., 51*, 277 - 292.

Strelitz, R. A., (1978). Moment tensor inversions and source models, *Geophys. J. R. Astr. Soc., 52*, 359 - 364.

Stump, B. W., and L. R. Johnson (1977). The determination of source properties by the linear inversion of seismograms, *Bull. Seism. Soc. Amer., 67*, 1489 - 1502.

Teledyne Geotech staff (1968). ADAPS, an automatic data association and processing system for seismological data, *TR-68-28*, Teledyne Geotech, Garland, Texas.

Teledyne Geotech staff (1982) Seismic Research Information System [SRIS] Documentation : Functional Description [FD], System-subsystem Specification [SS], Program Specification [PS], Data Base Specification [DS], Teledyne Geotech, Alexandria, Virginia

von Seggern, D., (1981). DISE, an interactive discrimination program for seismic events, *VSC-TR-82-4*, Teledyne Geotech, Alexandria, Virginia

(THIS PAGE INTENTIONALLY LEFT BLANK)

APPENDIX

MANUAL PAGES FOR PROGRAMS AT THE CSS

NAME: pearce - Pearce focal plane analysis program

SYNOPSIS

pearce infile [10,5] [inconsistencies]

DESCRIPTION

Pearce examines a gridded solution space of slip, dip and strike angles for possible double-couple focal mechanisms consistent with amplitude bounds and polarities on P, pP, and sP phases. The amplitude bounds on P, pP, and sP are converted to amplitude ratio bounds for either pP/P, sP/P, or sP/pP. These extremal ratio bounds are considered as seperate observations and the bounded three-dimensional solution space of (slip,dip,strike) is searched for all possible solutions consistent with the observations. The (slip,dip,strike) space may be gridded at either 5 or 10 degree intervals. The observations are provided in a formatted input file *infile*. Pearce creates two files called *printout*, and *plotout*. *Printout* is a comprehensive listing of the processing. *Plotout* is an unformatted file containing results for input to *fplanes*, or *histogram*.

The second command line argument is the step size either 5 or 10 degrees, and defaults to 5 degrees. The third command line argument is the total number of inconsistenices that will be checked for each respective solution. This option can speed up processing if the user is not interested in the total number inconsistent observations for each possible solution.

Infile is a formated input file;

title (80a1)

nobservations ppfact1 svel/pvel (i2,2f10.5)

followed by amplitude observations of the form;
name,azimuth,incidence,Ppolarity,amp1,amp2,pPpolarity,amp3,amp4,ppfact,(__sp,ra)

with format(a8,2f10.3,a1,2f10.3,a1,2f10.3,1f8.3,a2).

A sample of which is given below (blanks are specified by "_"):

```
  10 04/06/79 18:30:05.20  41.860   77.630  10 5.10 0.00   0
07__0.7___0.5
chto_____135.210___23.680-___3.000_____6.000+___14.000_____24.000___0.750__
chto_____135.210___23.680-___3.000_____6.000_____0.000_____24.000___0.500sp
chto_____135.210___23.680___14.000_____24.000_____0.000_____24.000___0.500ra
grfo_____303.600___21.030___37.000_____41.000___00.000_____91.000___0.500sp
grfo_____303.600___21.030___37.000_____41.000___141.000_____175.000___0.750__
majo_____75.620___20.810_____6.000_____7.000___13.000_____14.000___0.500sp
majo_____75.620___20.810_____6.000_____7.000___15.000_____19.000___0.750__
```

The default pP attenuation correction is ppfact1, svel/pvel is the s wave -to- p wave velocity ratio to be used in calculating the sP takeoff angle, and SV-to-P reflection coefficient. Amplitude ratio bounds are calculated from the bounds; amp1/amp4, and amp2/amp3 with the polarity information given by + _or -. Attenuation of the secondary phase may be indicated by ppfact or spfact. The type of ratio bounds, pP/P, sP/P, or sP/pP, are indicated by the last character string on the line as either blank (__) for pP/P, sp for sP/P, and ra for sP/pP.

SEE ALSO

histogram() *fplanes*()

BUGS

If the reduced redundancy check option is used, histogram will not give a true picture of the total number of inconsistencies for each observation. Maximum number of observations is 31, limited by the word size on the VAX. Pearce is a shell script that calls an f77 program, and the interface with UNIX through standard input should be changed to acces the comand line argumenst directly. SV-to-P reflection coefficient is simple minded. The incidence angle of SV at the surface is assumed equal to the takeoff angle at the source. Also, the format of the input file for a fortran program is unforgiving. Watch the blanks and field alignment.

AUTHOR

originally; R.G. Pearce AWRE report No O 4/79
latest modifications; K.L. McLaughlin Teledyne-Geotech, Alexandria Va Aug 83

NAME: fplanes - read pearce output and generate graphical output of solution space

SYNOPSIS

fplanes

DESCRIPTION

Fplanes is an interactive program for viewing the solution space derived from the pearce focal plane algorithm. The user is prompted for each input. Three versions of the solution space may viewed.

1) The vector diagram of [slip,dip,strike] space. Each acceptable solution is shown as a vector with the strike azimuth attached to a grid point representing the slip and dip.

2) equal area lower hemisphere projection of the acceptable focal planes, with or without P,T,B vectors. The stations used in the pearce focal plane analysis are shown at the projection of the P wave takeoff angle by the station 4 letter code.

3) equal area, or equal angle, lower hemisphere projection of just the P,T,B axis of the acceptable focal planes. The stations used in the analysis are shown at the P wave takeoff angle by their 4 letter code.

The acceptable number of inconsistencies the user is willing to tolerate in the solution space is an option. The user may wish to replot any of the solution space representations with a change of the number of inconsistencies tolerated. This option allows the user to examine the robustness of the solution space to loss of data. If the pearce analysis was done with a grid point of 5 degrees, the user may use either a 5 or 10 degree grid space for display of the solution space.

The input data is an unformatted output file from *histogram* and consists of a header followed by 93312 integers each representing a specific slip,dip,strike with a 5 degree grid. Each integer is the total number of inconsistencies for that possible solution that were found by *pearce*.

SEE ALSO

pearce() *histogram*()

BUGS

The user should be able to specify which data elements are to be elliminated from the analysis, and not just the total number of inconsistencies that are to be tollerated.

AUTHOR

K.L. McLaughlin Teledyne-Geotech, Alexandria Va Aug 83

NAME: histogram - read the pearce output and generate histogram

SYNOPSIS

histogram infile outfile [10,5] [y]

DESCRIPTION

Histogram reads the *plotout* file from *pearce* and generates statistics on the unacceptable solutions for each possible solution examined. Each observation has the total number of inconsistent solutions tabulated. A matrix of mutual inconsistencies is tabulated to examine the redundancies with pairs of observation. *infile*. Histogram creates one file called *outfile*. *Outfile* is a an unformated file for input to *fplanes* where the integer array from pearce has been converted from the coding of individual inconsistent observations to the total number of inconsistent observations.

The third command line argument is the step size either 5 or 10 degrees, and defaults to 5 degrees. The fourth command line argument is whether to do a long or short statistics. Statistics and histogram are standard output.

SEE ALSO

pearce() fplanes()

BUGS

If the reduced redundancy check option of pearce is used, histogram will not give a true picture of the total number of inconsistencies for each observation.

AUTHOR

K.L. McLaughlin Teledyne-Geotech, Alexandria Va Aug 83

(THIS PAGE INTENTIONALLY LEFT BLANK)

DISTRIBUTION LIST
(UNCLASSIFIED REPORTS)
DARPA FUNDED PROJECTS
(Last Revised 18 June 1984)

RECIPIENT	NUMBER OF COPIES
DEPARTMENT OF DEFENSE	
DARPA/GSD 1400 Wilson Boulevard Arlington, VA 22209	2
DARPA/PM 1400 Wilson Boulevard Arlington, VA 22209	1
Defense Technical Information Center Cameron Station Alexandria, VA 22314	12 2
Defense Intelligence Agency Directorate for Scientific and Technical Intelligence Washington, D.C. 20301	1
Defense Nuclear Agency Shock Physics Directorate/SS Washington, D.C. 20305	1
Defense Nuclear Agency/SPSS ATTN: Dr. Michael Shore 6801 Telegraph Road Alexandria, VA 22310	1
DEPARTMENT OF THE AIR FORCE	
AFGL/LW ATTN: Dr. J. Cipar Terrestrial Sciences Division Hanscom AFB, MA 01730	1
AFOSR/NPG ATTN: Director Bldg 410, Room C222 Bolling AFB, Washington D.C. 20332	1
AFTAC/TG Patrick AFB, FL 32925	3
AFTAC/TD (STINFO) Patrick AFB, FL 32925	1
AFWL/NTESC Kirtland AFB, NM 87171	1

DEPARTMENT OF THE ARMY

US Army Engineers
ATTN: Mr. J. Drake
Waterways Experiment Station
P.O. Box 631
Vicksburg, MS 39181 — 1

DEPARTMENT OF THE NAVY

NORDA
ATTN: Dr. J. A. Ballard
Code 543
NSTL Station, MS 39529 — 1

DEPARTMENT OF ENERGY

Department of Energy
ATTN: Dr. F. Dickerson (DP-52)
International Security Affairs
1000 Independence Avenue
Washington, D.C. 20545 — 1

Lawrence Livermore National Laboratory
ATTN: Dr. J. Hannon and Dr. M. Nordyke
University of California
P.O. Box 808
Livermore, CA 94550 — 2

Los Alamos Scientific Laboratory
ATTN: Dr. K. Olsen
P.O. Box 1663
Los Alamos, NM 87544 — 1

Sandia Laboratories
ATTN: Mr. P. Stokes
Geosciencies Department 1255
Albuquerque, NM 87115 — 1

OTHER GOVERNMENT AGENCIES

Central Intelligence Agency
ATTN: Dr. L. Turnbill
OSI/NED, Room 5G48
Washington, D.C. 20505 — 1

U.S. Arms Control and Disarmament Agency 2
ATTN: Mrs. M. Hoinkes
Division of Multilateral Affairs
Washington, D.C. 20301

U.S. Geological Survey 1
ATTN: Dr. T. Hanks
National Earthquake Research Center
345 Middlefield Road
Menlo Park, CA 94025

U.S. Geological Survey 1
ATTN: Dr. Robert Masse
Global Seismology Branch
Box 25046, Stop 967
Denver Federal Center
Denver, CO 80225

UNIVERSITIES

University of California, Berkeley 1
ATTN: DR. T. McEvilly
Department of Geology and Geophysics
Berkeley, CA 94720

California Institute of Technology 1
ATTN: Dr. D. Harkrider
Seismological Laboratory
Pasadena, CA 91125

University of California, San Diego 1
ATTN: Dr. J. Orcutt
Scripps Institute of Oceanography
La Jolla, CA 92093

Columbia University 1
ATTN: Dr. L. Sykes
Lamont-Doherty Geological Observatory
Palisades, NY 10964

Massachusetts Institute of Technology 3
ATTN: Dr. S. Soloman, Dr. N. Toksoz, Dr. T. Jordan
Department of Earth and Planetary Sciences
Cambridge, MA 02139

University of Nevada, Reno 1
ATTN: Dr. A. Ryall
Seismological Laboratory
Reno, NV 89557

The Pennsylvania State University 1
ATTN: Dr. S. Alexander
Department of Mineral Sciences
University Park, PN 16802

Southern Methodist University 1
ATTN: Dr. E. Herrin
Geophysical Laboratory
Dallas, TX 75275

CIRES 1
ATTN: Dr. C. Archambeau
University of Colorado
Boulder, CO 80309

Georgia Institute of Technology 1
ATTN: Professor Anton Dainty
The School of Geophysical Sciences
Atlanta, GA 30332

St. Louis University 1
ATTN: Dr. O. Nuttli
Department of Earth and Atmospheric Sciences
3507 Laclede
St. Louis, MO 63156

DEPARTMENT OF DEFENSE CONTRACTORS

Applied Research Associates, Incorporated 1
ATTN: Dr. N. Higgins
2101 San Pedro Boulevard North East
Suite A
Albuquerque, NM 87110

Applied Theory, Incorporated 1
ATTN: Dr. J. Trulio
930 South La Brea Avenue
Suite 2
Los Angeles, CA 90036

Center for Seismic Studies 2
ATTN: Dr. Carl Romney, and Dr. William Dean
1300 N. 17th Street, Suite 1450
Arlington, VA 22209

ENSCO, Incorporated 1
ATTN: Mr. G. Young
5408A Port Royal Road
Springfield, VA 22151

ENSCO, Incorporated 1
ATTN: Dr. R. Kemerait
1930 Highway A1A
Indian Harbour Beach, FL 32937

Pacific Sierra Research Corporation 1
ATTN: Mr. F. Thomas
12340 Santa Monica Boulevard
Los Angeles, CA 90025

Physics Applications, Incorporated 1
ATTN: Mr. C. Vincent
2340 Harris Way
San Jose, CA 95131

R&D Associates 1
ATTN: Dr. E. Martinelli
P.O. Box 9695
Marina del Rey, CA 90291

Rockwell International 1
ATTN: Dr. B. Tittmann
109 Camino Dos Rios
Thousand Oaks, CA 91360

Gould Incorporated 1
ATTN: Mr. R. J. Woodard
Chesapeake Instrument Division
6711 Baymeado Drive
Glen Burnie, MD 21061

Rondout Associates, Incorporated 1
ATTN: Dr. P. Pomeroy
P.O. Box 224
Stone Ridge, NY 12484

Science Applications, Incorporated 1
ATTN: Dr. H. Pratt
P.O. Box 2351
La Jolla, CA 92038

Science Horizons
ATTN: Dr. T. Cherry and Dr. J. Minster 2
710 Encinitas Blvd
Suite 101
Encinitas, CA 92024

Sierra Geophysics, Incorporated 2
ATTN: Dr. R. Hart and Dr. G. Mellman
15446 Bell-Red Road
Redmond, WA 98052

SRI International 1
333 Ravensworth Avenue
Menlo Park, CA 94025

S-Cubed
ATTN: Dr. Steven Day Dr. J. Savino 2
P.O. Box 1620
La Jolla, CA 92037

S-Cubed 1
ATTN: Mr. J. Murphy
11800 Sunrise Valley Drive
Suite 1112
Reston, VA 22091

Teledyne Geotech
ATTN: Dr. Z. Der and Mr. W. Rivers 2
314 Montgomery Street
Alexandria, VA 22314

Woodard-Clyde Associates 1
ATTN: Dr. Larry Burdick
380 West Del Mar Boulevard
Pasadena, CA 91105

Weidlinger Associates 1
ATTN: Dr. J. Isenberg
3000 Sand Hill Road
Building 4, Suite 245
Menlo Park, CA 94025

NON-U.S. RECIPIENTS

National Defense Research Institute 1
ATTN: Dr. Ola Dahlman
Stockholm 80, Sweden

Blacknest Seismological Center 1
ATTN: Mr. Peter Marshall
Atomic Weapons Research Establishment
UK Ministry of Defense
Brimpton, Reading RG7-4RS
United Kingdom

NTNF NORSAR 1
ATTN: Dr. Frode Ringdal
P.O. Box 51
N-2007 Kjeller
Norway